Iron Nanoparticles for In Situ Chemical Oxidation

by

Mohammed Al-Shamsi

A thesis

presented to the University of Waterloo

in fulfillment of the

thesis requirement for the degree of

Doctor of Philosophy

in

Civil Engineering

Waterloo, Ontario, Canada, 2013

Author's Declaration

I hereby declare that I am the sole author of this thesis. This is a true copy of the thesis, including any required final revisions, as accepted by my examiners.

I understand that my thesis may be made electronically available to the public.

Abstract

Recently, metal nanoparticles have attracted the attention of researchers in several fields of study due to their high surface area and other unique properties. Using metal nanoparticles as a component of an *in situ* chemical oxidation (ISCO) system is emerging and hence very little information is available.

In this research, nano zero valent iron (nZVI) particles and iron-based bimetallic zero valent nanoparticles (BZVNs) were employed to activate some common peroxygens (hydrogen peroxide (H_2O_2), persulfate ($S_2O_8^{2-}$), and peroxymonosulfate (HSO_5^-)) to degrade hazardous organic compounds. Aqueous and soil slurry batch systems were used along with a one-dimensional physical model.

The results from the aqueous batch systems showed that nZVI is a promising activator for $S_2O_8^{2-}$ compared to other conventional iron activators (e.g., granular-ZVI and Fe^{2+}). For example, the initial trichloroethylene (TCE) reaction rate by nZVI activated $S_2O_8^{2-}$ was 1.11 x 10^{-4} M L^{-1} min^{-1} compared to an initial reaction rate of 6.25 x 10^{-5} M L^{-1} min^{-1}, 5.18 x 10^{-6} M L^{-1} min^{-1}, and 1.8 x 10^{-7} M L^{-1} min^{-1} for Fe^{2+} activated $S_2O_8^{2-}$, granular-ZVI activated $S_2O_8^{2-}$, and non-activated $S_2O_8^{2-}$, respectively. However, the surfaces of nZVI particles were passivated quickly following exposure to $S_2O_8^{2-}$, causing the reaction rate to reduce to a magnitude representative of an un-activated $S_2O_8^{2-}$ system. An iron-sulfate ($FeSO_4$) complex was formed on the surfaces of the nZVI particles following exposure to $S_2O_8^{2-}$ compared to the iron oxyhydroxide (FeOOH) layer that was present on fresh nZVI surfaces.

BZVNs showed better treatment effectiveness than nZVI particles as activators for H_2O_2, $S_2O_8^{2-}$, and HSO_5^-. For example, the TCE reaction rate constant for nano-Ag-Fe^0 activated H_2O_2 was 9 to 18 fold higher than that for nZVI activated H_2O_2. Of the nine different BZVNs

investigated as activators, the greatest TCE degradation was achieved by nano-Pd-Fe^0 and nano-Zn-Fe^0 activated $S_2O_8^{2-}$ system, nano-Co-Fe^0 activated HSO_5^- system, and nano-Ag-Fe^0 activated H_2O_2 system. For all of these systems, an increase in the dosage of nanoparticles and peroxygens increased TCE degradation. The activated H_2O_2 system showed a lower TCE degradation rate compared to either the activated $S_2O_8^{2-}$ or the activated HSO_5^- systems, suggesting that a bridged group complex is formed between the activators and H_2O_2.

The dissolved TCE concentration remaining in the soil slurry batch systems after using the nano-Pd-Fe^0 activated $S_2O_8^{2-}$ system was two to three fold higher than that in an aqueous batch system. Furthermore, for five different aquifer materials used, the higher mass of aquifer materials the lower the TCE degradation, indicating that the aquifer materials compete with a target organic compound in the presence of activated $S_2O_8^{2-}$. A linear relationship was observed between the organic carbon (OC) content and the initial TCE decomposition rate. Although there is no direct evidence of the effect of OC on the treatment system, it is suggested that the OC may result in scavenging the generated free radicals or by directly consuming persulfate.

In the one-dimensional physical model systems, bimetallic nanoparticles were mobile in a non-geological porous medium and relatively immobile in a geological porous medium. In the non-geological porous medium, we found that adding a second metal (e.g., Pd) to nano-Fe^0 particles significantly improved their functionality and performance (e.g., mobility and suspension). For example, the results from mobility experiments using columns packed with glass beads showed that the effluent iron concentration was <6 % of the influent iron concentration for the nano-Fe^0 particles, while it was ~100 % for the nano-Pd-Fe^0 particles. In the geological porous medium, based on visual inspection, nano-Pd-Fe^0 particles could not travel

more than a few centimeters into columns packed with CFB Borden sand, and no iron was detected in the effluent.

To overcome the delivery issue in porous media, nano-Pd-Fe^0 particles were injected to create a zone of activation to activate $S_2O_8^{2-}$ for the treatment of TCE source zone. However, we found that the TCE mass destruction was only 9 % higher in the nano-Pd-Fe^0 activated $S_2O_8^{2-}$ system compared to the non-activated $S_2O_8^{2-}$ system as revealed by the effluent chloride concentration. In addition, the activation zone composed of nano-Pd-Fe^0 particles was rapidly deactivated after exposure to persulfate as visually observed by color change, indicating that the longevity of the activation zone is limited.

This research effort provides a contribution to the field of ISCO by evaluating the potential utility and applicability of a new class of activators for some common peroxygens.

Acknowledgments

Thank God for everything… the things that I know and the things that I don't.

I would like to thank the person without him this work could not see the light. I would like to express my gratitude to Prof. Neil R. Thomson (my supervisor) for his long patience all those years and for his generous advice and valuable comments.

I am also thankful to Prof. Steven P. Forsey (Chemistry Dep.) for helping me in many aspects of this work. I would like to thank Prof. Michael K. Tam (Chemical Engineering Dep.), Prof. Robert Gillham (Earth science dep.), Prof. James Barker (Earth science dep.), and Prof. Hyung-Sool Lee (Civil Engineering dep.) for being members in my Ph.D. committee. I am also thankful to Prof. John Bergendahl (Worcester Polytechnic Institute) for being the external examiner of this thesis.

I would like to express my gratitude…

To the guys who helped me a lot in the lab without being bored or tired… lots of thanks to Mark Sobon and Mark Merlau.

To my former and current colleagues (in Neil's research group, in Civil Eng. Dep., and Earth science dep.) who gave me a hand in the lab or taught me something that I don't know.

To King Abdulaziz City for Science & Technology (KACST) for providing me with the Ph.D. Scholarship and supporting me from distance.

To those who I love the most…to my dad, mom, brothers and sisters.

To my friends and relatives,

To my tribe… and my people,

Dedication

To Shamis (my 7th grand father), God bless him in his grave.

Poetry:

إلى شامس أهدي جهد المقل المقلل

ولئن بقيت إليك مني ذاك الحمل المثقل

حمل تنوء به عصب الرجال الكمل

و تذل له أعناق الأعادي وتخذل

Translation:

To Shamis I dedicate this little, tiny effort

If I survive in life, I will give you a heavy thing

A thing that hard for the wise men to achieve

And the opponents will be dazzled by it

Table of Contents

List of Figures

List of Tables

Chapter 1

Chapter 1.

Introduction

1.1. General background

More than two billion people worldwide depend on groundwater as a source of drinking water (Thiruvenkatachari et al., 2008). Groundwater can be contaminated by many sources such as accidental spills, leaking underground storage tanks (USTs), and municipal and industrial landfill leachate. In the United States, there are more than 300,000 contaminated sites, and the estimated cost to treat these sites may be as high as US$ 500 billion (NRC, 1999). The average cost of cleaning up a leaking UST site is about US$ 200,000 (Billings and Gale, 1999).

Initially, soil excavation and the pump-and-treat methods were used to clean up these sites; however, both approaches were costly and had limitations. For example, NRC (1994) found that 69 of 77 sites reviewed did not achieve their treatment goals (return aquifer to drinking water standards) after employing the pump-and-treat method. As a result, novel subsurface remediation technologies were developed and tested (NRC, 1999) (see section A.12 in Appendix A).

In situ chemical oxidation (ISCO) is one of these novel technologies and has its own advantages and limitations. ISCO is a fast and effective method to treat a wide range of organic compounds (even biorefractory organics) (Huling and Pivetz, 2006; Siegrist et al., 2011), but some oxidants (e.g., hydrogen peroxide) have a short life span *in situ* (Kakarla and Watts, 1997; Ravikumar and Gurol, 1994; Watts, 1998) and some others (e.g., permanganate) reduce the permeability of the aquifer by the formation of manganese dioxide precipitates (Conrad et al., 2002; MacKinnon and Thomson, 2002). In recent years, persulfate has gained considerable

attention as an alternative oxidant. Unlike hydrogen peroxide, persulfate has a long life span *in situ* (Dahmani et al., 2006; Liang et al., 2003; Sra et al., 2010). Persulfate can be activated by a variety of methods such as transition metals, and photochemical and thermal processes (House, 1962). Ferrous ion (Fe^{2+}) is the most common method to activate peroxygens, but of course it has some drawbacks (Pignatello and Baehr, 1994).

Recently, zero-valent iron (ZVI) (in granular and micro -forms) has been used to activate persulfate (Liang and Lai, 2008). ZVI activated persulfate has been shown to oxidize organic compounds (i.e., TCE, 2,4-dinitrotoluene, and phenyl alcohols) more effectively than Fe^{2+} activated persulfate (Oh et al., 2010; Oh et al., 2009; Padmanabhan, 2008). In spite of ZVI being a promising alternative to activate persulfate, it cannot be injected into a geological porous medium (due to the size of the materials). Nano zero-valent iron (nZVI) has been claimed to be injected successfully *in situ* when it is coupled with stabilizing agents (Elliott and Zhang, 2001; Saleh et al., 2007; Zhan et al., 2008). One of the first efforts to use nZVI with hydrogen peroxide was performed by Liao et al. (2007); however, nZVI has not been examined as a potential activator for other peroxygen systems (e.g., persulfate and peroxymonosulfate). Other types of synthesized metal nanoparticles (e.g., nano-Pd-Fe^0 and nano-Zn-Fe^0), that have shown promising results (e.g., chemical reduction) (Wang and Zhang, 1997; Zhang et al., 1998b) have not been tested as potential activators for oxidants.

1.2. Research scope and objectives

This research investigated the applicability of metal nanoparticles (nZVI and bimetallic nanoparticles) for some peroxygen systems to degrade hazardous organic compounds.

The objectives of this thesis were:

1) to explore the utility of nano-scale zero-valent iron as a persulfate activator and to advance our understanding of the role of nZVI particles in the persulfate system (Chapter 2);
2) to evaluate the potential of using various types of iron-based bimetallic nanoparticles as activators for three common peroxygens (i.e., hydrogen peroxide, persulfate, and peroxymonosulfate) (Chapter 3);
3) to investigate the potential treatability of a typical dissolved phase organic compound (i.e., trichloroethylene) in the presence of five different aquifer materials using nano-Pd-Fe^0 (or nano-Zn-Fe^0) activated persulfate (Chapter 4); and
4) to examine the treatability of a trichloroethylene source zone using the nano-Pd-Fe^0/persulfate system in a one-dimensional physical model (Chapter 5).

1.3. Contributions

Using metal nanoparticles as part of ISCO technology is still in the very early stage of investigation. This work helps to advance our knowledge about the utility and applicability of metal nanoparticles in some ISCO systems.

In this study, we found some advantages of using metal nanoparticles in the ISCO over the conventional activation methods. Accelerating and enhancing the treatment process is considered one of the most promising advantages of using metal nanoparticles (Chapter 2 and 3). The small size of metal nanoparticles is an advantage especially for *in situ* applications. The metal nanoparticles are injected in the subsurface (Chapter 5). The main limitation of using metal nanoparticles was identified in this research as the passivation (or deactivation) of the surfaces of metal nanoparticles. However, the results of this research surrounding this phenomenon will help others to seek potential solutions to this identified problem (Chapter 2).

Each type of metal nanoparticles has a different activation ability toward the different peroxygens investigated. Although the mechanism is unknown, the differences are significant. This contribution may inspire others 1) to investigate the utility of new types of metal nanoparticles, and 2) to discover the unknown mechanisms (Chapter 3).

It has been long debated in the literature whether the soil organic carbon can compete with the target organic contaminants in activated peroxygen systems. However, in this research, we found that the treatment of the target dissolved organic contaminant using the activated peroxygen system is affected by the aquifer material constituents (Chapter 4).

The implementation of metal nanoparticles as an *in situ* activation zone to assist peroxygens in the subsurface was limited by the poor mobility and the surface deactivation of nanoparticles (Chapter 5).

1.4. Thesis design

This thesis was built as a paper-based document where the main four chapters comprise four independent journal articles.

Chapter 1 consists of this introduction along with the objectives and the contributions of the research performed. A general literature on the subject of ISCO and related activators is provided in Appendix A.

Chapter 2 entitled "Treatment of Organic Compounds by Activated Persulfate Using Nano-scale Zero Valent Iron" was accepted by Industrial & Engineering Chemistry Research (ACS publications in 4th August 2013). This article highlights the usefulness of nano-scale ZVI with persulfate compared to some conventional activators, and the issue of passivation. The experiments were performed by M. A. Al-Shamsi. Interpretation of the results was conducted by

M. A. Al-Shamsi and N. R. Thomson. The text was written by M. A. Al-Shamsi, and edited by N. R. Thomson.

Chapter 3 entitled "Iron Based Bimetallic Nanoparticles to Activate Peroxygens" was accepted by the Chemical Engineering Journal (27 July 2013). In this chapter, various bimetallic nanoparticles were examined as potential activators for common peroxygnes. The experiments were performed by M. A. Al-Shamsi. Interpretation of the results was conducted by M. A. Al-Shamsi and N. R. Thomson and S. Forsey. The text was written by M. A. Al-Shamsi, and edited by N. R. Thomson and S. Forsey.

Chapter 4 is entitled "Competition by Aquifer Materials in a Bimetallic Nanoparticles/persulfate System for The Treatment of Trichloroethylene" was accepted by the journal of Environmental Science: Processes & Impacts (as a technical note in 9th August 2013). In this chapter, the degradation of the dissolved phase of organic contaminant was evaluated using nano-Pd-Fe^0 (or nano-Zn-Fe^0) activated persulfate in the presence of various aquifer materials. The experiments were performed by M. A. Al-Shamsi. Interpretation of the results was conducted by M. A. Al-Shamsi and N. R. Thomson. The text was written by M. A. Al-Shamsi, and edited by N. R. Thomson.

Chapter 5 is entitled "Treatment of a Trichloroethylene source zone using persulfate activated by an emplaced nano-Pd-Fe^0 zone" was submitted in 4th June 2013 to the journal of Water, Air, & Soil Pollution. In this article, a one-dimensional physical model was used to evaluate the applicability of a nano-Pd-Fe^0 activation zone approach to assist in the treatment of a TCE source zone using persulfate. The experiments were performed by M. A. Al-Shamsi. Interpretation of the results was conducted by M. A. Al-Shamsi and N. R. Thomson. The text was written by M. A. Al-Shamsi, and edited by N. R. Thomson.

Chapter 6 consists of a summary of the main conclusions and recommendations.

As a result of this thesis format, a repetition of some chemical reactions and other information is inevitable across the four main chapters. In addition, each chapter has its own reference style to suit the journal submission requirements.

Chapter 2

Chapter 2.

Treatment of Organic Compounds by Activated Persulfate using Nano-scale Zero Valent Iron

Outline

Recently, persulfate has caught the attention of groundwater remediation practitioners as a promising oxidant for *in situ* chemical oxidation. In this study, a method was applied to treat a selection of hazardous organic compounds using nano-scale zero valent iron (nZVI) particles as activators for persulfate. The results show that degradation of these organic compounds using nZVI activated persulfate is more effective than nZVI alone. For example, the degradation of naphthalene by nZVI activated persulfate was >99% compared to <10% by nZVI alone. Despite the higher effectiveness, the nZVI particles were passivated quickly following exposure to persulfate causing the reaction rate to reduce to a magnitude representative of an un-activated persulfate system. X-ray photoelectron spectroscopy (XPS) analyses indicated that an iron sulfate layer was formed on the nZVI particle surfaces following exposure to persulfate compared to the FeOOH layer that was present on the fresh nZVI surfaces. Although the nZVI particle surfaces are passivated, nZVI appears to be a promising persulfate activator compared to the conventional persulfate activators such as Fe^{2+} and granular ZVI.

2.1. Introduction

Many of the organic compounds used widely by industry are classified as hazardous and toxic substances, and thus threaten human and ecosystem health. Some of these organic compounds are known potential human carcinogens such as trichloroethylene (TCE) (an industrial solvent),[1-2] methyl tertiary-butyl ether (MTBE) (a gasoline additive),[3] naphthalene (a petroleum and coal tar product),[4] and chlorobenzene (used widely in pesticide manufacturing process).[5] Effective treatment solutions for soil and groundwater contaminated with hazardous organic compounds is required by remediation scientists and engineers.

In situ chemical oxidation (ISCO) is a promising technology that can be used to oxidize a wide range of organic compounds.[6] Hydrogen peroxide,[7] permanganate,[8] and ozone[9] have been used in the subsurface and recently persulfate[10-11] has gained popularity due to its stability in the subsurface and high oxidation potential (E_h = 2.01 V):

$$S_2O_8^{2-} + 2e^- \rightarrow 2SO_4^{2-} \quad (2.1)$$

Treatment of some organic compounds can be enhanced and accelerated by employing activation methods. Activation methods can generate the sulfate free radical ($SO_4^{-\bullet}$) from persulfate which is a much stronger oxidant (E_h = 2.6 V) than the persulfate anion. When transition metals are used (denoted by M^{n+}), then the following reaction can occur[12]:

$$M^{n+} + S_2O_8^{2-} \rightarrow M^{n+1} + SO_4^{2-} + SO_4^{-\bullet} \quad (2.2)$$

Sulfate free radicals can produce hydroxyl free radicals ($OH^{\bullet}$) which are less selective than sulfate free radicals with a higher redox potential (E_h ($OH^{\bullet}/OH^-$) = 2.7 V)[12-13]:

$$SO_4^{-\bullet} + H_2O \rightarrow SO_4^{2-} + OH^{\bullet} + H^+ \qquad K[H_2O]= 2 \times 10^{-3}\ s^{-1} \quad (2.3)$$

$$SO_4^{-\bullet} + OH^- \rightarrow SO_4^{2-} + OH^{\bullet} \qquad K= 6.5 \times 10^{7}\ M^{-1}\ s^{-1} \quad (2.4)$$

These free radicals can attack organic compounds and break them down to non-toxic or less toxic compounds.[14-15]

Iron was used initially in a soluble form (dissolved phase) as ferrous ion (Fe^{2+}) to activate persulfate[16]; however, aqueous Fe^{2+} is relatively insoluble at the ambient pH ≥5 of most aquifer systems.[17] A variety of chelating agents (e.g., ethylenediaminetetraacetic acid (EDTA), diethylene triamine pentaacetic acid (DTPA), and nitrilotriacetic acide (NTA)) are normally used to enhance the solubility of iron. Chelating agents are organic-based compounds which can be degraded in the presence of an oxidant and they also compete with the target organic compounds for the oxidant and the generated free radicals in the system.[17-18]

As an alternative activator, zero valent iron (ZVI), an in-soluble form of iron, has been employed with promising results.[19-22] However, due to the small pore size associated with geological porous media, ZVI in a granular form (millimeter) or powder form (micrometer) cannot be injected into the subsurface and hence is not suitable.

In this study, we use nano-scale ZVI (nZVI) to activate persulfate and to treat an aqueous organic compound of interest. Our objective was to investigate treatment of selected organic compounds (e.g., TCE, MTBE, naphthalene, and chlorobenzene) by persulfate in the presence of a variety of iron-activators (i.e., nZVI, granular ZVI, and Fe^{2+}). The findings from this work advance our understanding of the role of nZVI as a persulfate activator.

In terms of reaction mechanisms, ZVI can activate persulfate by three possible mechanisms (all these mechanisms can generate Fe^{2+} through ZVI corrosion): (1) direct release of Fe^{2+} by persulfate, (2) indirect release of Fe^{2+} by oxygenated water, and (3) indirect release of Fe^{2+} in deoxygenated water as given by[20, 23]:

$$Fe^0 + S_2O_8^{2-} \rightarrow Fe^{2+} + 2SO_4^{2-} \qquad (2.5)$$

$$Fe^0 + \tfrac{1}{2}O_2 + H_2O \rightarrow Fe^{2+} + 2OH^- \quad (2.6)$$

$$Fe^0 + 2H_2O \rightarrow Fe^{2+} + 2OH^- + H_2 \quad (2.7)$$

The corrosion of the ZVI surface, in the direct reaction pathway, is much faster than the corrosion taking place along the other two pathways. Following release from the ZVI, Fe^{2+} can activate persulfate to generate sulfate free radicals by[21-22]:

$$Fe^{2+} + S_2O_8^{2-} \rightarrow Fe^{3+} + SO_4^{2-} + SO_4^{-\bullet} \qquad K= 2 \times 10^1\ M^{-1}\ s^{-1} \quad (2.8)$$

However, at higher ZVI dosages, a chain of inhibiting reactions (radical scavenging reactions) occurs and this reduces treatment effectiveness. The reaction rates of these radical scavenging reactions are much faster than the free radical formation reactions as shown by[21-22, 24]:

$$Fe^{2+} + SO_4^{-\bullet} \rightarrow Fe^{3+} + SO_4^{2-} \qquad K= 4.6 \times 10^9\ M^{-1}\ s^{-1} \quad (2.9)$$

Also, Fe^{2+} can be recycled by reacting with Fe^{3+} that is present with the ZVI surface as follows[22]:

$$2Fe^{3+} + Fe^0 \rightarrow 3Fe^{2+} \quad (2.10)$$

2.2. Materials & Methods

2.2.1. Materials and Chemicals

The following materials were assembled: nZVI particles (average particle size 66-187 nm with a specific surface area of 37 - 58 m^2/g) from Polymetallix, USA; granular-ZVI (1000 to 2000 µm size, 99.98%) from Alfa Aesar; ferrous sulfate, 7-hydrate granular (99.86%) from J.T.Baker; trichloroethylene (99.8%), naphthalene (99%), and chlorobenzene (99.5%) from BDH, England; sodium persulfate (≥98%), hydroxylamine (99%), 1,10-phenanthroline monohydrate (99%), ammonium acetate (>98%) and sodium bicarbonate (99.5%) from Sigma-

Aldrich, USA; potassium iodide (>99%) and hydrochloric acid (34-37%) from EMD Chemicals Inc., Germany; and MTBE (99.95%) from EM Science, Germany. All chemicals were reagent grade and were used as received.

2. 2.2. Procedures and Preparation

The stock solutions of persulfate and the organic compounds were prepared by mixing the desired amount of laboratory-grade chemicals and Milli-Q water (resistivity of 18.2 MΩ cm^{-1}). All the aqueous experiments were performed in 40 mL batch reactors (borosilicate glass vial fitted with polytetrafluoroethylene septa). The solutions were added to each reactor starting with the persulfate solution, then the organic solution (TCE, MTBE, napthalene, or chlorobenzene solutions), then the activators (soluble Fe^{2+}, granular-ZVI, or nZVI), and finally the reactors (three to five treatment replicates) were filled with Milli-Q water (zero head space), and placed on an orbital shaker (200 rpm) in a dark room (temperature 20.5 ± 4 °C). nZVI and ZVI were added as received. At the selected sampling times, a gas-tight syringe (1 mL, 1001 Hamilton syringe series, Sigma-Aldrich, USA) was used to collect aqueous samples through the reactor septa for organic compound and persulfate analyses.

A range of TCE/persulfate/activator molar ratios from 1/20/0 (for the non-activated persulfate system) up to 1/40/150 was explored, and the initial concentration of TCE was 50 or 375 mg/L. To determine the optimal TCE treatment capability, a sequence of experiments was performed using different nZVI and persulfate molar ratios. For the other organic compounds, a 1/20/20 molar ratio of organic compound/persulfate/activator was used, and the initial concentration of MTBE, naphthalene, and chlorobenzene was 300, 13, and 300 mg/L, respectively.

2.2.3. Analysis

Samples (0.7 mL) for organic compound analyses were injected into 2 mL glass vials and shaken on a mini vortexer (VWR Scientific) for 10 seconds prior to gas chromatography (GC) analysis. The organic compound concentration was determined by a head-space solid phase micro-extraction (HS-SPME) method [25] using a HP 6890 series GC equipped with a flame ionization detector (FID), column length 30 m x 0.53 mm and 0.5 μm film (Supelco), SPME fiber 100 μm coated by PDMS (Supelco), and Varian 8200 series auto sampler.

Persulfate was determined by the spectrophotometric method developed by Liang et al.[26] with slight modifications. Potassium iodide (100 g), sodium bicarbonate (5 g), and 100 mL of Milli-Q water were mixed to create a stock solution. A 4 mL aliquot was taken from the stock solution using a pipette and added to 0.1 mL of persulfate sample, and then 36 mL of Milli-Q water was added. The concentration of persulfate was measured spectrophotometrically (after 15 min) using a HACH spectrophotometer (DR/2010) at 400 nm.

Total iron, dissolved iron, and ferrous ion were analyzed spectrophotometrically using 1**,**10-phenanthroline monohydrate as a detector with a HACH spectrophotometer (DR/2010) at 500 nm.[27] Suspended or solid iron was estimated as the difference between the total iron and dissolved iron, and ferric iron was estimated as the difference between dissolved iron and ferrous iron. We assumed that the nZVI particles that were added were 100% metallic iron and neglected the thin iron-oxide shell.

The surface of the nano-iron particles was characterized b**y** X**-**ray photoelectron spectroscopy (XPS) (Thermo-VG Scientific ESCALab 250)**.** XPS spectra were analyzed by using the CasaXPS software (version 2.3.15 CasaXPS software Ltd.). All spectra were calibrated against a carbon peak (C1 s) at the binding energy (BE) of 284.6 eV.

Aqueous pH and Eh were determined using a pH/ISE meter (Orion, 710A), and pH/ISE meter (Orion 4 star, Thermo Electron Corporation).

2.3. Results & Discussion

2.3.1. Chemical Oxidation vs Chemical Reduction

Naphthalene concentration was below the method detection limit (<MDL) using activated persulfate (for all three activator systems), while the remaining naphthalene concentration was >90% of the initial naphthalene concentration for the nZVI only system (Figure 2.1a). The data for naphthalene for the un-activated persulfate system and the granular-ZVI only system are not available.

The remaining chlorobenzene concentration was <3% of the initial chlorobenzene concentration using Fe^{2+} and nZVI activated persulfate system, and 29% using the granular-ZVI activated persulfate system, while the chlorobenzene concentration was >70% of the initial chlorobenzene concentration using either granular-ZVI or nZVI (Figure 2.1b).

In the case of TCE, the remaining TCE concentration was <6% of the initial TCE concentration using the nZVI activated persulfate system compared to 70% using the nZVI only system. Similarly, the remaining TCE concentration was ~20% of the initial TCE concentration using granular-ZVI activated persulfate compared to >85% using granular-ZVI only system (Figure 2.1c). The results from a statistical analysis showed that there is a statistically significant difference ($p < 0.05$) between the mean observed TCE degradation over 24 hours for the nZVI and the Fe^{2+} activated persulfate systems.

The remaining MTBE concentration was ~60% of the initial MTBE concentration using nZVI activated persulfate compared to >80% using either granular-ZVI or nZVI systems (Figure 2.1d).

MTBE is more recalcitrant than the other organic compounds explored because of the binding of tertiary-butyl with ether.[28]

These findings clearly indicate that nZVI activated persulfate is a promising system to treat hazardous organic compounds (e.g., TCE, MTBE, naphthalene, and chlorobenzene) compared to iron reduction methods (e.g., granular-ZVI and nZVI). Based on these screening data, we choose to further investigate the behavior of the nZVI activated persulfate system to treat TCE since nZVI activated persulfate system was more effective to treat TCE compared to the other hazardous organic compounds.

2.3.2. TCE Treatment

The degradation of TCE by the various persulfate systems explored (Figure 2.2) illustrate how the various systems behave. Over a three-hour reaction period, TCE treatment using Fe^{2+} activated persulfate and granular-ZVI activated persulfate was very similar. In comparison, Oh et al.[19] indicated that the oxidation of polyvinyl alcohol (PVA) with ZVI activated persulfate (>99%) was higher than that of Fe^{2+} activated persulfate (~70%) over a two-hour reaction period for an activator to persulfate molar ratio of 1/1. Padmanabhan[29] reported the same observation with TCE; however, Padmanabhan[29] and Oh et al.[19] used micro-sized ZVI and not the granular size as used in this study. Thus, we hypothesize that the difference between these findings is due to the size of ZVI materials used where the larger surface area gives rise to an increased capability to activate persulfate (and other like oxidants).

The initial TCE degradation rate (defined over the initial 3 mins) by nZVI activated persulfate was 1.11×10^{-4} M min^{-1} compared to an initial degradation rate of 6.25×10^{-5} M min^{-1}, 5.18×10^{-6} M min^{-1}, and 1.8×10^{-7} M min^{-1} for Fe^{2+} activated persulfate, ZVI activated persulfate, and

non-activated persulfate, respectively. Although the initial TCE reaction rate by nZVI activated persulfate was very fast, after 45 min the reaction rate drastically reduced.

The late time (>26 min) pseudo first-order TCE degradation rate coefficients[30] for nZVI activated persulfate, ZVI activated persulfate, Fe^{2+} activated persulfate, and non-activated persulfate were 1.1 x 10^{-5} (r^2 = 0.98), 4.3 x 10^{-5} (r^2 = 0.93), 2.7 x 10^{-5} (r^2 = 0.94), and 1.8 x 10^{-5} s^{-1} (r^2 = 0.94), respectively. The change from this initially fast TCE reaction rate to a very slow reaction rate for the nZVI activated persulfate system is suspected to be caused by consumption of persulfate, depletion of nZVI particles, or passivation of reaction sites on the nZVI particles. We explore and discuss these potential causes below.

To advance our understanding of the role nZVI plays as an activator for persulfate, we conducted a separate series of experiments in the absence of TCE. As expected, the more nZVI in the system, the more persulfate was consumed (Figure 2.3a). At a persulfate/nZVI molar ratio of 1/5, >99% of the persulfate was consumed while at a persulfate/nZVI molar ratio of 1/1 [as we used in the previous experiment to treat TCE], <30% of the persulfate was consumed over a 5 day reaction period. Thus, there was an excess of persulfate in the system at a persulfate/nZVI molar ratio of 1/1.

Similarly, when Fe^{2+} is used as an activator for persulfate at a persulfate/Fe^{2+} molar ratio of 1/1 only ~20% of persulfate is consumed (Figure 2.3b). However, the ability of the nZVI system to consume persulfate was higher than that of the Fe^{2+} system. For example, the persulfate residual at a persulfate/Fe^{2+} and persulfate/nZVI system molar ratio of 1/4 was ~25% and 7%, respectively. Liang et al.[31] found that at the TCE/persulfate/Fe^{2+} molar ratio of 1/20/20, 43% of persulfate and 36% of TCE remained in the system at the end of the reaction period. At the same molar ratio, we found that ~45% of TCE and ~80% of persulfate remained. The difference in

these results may be related to the system pH. The initial pH in the study by Liang et al.[31] was 4.5 while the pH in our study was ~6.5. At a lower pH, Fe^{2+} is more soluble and available in the aqueous system[17-18]; however, both studies are in general agreement on the residual amount of persulfate and TCE in the system.

The form of the iron in the persulfate/nZVI system was investigated (Figure 2.4a). In the absence of persulfate, ≤ 8% of nZVI was transferred into the dissolved phase (Fe^{2+} and Fe^{3+}) due to the natural corrosion of nZVI in an aqueous system (Eq. 2.6). In the presence of persulfate, >30% of nZVI was transferred into the dissolved phase, and most of this was in the Fe^{3+} state due to the high corrosion of nZVI by persulfate (Eq. 2.5). As mentioned earlier, nZVI can activate persulfate indirectly by, initially, releasing Fe^{2+} into the aqueous systems, and then the released Fe^{2+} can activate persulfate directly to generate free radicals (Eq. 2.8). The final iron state in this system is Fe^{3+} (Eq. 2.8). Theoretically, all nZVI should be converted into Fe^{3+} as an indicator of the complete depletion of nZVI. Experimentally, we found that only 23% of nZVI was converted into Fe^{3+}, but the amount of Fe^{3+} in the persulfate/nZVI system was almost four times higher than that in the system with only nZVI present. However, the remaining nZVI was not able to react with persulfate suggesting that deactivation of the nZVI surfaces occurred.

In contrast to the persulfate/nZVI system, >85% of Fe^{2+} was converted into Fe^{3+} in the persulfate/Fe^{2+} system (Figure 2.4b). The remaining dissolved Fe^{2+} in the persulfate/Fe^{2+} system is not able to react with persulfate. In addition, we visually observed precipitates and quantified the suspended iron which is likely a result of the following reaction pathway:

$$Fe^{3+} + 3H_2O \rightarrow Fe(OH)_3 \downarrow + 3H^+ \quad (2.11)$$

Moreover, the small amount of Fe^{2+} (~8%) which was left in the system (Figure 2.4b) is below the minimum threshold concentration which allows the reaction to proceed.

2.3.3. Characterization of nZVI Surface

2.3.3.1. Fresh nZVI Surface

The main form of iron on the active activator surface (not exposed to persulfate) was found to be FeOOH (ferric oxyhydroxide) which is consistent with Li et al.[32], Li et al.[33], and Sun et al.[34]. Figure S1a (see electronic supplemental information) shows that the binding energy of the main peak in the iron spectra (Fe 2P 3/2) was at 710.7 eV. Two main peaks were detected in the oxygen spectra (O 1s) at the binding energy of 529.4 eV, and 530.7 eV (Figure S1b. The first main peak in the oxygen spectra (O 1s) implies the presence of the lattice oxygen (O^{2-}) while the second main peak is an indication of the presence of HO^- (hydroxyl group) as found by Haber et al.[35]. FeO, Fe_3O_4, Fe_2O_3, or $Fe(OH)_3$ have only one main peak in their oxygen spectra (O 1s), but we observed two main peaks in the oxygen spectra which supports the presence of FeOOH on the fresh nZVI particles. Furthermore, Li et al.[33], Baltrusaitis et al.[36], and Legrand et al.[37] found that FeOOH has a main peak in the iron spectra (Fe 2P 3/2) at the binding energy of 710.8 eV (± 0.2), and two main peaks in oxygen spectra (O 1s) one at 529.6 eV (± 0.1) for O^{2-} and the second at 530.8 eV (± 0.2) for HO^-. Our results are consistent with these observations. Thus, FeOOH is most likely formed on the surface of the fresh nZVI particles.

The mechanism responsible for forming FeOOH on the surface of nZVI particles starts by the release of Fe^{2+} into the aqueous system (Eq. 2.7), followed by the generation of Fe^{3+} under anaerobic conditions as given by:

$$Fe^{2+} + H_2O \rightarrow Fe^{3+} + OH^- + \tfrac{1}{2}H_2 \qquad (2.12)$$

Fe^{3+} is adsorbed on the surface of nZVI particles as suggested by Fu et al.[38], and then continues reacting to yield $Fe(OH)_3$ as an intermediate product to form FeOOH[33]:

$$Fe^{3+}{}_{(ads)} + 3OH^- \rightarrow Fe(OH)_{3(s)} \qquad (2.13)$$

$$Fe^{3+}_{(ads)} + 3H_2O \rightarrow Fe(OH)_{3(s)} + 3H^+ \quad (2.14)$$

$$Fe(OH)_{3(s)} \rightarrow FeOOH_{(s)} + H_2O \quad (2.15)$$

2.3.3.2 Deactivated nZVI Surface

The main form on iron of the deactivated nZVI surface (exposed to persulfate) was found to be iron sulfate. Figure S1d displays the iron spectra (Fe 2P 3/2) of the deactivated nZVI surface which was found at the binding energy of 711.1 eV. The main peak in the oxygen spectra (O 1s) was found at the binding energy of 531.5 as shown in Figure S1e. Grosvenor et al.[39], and Frost et al.[40] detected $FeSO_4$ at the binding energy of 710.9 eV (± 0.2) in the iron spectra (Fe 2P 3/2), and at the binding energy of 532.0 eV in oxygen spectra (O1s). These findings are similar to those that we observed.

In addition, Figure S1c and S1f show the sulfur spectra (S 2P) of fresh and deactivated surfaces, respectively. Sulfur was not detectable on the fresh nZVI surface compared to a significant detectable sulfur peak on the deactivated nZVI surface at the binding energy of 168.6 eV which implies the presence of sulfur as sulfate (e.g., $FeSO_4$, $Fe_2(SO_4)_3$) rather than sulfide (e.g., FeS, FeS_2) or other sulfur forms.[36, 39-46] In the peer-reviewed literature[42, 44, 46], the reference peaks of $FeSO_4$ in the sulfur spectra (S 2P) were detected at 169.0 eV (± 0.2). Therefore, ferrous sulfate ($FeSO_4$) is most likely formed on the deactivated nZVI surface.

The proposed mechanism to form ferrous sulfate ($FeSO_4$) on the deactivated nZVI surface from ZVI (directly) or from FeOOH (indirectly) is based on adsorbing sulfate anions (SO_4^{-2}) on the surfaces of iron particles as follows:

$$Fe^0_{(s)} + SO_4^{2-} + 2H_2O \rightarrow FeSO_{4(s)} + 2OH^- + H_{2(g)} \quad (2.16)$$

$$FeOOH_{(s)} + SO_4^{2-} + H_2O \rightarrow FeSO_{4(s)} + 2OH^- + \tfrac{1}{2}H_{2(g)} + \tfrac{1}{2}O_{2(g)} \quad (2.17)$$

Parfitt and Smart[47-48] suggested that the sulfate anion (SO_4^{2-}) is adsorbed on the surface of iron oxides such as FeOOH by replacing two surface hydroxyl groups (OH^-) by one sulfate ion (SO_4^{2-}) to make a complex with binuclear bridging Fe—O—S(O_2)—O—Fe. In addition, a mononuclear bridging complex can be formed on the surface of iron oxides (i.e., FeOOH) like Fe—O—S(O_2)—O—H as observed by Peak et al.[49].

Figure 2.5 provides a conceptual model that illustrates the sequence required to form the iron sulfate complex on the surface of a nZVI particle.

2.3.4. Optimal TCE Treatment Conditions

Generally, increasing the nZVI concentration enhanced TCE treatment until the persulfate/nZVI molar ratio of 1/1 was reached (Figure 2.6). Subsequently, further increases in nZVI resulted in no further improvement in TCE treatment, likely as a result of the various scavenging reaction pathways (Eq. 2.9).

TCE residuals (~7%) were similar between the TCE/persulfate/nZVI molar ratio of 1/20/20 and 1/40/20. The highest TCE treatment was at the molar ratio of 1/40/40 (96.3%) and 1/20/150 (96.1%). However, the optimum molar ratio was chosen to be at the TCE/persulfate/nZVI molar ratio of 1/20/20 (92.9%) based on the amount of materials (activator and oxidant) that was used to achieve this treatment level.

According to Oh et al.[19], the treatment of PVA was maximized when the molar ratio between persulfate to Fe^{2+} (and also with persulfate to granular-ZVI) was 1/1. Likewise, Liang et al.[31] found that the highest TCE treatment was at the TCE/persulfate/Fe^{2+} molar ratio of 1/20/15, and increased Fe^{2+} concentrations caused a decrease in TCE treatment. Thus, their observations are consistent with the results we present here.

The pH and redox potential of the persulfate/nZVI system was also investigated (Figure 2.7). As the amount of nZVI is increased in this system, the pH decreases from 4.5 for a persulfate only system to just above 2 for a persulfate/nZVI molar ratio of 1/1 due to the production of HSO_4^- from persulfate decomposition as given by[50]:

$$S_2O_8^{2-} + OH^- \rightarrow HSO_4^- + SO_4^{2-} + \tfrac{1}{2}O_2 \quad (2.18)$$

and then increases to near 7 for a persulfate/nZVI molar ratio of 1/8. At a persulfate/nZVI molar ratio of 1/5, insignificant persulfate mass remains (Figure 2.3a) and the pH is controlled by the production of hydroxyl anions (OH^-) (Eqs. 2.6 and 2.7) and the passivation state of the nZVI particles present. Once all the persulfate is consumed in the vicinity of a persulfate/nZVI molar ratio of 1/5 the system transitions from oxidizing to reducing conditions.

Despite a general decrease in TCE treatment effectiveness above a persulfate/nZVI molar ratio of 1/1, there was an apparent anomaly for a TCE/persulfate/nZVI molar ratio of 1/20/150 (Figure 2.6). We speculate that this anomaly was a result of the initial degradation of TCE due to oxidation reactions until all the persulfate was depleted and then the system became reducing and further degradation of TCE was a result of the reaction between nZVI and TCE following the reductive dechlorination pathway given by

$$3Fe^0 + C_2HCl_3 + 3H^+ \rightarrow 3Fe^{2+} + C_2H_4 + 3Cl^- \quad (2.19)$$

This reaction pathway is supported by the pH and redox observations of the nZVI/persulfate system (Figure 2.7).

2.4. Summary

In this study, a method was applied to treat selective hazardous organic compounds (i.e., TCE, MTBE, naphthalene, and chlorobenzene) using nZVI particles and persulfate. The results show

that coupling nZVI or granular-ZVI with persulfate is more effective to treat the selective organic compounds than using either nZVI or granular-ZVI alone.

The focused investigation of the degradation of TCE by the nZVI activated persulfate system indicated that the degradation rate was initially very fast but then reduced in <50 min to a magnitude representative of an un-activated persulfate system. The suggested scenario is that the nZVI surfaces were deactivated or passivated as a result of the reaction with persulfate. To support this hypothesis, the persulfate/nZVI system without TCE present was explored. After ~5 days of exposure to persulfate the reaction with nZVI essentially stopped with <25% of the nZVI mass converted into dissolved Fe^{3+} and >70% of the initial persulfate remaining. The results from XPS analyses showed that iron sulfate (i.e., ferrous sulfate $FeSO_4$) was present on the nZVI surface following exposure to persulfate compared to iron oxide-hydroxide (i.e., FeOOH) on the fresh nZVI surface.

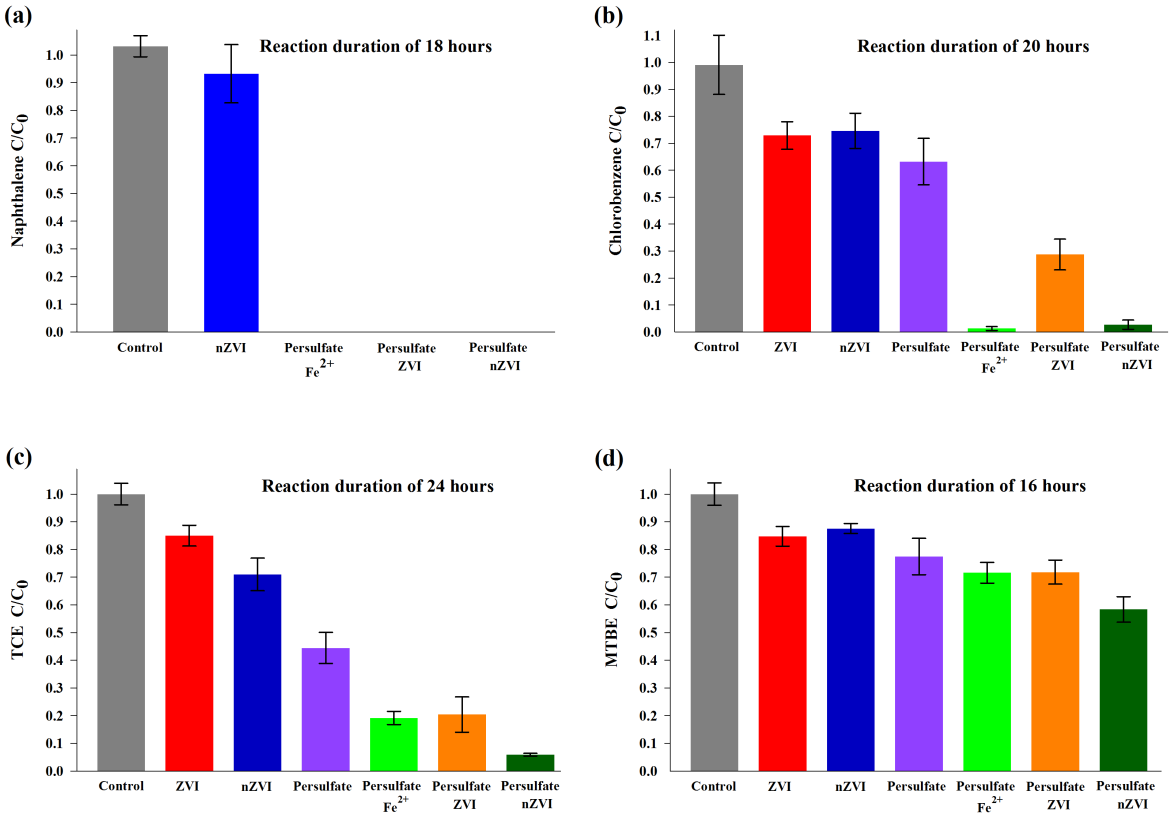

Figure 2.1.1 Degradation of selected organic compounds by various treatment systems. The error bars represent the standard deviation from five replicates. The data of naphthalene for the un-activated persulfate system and granular-ZVI only system is not available.

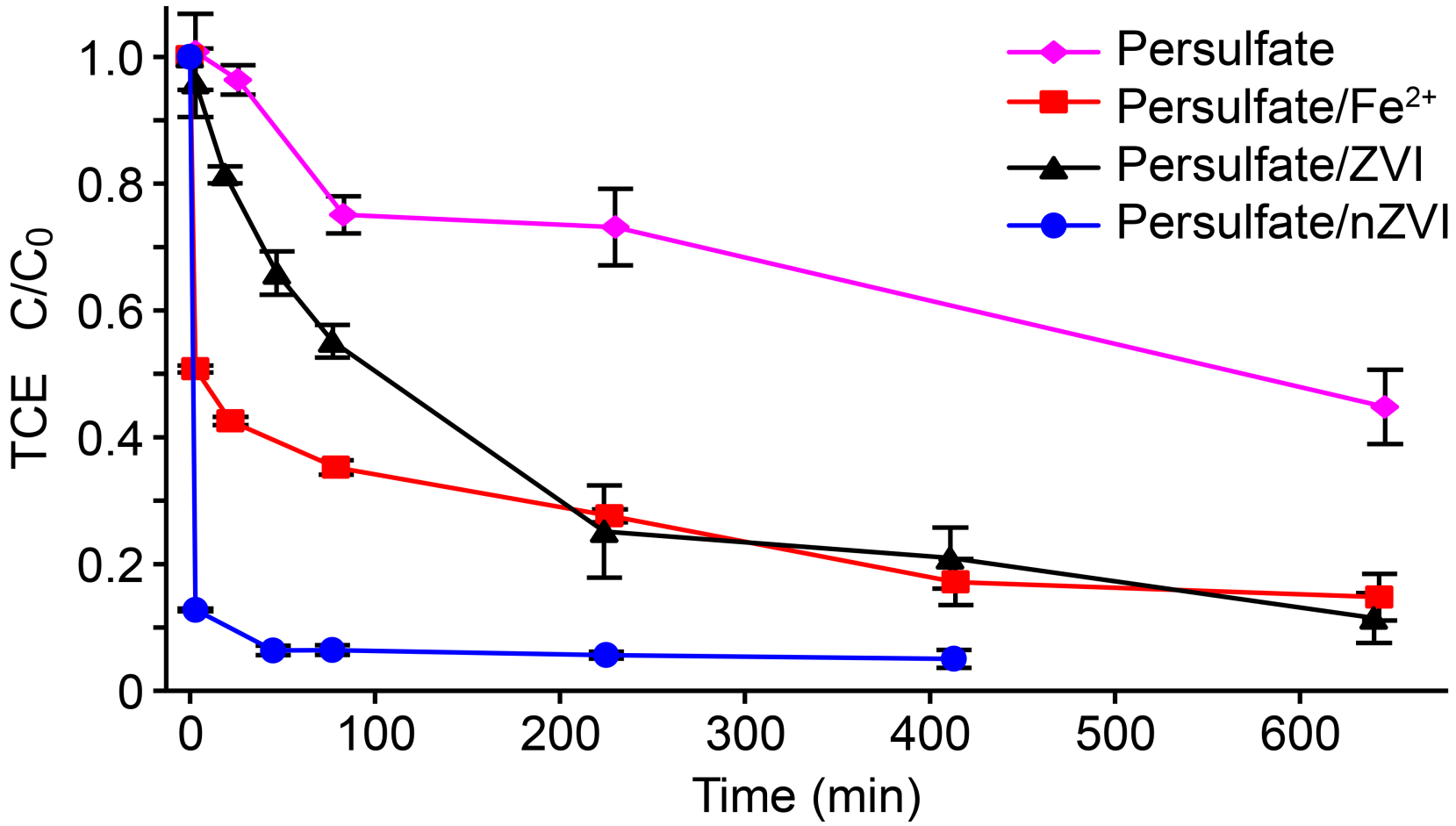

Figure 2.2. TCE treatment by activated and non-activated persulfate. The activators are Fe^{2+}, granular ZVI and nZVI particles. The error bars represent the standard deviation from three replicates.

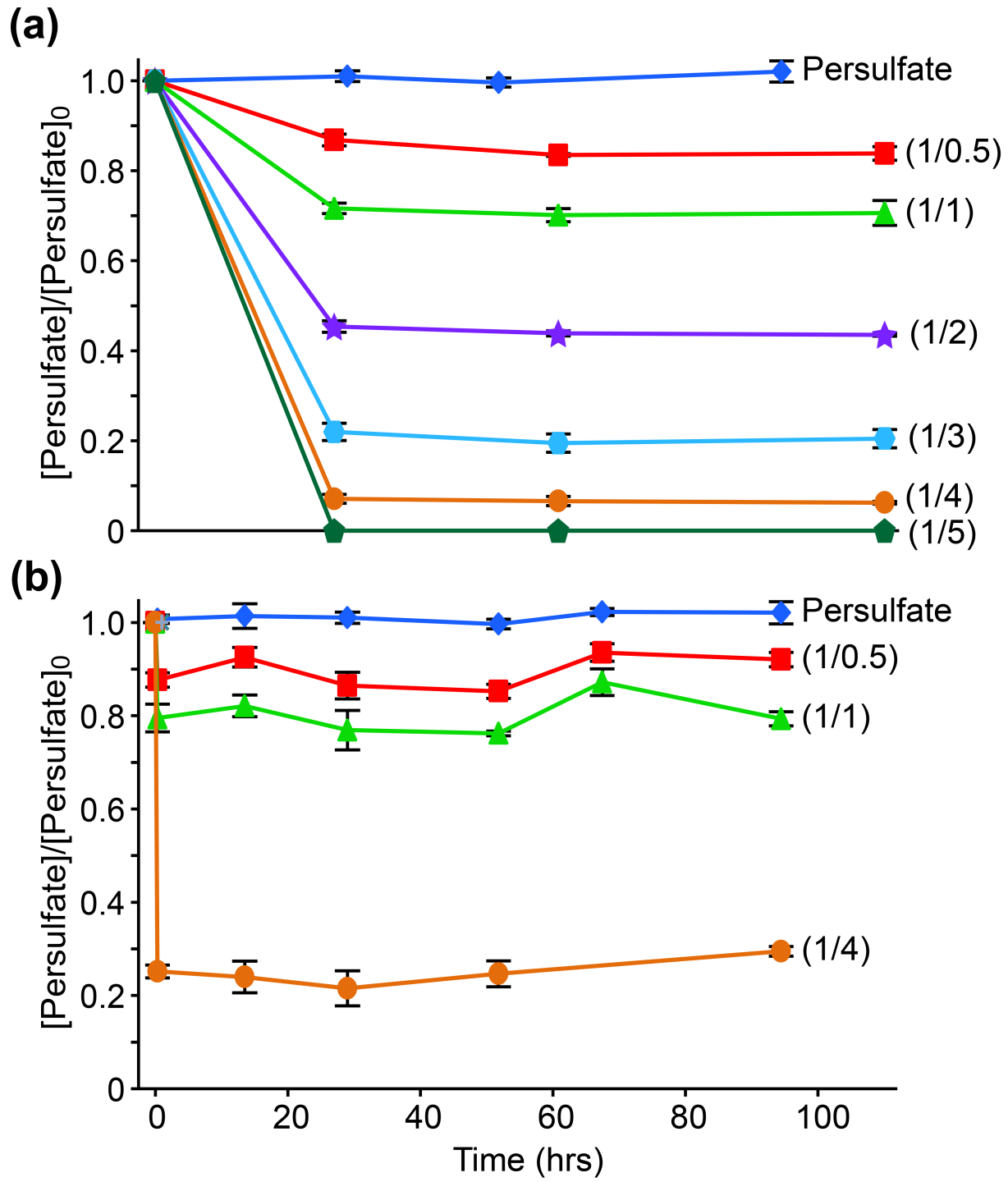

Figure 2.3. Persulfate decomposition at different molar ratios in a (a) persulfate/nZVI system and (b) persulfate/Fe^{2+} system. The initial persulfate concentration was 1.8 g/L. The error bars represent the standard deviation from three replicates.

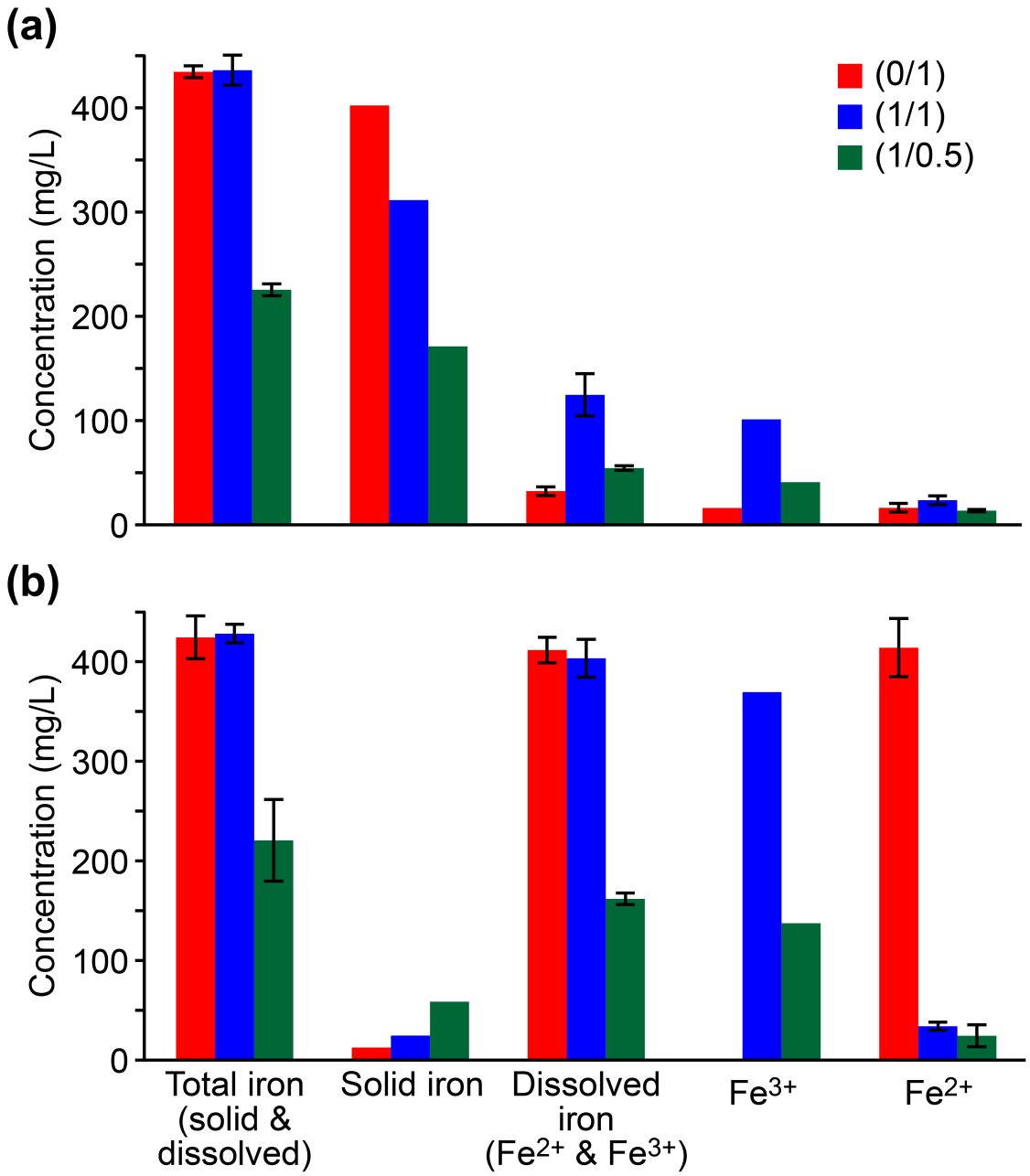

Figure 2.4. The state of iron for different molar ratios of (a) persulfate/nZVI and (b) persulfate/Fe^{2+}. The reaction period was 26 hr for the persulfate/nZVI system and 50 min for the persulfate/Fe^{2+} system. The error bars represent the standard deviation from three replicates.

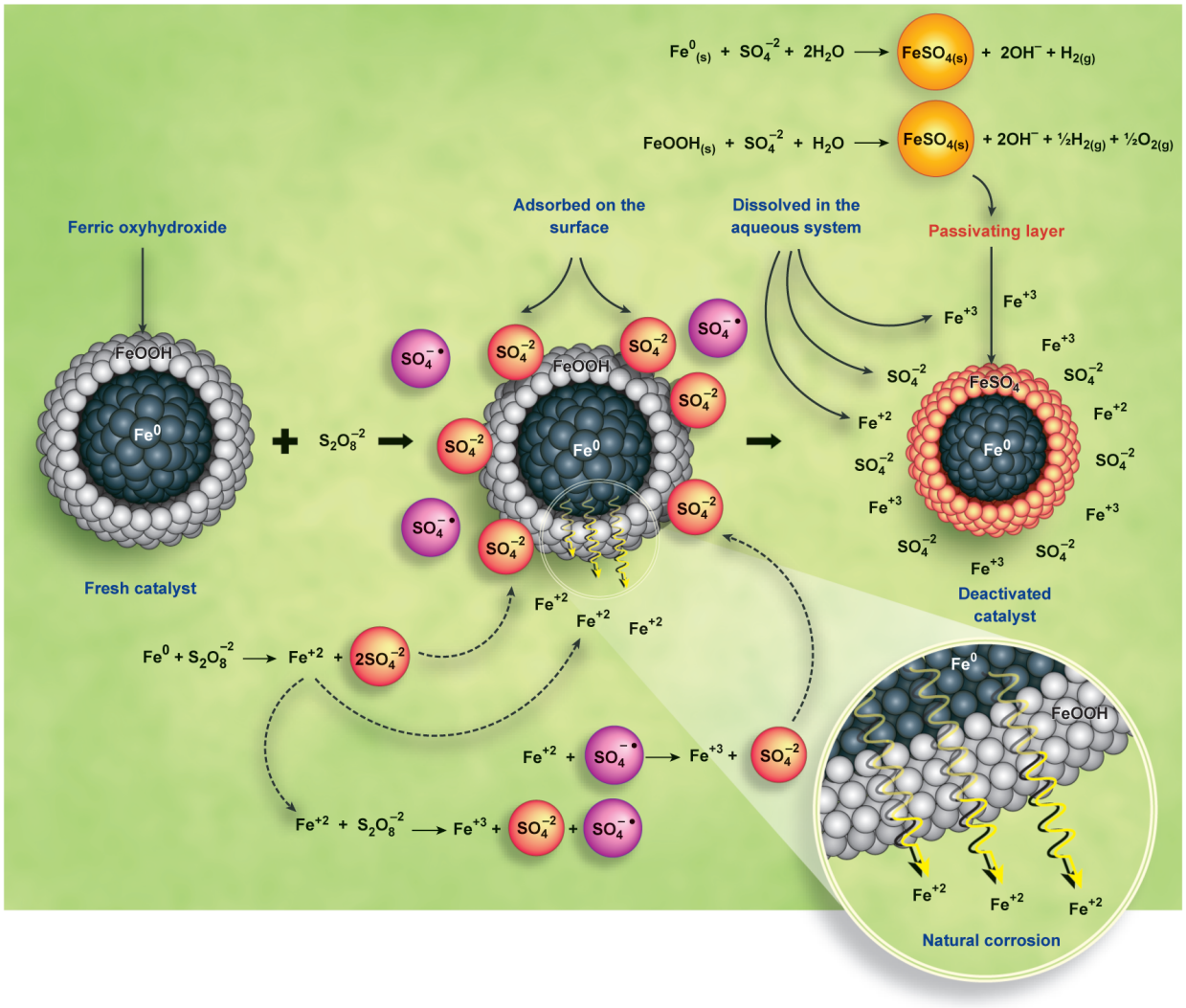

Figure 2.5. A conceptual model that illustrates the formation of an iron sulfate complex on the surface of a nZVI particle.

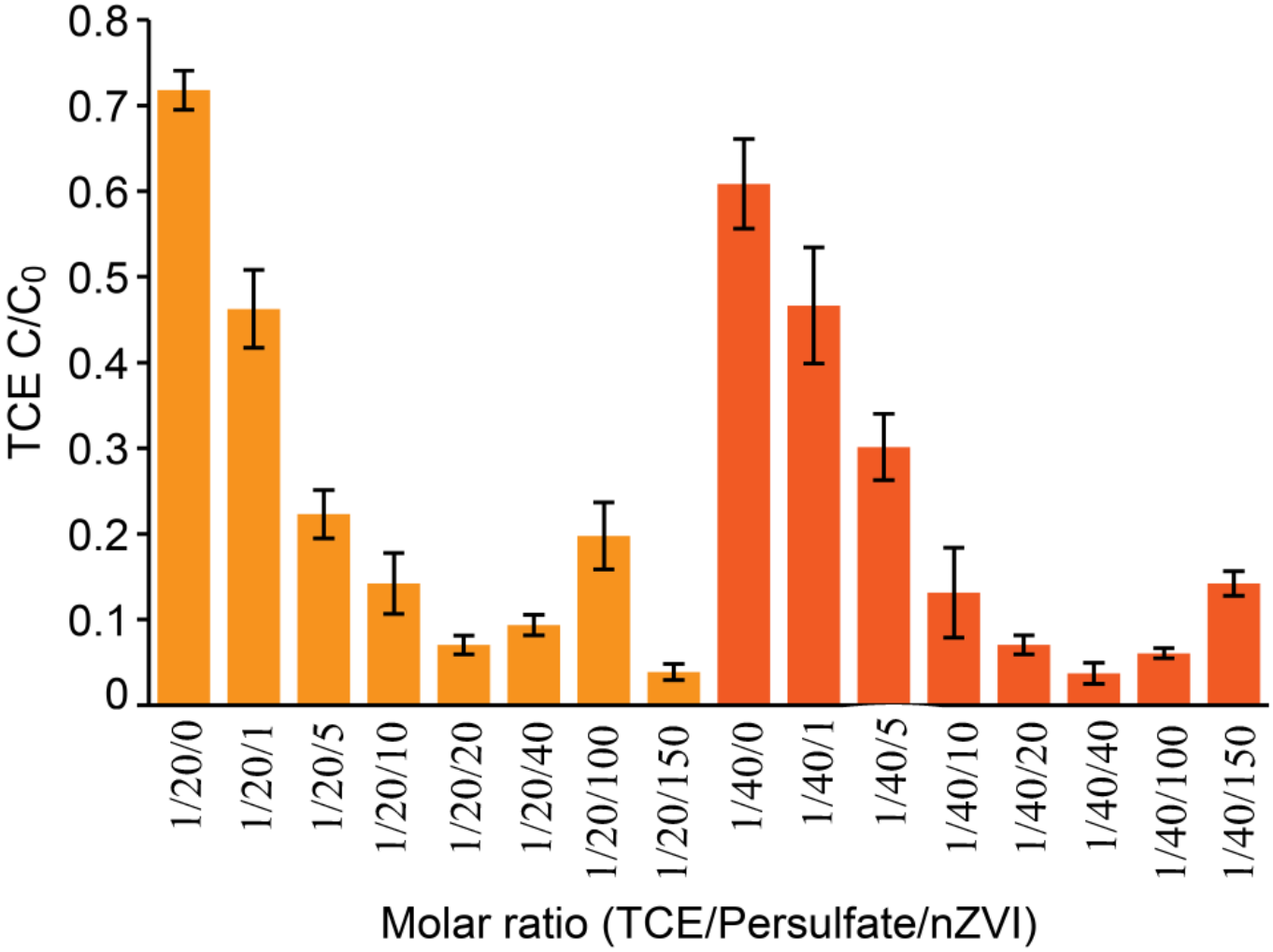

Figure 2.6. TCE treatment for different TCE/persulfate/nZVI molar ratios. Reaction period of 16 hours. The error bars represent the standard deviation from five replicates.

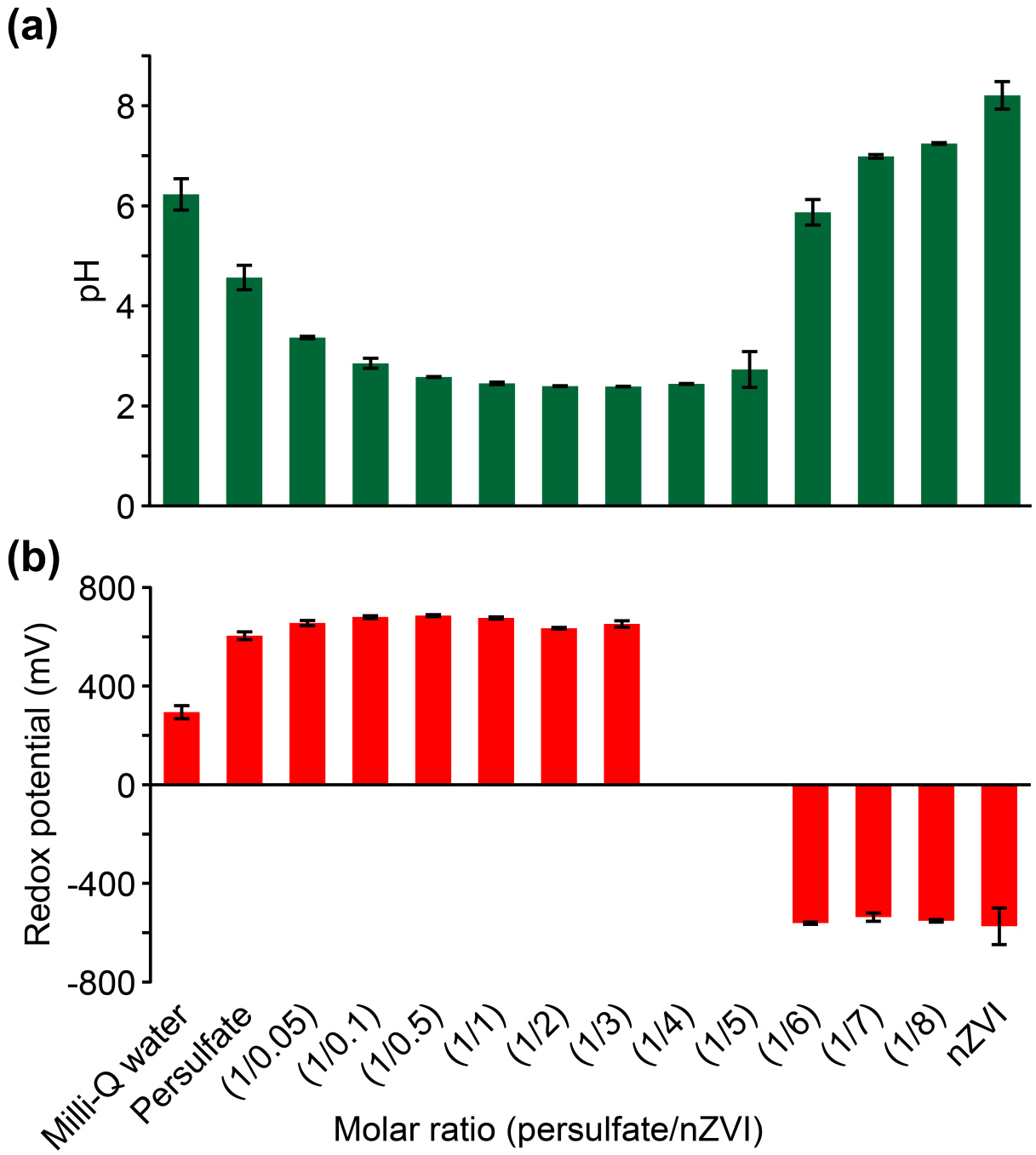

Figure 2.7. pH and redox potential for a persulfate/nZVI system at different molar ratios. The error bars represent a standard deviation from three replicates.

Supporting information:

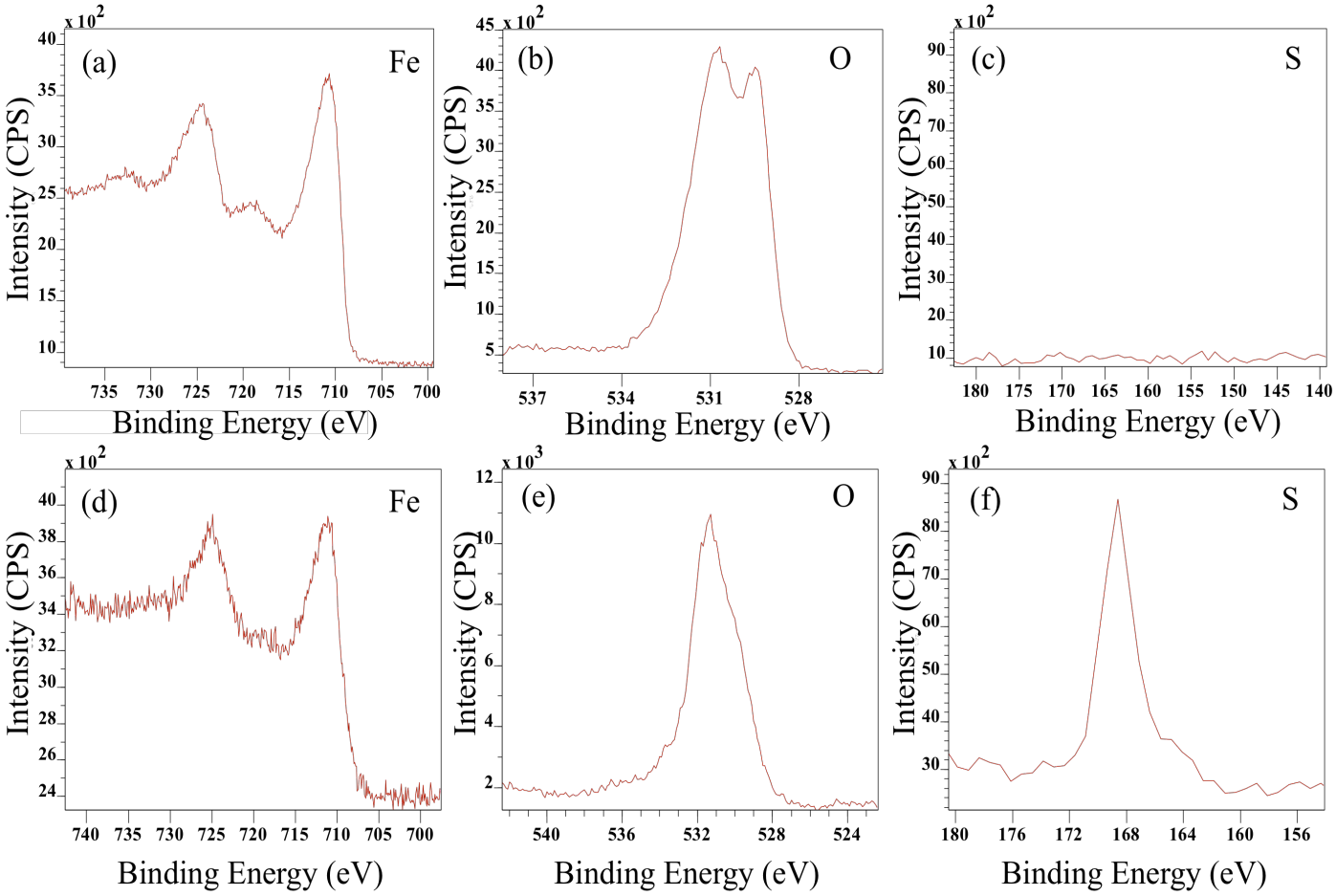

Figure I-1. XPS spectra of Fe (2P $^{3}/_{2}$ and $^{1}/_{2}$), O (1S), and S (2P) species on the surface of nZVI particles before (a, b, c) and after (d, e, f) using them as persulfate activators.

Chapter 3

Chapter 3.

Iron Based Bimetallic Nanoparticles to Activate Peroxygens

Outline

Recently, metal nanoparticles have been used to generate highly reactive free radicals from peroxygens to treat hazardous organic compounds. A novel method of treating trichloroethylene (TCE) was applied using bimetallic zero valent nanoparticles (BZVNs) and peroxygens. In the investigation of nine different BZVNs as activators, the highest TCE oxidation was achieved by nano-Pd-Fe^0 and nano-Zn-Fe^0 in the activated persulfate system, nano-Co-Fe^0 in the activated peroxymonosulfate system, and nano-Ag-Fe^0 in the activated hydrogen peroxide system. In all three systems, increasing the dosage of metal nanoparticles and peroxygens increased the oxidation of TCE. We also found that BZVNs are promising activators for hydrogen peroxide, persulfate, and peroxymonosulfate compared to monometallic zero valent nanoparticles. For example, the TCE reaction rate constant by nano-Ag-Fe^0 activated H_2O_2 is 9- to 18-fold higher than that with nano-Fe^0 activated H_2O_2. The activated H_2O_2 system showed a much lower TCE oxidation rate compared to either activated persulfate or activated peroxymonosulfate, suggesting that a bridged group complex is formed between the activators and H_2O_2, causing a lower TCE oxidation rate.

3.1. Introduction

Municipal and industrial wastewater may contain toxic and hazardous organic compounds. Due to increased health and environmental concerns over the toxicity of some hazardous organic compounds, regulators have established very strict water quality regulations. Achieving the target treatment levels imposed by these strict regulations has become a paramount concern for the water and wastewater industry.

Advanced oxidation technologies (AOTs), which are based on the generation of highly reactive free radicals such as the hydroxyl and sulfate free radicals ($HO^{\bullet}$, $SO_4^{-\bullet}$), are reliable techniques used by the drinking water and wastewater treatment industry to oxidize a wide range of organic compounds [1-2].

Recently, metal nanoparticles have attracted attention as effective activators in AOTs due to their high surface area per unit weight, and their other unique properties compared to bulk (large scale) and dissolved metals (salts) [3]. For example, iron oxide nanoparticles (such as nano-Fe_3O_4) and copper oxide nanoparticles (nano-CuO) have been successfully used with H_2O_2 to oxidize various organic compounds [4-7]. In addition, a novel application of using bimetallic oxide nanoparticles (BONs) as activators for peroxygens showed promising results with cobalt-iron oxide nanoparticles (nano-$CoFe_2O_4$) and peroxymonosulfate [8]. Iron nanoparticles synthesized in a zero valent state have a relatively high reductivity in aqueous systems (E_h = -0.44 V) [9], and have been successfully employed as activators for H_2O_2 [10-15] and persulfate [3] to degrade various organic compounds.

Iron-based bimetallic zero valent nanoparticles (BZVNs) are widely used as a chemical reductant because of their higher reactivity and dispersivity in aqueous systems compared to monometallic systems [16-17]. For example, Wang and Zhang [17] found that > 99 %

degradation of TCE was achieved using nano-Pd-Fe^0 as a treatment method over 0.25 hours compared to a reaction period of 1.7 hours with nano-Fe^0. Although BZVNs are widely used as a reductive treatment method, they have not been examined as potential activators for peroxygens.

The major goal of this research is to investigate the degradation of a model hazardous organic compound (i.e., TCE) using iron based bimetallic zero valent nanoparticles (BZVNs) as activators for three common peroxygens (hydrogen peroxide, persulfate, and peroxymonosulfate).

3.1.1. Generation of Free Radicals

The O-O bond (peroxo bond), which is present in the three peroxygens (H_2O_2, $S_2O_8^{2-}$, and HSO_5^-), breaks down in the presence of transition metals to form highly reactive species such as $OH^{\bullet}$ and $SO_4^{-\bullet}$. Initially, Fe^{2+} is released from nano-Fe^0 by the interaction with the various peroxygens (Eqs. 3.1 and 3.2) or naturally in aqueous systems (Eqs. 3.3 and 3.4), and can generate free radicals by activating peroxygens by providing an electron which cleaves the O-O bond. The reaction mechanisms that generate highly reactive free radicals in the nano-Fe^0/peroxygen system are presented in Table 3.1.

The sulfate free radicals can further react to generate hydroxyl free radicals as given by [26-29]:

$$SO_4^{-\bullet} + H_2O \rightarrow SO_4^{2-} + H^+ + OH^{\bullet} \quad (3.9)$$

$$SO_4^{-\bullet} + OH^- \rightarrow SO_4^{2-} + OH^{\bullet} \quad (3.10)$$

To avoid the possible scavenging of the highly reactive free radicals in the reaction due to the excessive addition of the metal-activators (Eqs. 3.11 and 3.12), a molar ratio of 1 to 1 between nano-Fe^0 and peroxygens should be maintained.

$$Fe^{2+} + SO_4^{-\bullet} \rightarrow Fe^{3+} + SO_4^{2-} \qquad K= 4.6 \times 10^9\ M^{-1}\ s^{-1} \qquad [21] \qquad (3.11)$$

$$Fe^{2+} + OH^{\bullet} \rightarrow Fe^{3+} + OH^{-} \qquad K= 3.0 \times 10^8\ M^{-1}\ s^{-1} \qquad [23] \qquad (3.12)$$

This molar ratio is believed to be the optimum ratio between the metal-activators and peroxygens. In homogenous systems, Rastogi et al. [2] indicated that a 1 to 1 molar ratio is the optimum ratio between Fe^{2+} and HSO_5^-. Burbano et al. [30] found the same with the Fe^{2+}/H_2O_2 system, while Liang et al. [31] found relatively similar results with an optimal molar ratio of 3 to 4 for the $Fe^{2+}/S_2O_8^{2-}$ system. In heterogeneous systems, 1 to 1 was also the optimum molar ratio between the metal activators and peroxygens as found by Oh et al. [32] in the Fe^0/H_2O_2 system and Al-Shamsi & Thomson [3] in the nano-$Fe^0/S_2O_8^{2-}$ system.

3.1.2. TCE Oxidation Mechanisms

Trichloroethylene (TCE), which is used in many industrial fields as a degreasing and cleaning agent [33], was chosen in this research as a model hazardous organic compound. Although Fe^0 is known as a relatively highly reductive species with a redox potential of E_h (Fe^0/Fe^{2+}) = -440 mV [9], coupling Fe^0 with peroxygens provides an oxidative environment in various aqueous systems, for Fe^0/H_2O_2 [34], nano-Fe^0/H_2O_2 [10], $Fe^0/S_2O_8^{2-}$ [20], and nano-$Fe^0/S_2O_8^{2-}$ [3].

The degradation of TCE by hydroxyl radicals generated from H_2O_2 that has been achieved by a metal involves the electrophilic addition of hydroxyl radical to the electron rich double bond to create a geminal chorohydrin radical. Further oxidation produces stable intermediates such as

dichloroacetic acid (Cl_2CHCO_2H), formic acid (HCOOH), and glyoxylic acid (OHCCOOH) [35-37]. Complete mineralization of TCE produces CO_2 and HCl as the final products [35, 37]:

$$C_2HCl_3 \xrightarrow{OH^\bullet} \text{organic radicals} \xrightarrow{OH^\bullet} Cl_2CHCO_2H \xrightarrow{OH^\bullet} CO_2 + 3HCl \quad (3.13)$$

Similarly, the reaction pathway of the sulfate radical ($SO_4^{-\bullet}$) is based on the electrophilic addition of the $SO_4^{-\bullet}$ radical to the electron rich double bond found in unsaturated hydrocarbons [29].

3.2. Materials & Methods

3.2.1. Materials and Chemicals

The following materials were assembled: ferric chloride hexahydrate (> 99 %) and chromium (III) chloride hexahydrate (> 98 %) from Fluka, Germany; zinc sulfate heptahydrate (> 99.5 %) from EM science, Germany; manganese chloride 4-hydrate (99.5 %) from J.T. Baker, USA; trichloroethylene (99.8 %) from BDH, England; sodium persulfate (≥ 98 %), palladium (II) chloride (≥ 99.9 %), cadmium chloride hemi(pentahydrate) (≥ 79.7 %), cobalt (II) chloride (≥ 98 %), nickel (II) sulfate (99.99 %), copper (II) sulfate (≥ 99 %), silver sulfate (> 99.99 %), and sodium borohydride (98 %) from Sigma-Aldrich, USA; peroxymonosulfate (Oxone) from Du Pont Inc., USA; hydrogen peroxide (30 %) from VWR International, USA; and hydrochloric acid (34-37 %) from EMD Chemicals Inc., Germany.

3.2.2. Synthesis of Nanoparticles

Zero valent iron nanoparticles were synthesized in accordance with [16-17, 38-40]. A peristaltic pump (flow rate of 1.67 mL/min) was used to slowly drop $NaBH_4$ (0.25 M) onto the

side of a Erlenmeyer flask containing $FeCl_3.6H_2O$ (0.045 M) to a volume ratio of 1:1 $NaBH_4$: $FeCl_3.6H_2O$ (Figure S1; in the electronic supplementary information) so that the following reaction occurs [16-17]:

$$Fe(H_2O)_6^{3+} + 3BH_4^- + 3H_2O \rightarrow Fe^0{}_{(s)\downarrow} + 3B(OH)_3 + 10.5H_2 \quad (3.14)$$

This reaction occurred under nitrogen gas at ambient room (20 °C) temperature with vigorous mixing using a magnetic stirrer. The stock solutions of $NaBH_4$ and $FeCl_3 \bullet 6H_2O$ were prepared with deoxygenated ultra-pure water. The precipitated iron was washed to remove excess cations and anions such as Cl^- and Na^+ (from $NaBH_4$ and $FeCl_3 \bullet 6H_2O$) by centrifuging for 10 min at 15,000 rpm (Sorvall RC5B plus, Du Pont Company, USA). The mass of the zero valent iron nanoparticles produced was 2.57± 0.22 g/L of the mixture.

The process of depositing the second metal (Pd, Zn, Cr, Cu, Co, Cd, Ag, Mn, or Ni) on the zero valent iron surfaces was accomplished by acidifying the nanoparticle surfaces with HCl (1 M) for a period of 60 seconds, followed by adding 1 % (wt/wt) [all the experiments were performed by adding 1 % load of the second metal except in one experiment in which a range of 0.1 % to 10 % was added] of the respective salts (e.g., $PdCl_2$) into the solution of zero valent iron nanoparticles. The mixture was stirred for a minimum of two hours in zero headspace containers at ambient room temperature. The bimetallic nanoparticles were washed by centrifugation and re-dispersed in deoxygenated ultra-pure water. The reaction required to deposit the second metal on the zero valent iron surfaces (Figure S2) is given by [16-17]:

$$Pd^{2+} + Fe^0_{(s)} \rightarrow Pd^0_{\downarrow(s)} + Fe^{2+} \quad (3.15)$$

3.2.3. Characterization of Nanoparticles

The synthesized bimetallic zero valent nanoparticles (BZVN) were characterized by high resolution scanning electron microscopy (HR-SEM) (Leo 1530, Zeiss, Germany), energy dispersive X-ray spectroscopy (EDX), X-ray photoelectron spectroscopy (XPS) (Thermo-VG Scientific ESCALab 250, USA), and dynamic light scattering (DLS) (Brookhaven Instrument Corporation, BI-APD, USA).

For SEM, EDX, and XPS analyses, dried samples of nanoparticles were obtained by drying the slurry solution of nanoparticles on a silicon wafer (one side polished, Sigma-Aldrich, USA) in small chambers connected to a nitrogen gas cylinder in order to prevent the oxidation of the nanoparticles during the drying process. Image J software was used to determine the size of the particles on the SEM images. For DLS analysis, the GENDIST software package was used to analyze the time correlation functions, and Origin 7 software was used to calculate the size distribution. For XPS analysis, XPS spectra were analyzed using CasaXPS software. All spectra were calibrated against a carbon peak (C1 s) at a binding energy (BE) of 284.6 eV.

3.2.4. Procedures and Preparation

The stock solutions of hydrogen peroxide, persulfate, peroxymonosulfate, and TCE were prepared by mixing the desired amount of laboratory-grade chemicals and Milli-Q water (resistivity of 18.2 MΩ cm^{-1}). All of the aqueous experiments were performed in 40 mL batch reactors (borosilicate glass vials fitted with polytetrafluoroethylene septa). The solutions were added to each reactor starting with the oxidant solution, then the TCE solution, then the activators (e.g., BZVN), and finally the reactors (three treatment replicates) were filled with Milli-Q water (zero head space) and placed on an orbital shaker set to 200 rpm in a dark room

(temperature 20.5 ± 4 °C). The initial concentration of TCE in all of the experiments was 50 mg/L. At the end of the reaction period, a gas-tight syringe (1 mL, 1001 Hamilton syringe series, Sigma-Aldrich, USA) was used to collect aqueous TCE samples (0.7 mL) through the reactor septa. TCE analyses were conducted by a head-space solid phase micro-extraction (HS-SPME) method [41] using a gas chromatography (GC) (HP 6890 series) equipped with a flame ionization detector (FID) and Varian 8200 series auto sampler.

3.3. Results

3.3.1. Characterization of Nanoparticles

DLS analysis showed that the BZVNs are poly-dispersed in aqueous systems with three different size populations: 68± 15 nm, 277.6± 20 nm, and > 500 nm. The size distribution was obtained from 198 nanoparticles observed across several SEM images (Figure S3). The average size of the BZVNs was 99.5± 30.3 nm. The morphology of the synthesized nanoparticles appeared as both a spherical and cubic crystalline structure as shown in Figure S4. The elemental analysis as determined by EDX showed that the nanoparticles contained 85.6 % iron, 11 % oxygen, and 3.4 % palladium (Figure S5). XPS analysis showed that the surface of the fresh synthesized nanoparticles (either nano-Fe^0 or nano-Pd-Fe^0 particles) contained FeOOH.

3.3.2. BZVNs as Persulfate Activators

TCE degradation by persulfate ($S_2O_8^{2-}$) with nine different types of BZVNs (1 % (wt/wt) load of metal additives on zero valent iron nanoparticles) for a reaction period of 30 min is shown in Figure 3.1 (a). TCE degradation by $S_2O_8^{2-}$ was greater with some of the BZVNs than with the mono-metallic iron system. The highest TCE degradation was achieved by the nano-Pd-Fe^0 and nano-Zn-Fe^0 activators; however, for some of the BZVNs (i.e., nano-Cd-Fe^0 nano-Ag-Fe^0 nano-

Cu-Fe^0, and nano-Mn-Fe^0) there was no improvement in TCE degradation compared to the mono-metallic system.

TCE treatment with nano-Fe^0 or nano-Pd-Fe^0 without peroxygens was only able to achieve 36 % degradation over the 30 min reaction period, compared to > 50 % by nano-Fe^0 activated $S_2O_8^{2-}$, and > 70 % by nano-Pd-Fe^0 activated $S_2O_8^{2-}$ Figure 3.1 (b). The effect of palladium on the nano-Fe^0 as a $S_2O_8^{2-}$ activator to treat TCE was investigated (Figure S6). We found that increasing the palladium dosage did not improve the effectiveness of TCE degradation using nano-Fe^0 activated $S_2O_8^{2-}$ system. The effect of adding a 0.1 % load of palladium was similar to the effect of adding a 10 % load. It appears that a small amount of metal additives such as 0.1 % (wt/wt) might be enough to be deposited on the bare nano-Fe^0 particles.

TCE oxidation by different molar ratios of $S_2O_8^{2-}$ with nano-Pd-Fe^0 or nano-Zn-Fe^0 particles (1 % (wt/wt) load of Pd or Zn) was investigated (Figure 3.2 (a) and (b)). The oxidation of TCE was proportional to the dosage of $S_2O_8^{2-}$ and the nano-bimetallic activators. 96 % of TCE was oxidized over a 3 min reaction period using nano-Pd-Fe^0 activated $S_2O_8^{2-}$ at a molar ratio of 1/100/96 (TCE/$S_2O_8^{2-}$/nano-Pd-Fe^0), and 91 % of TCE was oxidized over a 3 min reaction period using nano-Zn-Fe^0 activated $S_2O_8^{2-}$ at a molar ratio of 1/60/60 (TCE/$S_2O_8^{2-}$/nano-Zn-Fe^0).

3.3.3. BZVNs as Peroxymonosulfate Activators

Peroxymonosulfate (HSO_5^-) was activated by different types of BZVNs, each with a 1 % (wt/wt) load of the metal additives, to treat TCE at molar ratios of 1/20/20 (Figure 3.3 (a)) and 1/10/10 (Figure 3.3 (b)) for TCE/HSO_5^-/nano-activator. Over a reaction period of 20 seconds, > 99 % of TCE was oxidized when using all nine variants of BZVN activated HSO_5^- at the molar ratio of 1/20/20, while 72 % of the TCE was oxidized by nano-Fe^0 activated HSO_5^-, and < 4 % of TCE was oxidized by non-activated HSO_5^-.

At the molar ratio of 1/10/10 for TCE/HSO_5^-/nano-activators, the highest TCE oxidation, over a 6 hour reaction period, was achieved by nano-Co-Fe^0 activated HSO_5^-. Therefore, the best peroxymonosulfate activator for TCE oxidation was found to be nano-Co-Fe^0 particles [Co-Fe^0 > Pd-Fe^0 = Mn-Fe^0 = Cd-Fe^0 > Ni-Fe^0 > Cr-Fe^0 > Zn-Fe^0 > Cu-Fe^0 > Ag-Fe^0].

3.3.4. BZVNs as Hydrogen Peroxide Activators

TCE oxidation by different molar ratios of nano-Fe^0 particles and hydrogen peroxide (H_2O_2) was investigated (Figure 3.4 (a)). In general, increasing the dosage of nanoparticles and H_2O_2 increased the oxidation of TCE. For instance, at the molar ratio of 1/100/120 between TCE/H_2O_2/nano-Fe^0, the oxidation of TCE was > 90 % over a 46 hour reaction period compared to ~ 50 % TCE oxidation at the molar ratio of 1/20/20 between TCE/H_2O_2/nano-Fe^0.

TCE oxidation by all nine BZVN activated H_2O_2 reactions was higher than that seen with the bare nano-Fe^0 activated H_2O_2 even at a high molar ratio of 1/100/120 for TCE/H_2O_2/nano-Fe^0 as shown in Figure 3.4 (b). TCE oxidation over a reaction period of ~ 25 hours was > 99 % and 56 % for nano-Ag-Fe^0 activated H_2O_2 and nano-Fe^0 activated H_2O_2, respectively. Nano-Ag-Fe^0 particles were the most promising hydrogen peroxide activators [nano-Ag-Fe^0 > nano-Cu-Fe^0 > nano-Cr-Fe^0 > nano-Zn-Fe^0 > nano-Mn-Fe^0 > nano-Pd-Fe^0 > nano-Cd-Fe^0 > nano-Ni-Fe^0 > nano-Co-Fe^0 > nano-Fe^0].

We extended the investigation of nano-Ag-Fe^0 particles using different molar ratios of nano-Ag-Fe^0/ H_2O_2 to treat TCE (Figure 3.4 (c)). The oxidation of TCE over a 3 hour reaction period was 97 % for TCE/H_2O_2/nano-Ag-Fe^0 molar ratios of 1/100/100, while 46 % of the TCE was oxidized at the molar ratio of 1/10/10. Again, increasing dosage increased the oxidation rate.

3.4. Discussion

3.4.1. Characterization of Nanoparticles

The smaller size population as found by DLS (i.e., 68 nm as an average particle size) was created by the initial precipitation reaction of $NaBH_4$ with $FeCl_3.6H_2O$. The two larger size populations are likely caused by the aggregation of nanoparticles due to their attractive forces. The main shape of the BZVNs as observed by HR-SEM is a cubic crystalline structure, which is similar to that found by Wang and Zhang [17] and Chun et al. [9] using TEM.

Very small peaks were identified for the second metals (e.g., Pd, Cu, Ag) on the surface of the zero valent iron particles by XPS (data not shown) and EDX. The same observation was also found by Zhu and Lim [42]. The diameter of the second metal that was deposited heterogeneously on the surface of zero valent iron particles was smaller than 20 nm as measured from HR-SEM images, which is in agreement with the findings of Chun et al. [9].

The presence of an iron-oxide shell in the form of FeOOH was identified by XPS for the mono and the bimetallic zero valent iron nanoparticles which is consistent with the observation of Li et al. [43] and Sun et al. [44].

3.4.2. The Effectiveness of the Various Activated Peroxygens

In the various BZVN/peroxygens systems, BZVN activated H_2O_2 takes several hours to oxidize TCE even with the best reaction conditions (high dosage and silver as the second metal) compared to minutes with either BZVN activated HSO_5^- and $S_2O_8^{2-}$ (Figure 3.4). This indicates that the activated H_2O_2 is less able to oxidize TCE than either the activated $S_2O_8^{2-}$ and HSO_5^- systems.

These results are consistent with the findings of Anipsitakis and Dionysiou [25] who found that H_2O_2 in a homogenous system with various transition metal activators (e.g., Fe^{2+}, Co^{2+}, Ni^{2+}) was less able to oxidize 2,4 dichlorophenol (2,4-DCP) than either transition metal activated $S_2O_8^{2-}$ or transition metal activated HSO_5^-. Masarwa et al. [45] also found that Cu^+ reacts with $S_2O_8^{2-}$ much faster than H_2O_2. Yang et al. [46] indicated that the oxidation of Azo dyes by heat-activated $S_2O_8^{2-}$ and HSO_5^- is higher than that seen by heat-activated H_2O_2. Likewise, Anipsitakis and Dionysiou [47] found that the oxidation of 2,4-DCP is higher using UV activated $S_2O_8^{2-}$ and HSO_5^- than UV activated H_2O_2. In heterogeneous systems, Clausen et al [48] found that the reaction rate of degrading direct red 32 (DR 32) by $TiO_2/UV/H_2O_2$ system was less than that by either $TiO_2/UV/S_2O_8^{2-}$ or $TiO_2/UV/ClO_3^-$ systems.

Although some have found that the oxidation of organic compounds by the activated $S_2O_8^{2-}$ system is higher than that by the activated HSO_5^- system [46-47], they are all in agreement that the activated H_2O_2 system has the weakest ability to oxidize organic compounds compared to other activated peroxygen systems. We found that the oxidation of organic compounds (i.e., TCE) by the activated HSO_5^- system is higher than that by the activated $S_2O_8^{2-}$ system, which is in agreement with the findings of Anipsitakis and Dionysiou [25]. It is clear that the response of peroxygens to the various activation methods are not the same, as has been discussed elsewhere.

The $OH^\bullet$ that is generated by the decomposition of H_2O_2 in the presence of an activator is higher in redox potential (E_h $OH^-/OH^\bullet$ = 2.7 V) than that of $SO_4^{-\bullet}$ (E_h ($SO_4^{2-}/SO_4^{-\bullet}$) = 2.4 V) [20], however the $OH^\bullet$ produced by the activated decomposition of H_2O_2 has a lower oxidative capacity than $SO_4^{-\bullet}$ as illustrated by the examples above. One possible explanation for this phenomenon is that the electron transfer from the surface of metals to H_2O_2 occurs through an inner sphere electron transfer as opposed to the faster outer sphere electron transfer that may

occur with the activated $S_2O_8^{2-}$ and HSO_5^- with a metal activator. An inner sphere electron transfer mechanism, which is proposed by Taube et al. [49] as a bridged transition state, is most likely responsible for the slow oxidation of TCE and other organic compounds in the activated H_2O_2 system, regardless of the type of activators being used.

The inner sphere electron transfer mechanism is not like the outer sphere electron transfer mechanism (i.e., the classical theory) where electrons are transferred between the reductant (electron donor) and the oxidant (electron accepter) without bridging or sharing ligands. In the inner sphere electron transfer reaction, the reductant and the oxidant are sharing ligands and connected by a chemical bond, forming an intermediate (bridging group complex) followed by an electron transfer between the reductant and the oxidant. The most important aspect of the inner sphere electron transfer is that the bridging group complex that is produced in the first step of the mechanism can be an active intermediate and react without the separation of the bridging group complex or transferring electrons between the reductant and the oxidant causing a decrease of the oxidation efficiency. Even in the case of generating free radicals after the separation of the bridging group complex, the oxidation process by inner sphere electron transfer always takes longer than by an outer sphere electron transfer [50-51].

This possible explanation is supported by Rastogi et al. [2] who indicated that the activated H_2O_2 system is less able to oxidize organic compounds compared to the activated HSO_5^- system due to the differences in outer and inner sphere electron transfer reactions.

Since dissolved-Fe^{2+} is released from solid-Fe^0 particles as indicated in section 3.1.2., the electron transfer reaction in nano-Fe^0 activated H_2O_2 might be similar to that of Fe^{2+} activated H_2O_2. In the case of Fe^{2+} activated H_2O_2, the outer sphere electron transfer reaction does not occur due to the production of a bridged group complex with H_2O_2 and Fe^{2+} as a hydrated

iron(II)- H_2O_2 complex $\left[Fe(OH)(H_2O_2)(H_2O)_4\right]^+$, followed by the formation of an intermediate iron (IV) complex $\left[Fe(OH)_3(H_2O)_4\right]^+$ [52-53]:

$$\left[Fe(OH)(H_2O_2)(H_2O)_4\right]^+ \rightarrow \left[Fe(OH)_3(H_2O)_4\right]^+ \quad (3.16)$$

The intermediate iron (IV) complex may react further to generate $OH^\bullet$, as shown by

$$\left[Fe(OH)_3(H_2O)_4\right]^+ + H_2O \rightarrow \left[Fe(OH)(H_2O)_5\right]^{2+} + OH^\bullet + OH^- \quad (3.17)$$

$OH^\bullet$ may not even be formed in some cases as found in the mixture of Cu^+ and H_2O_2 by Masarwa et al. [45]. In such cases, the bridged group complex is not broken down to generate free radicals, and thus the bridged group would react as a whole with the organic compounds, causing a lower reaction rate. Another term that has been used to describe such a phenomena is "non-free $OH^\bullet$" in which the $OH^\bullet$ in a Fenton reaction is not totally free in the solution [52].

Rastogi et al. [2] suggested the possibility of an outer sphere electron transfer reaction in a activated HSO_5^- system, and Masarwa et al. [45] suggested the same electron transfer mechanism in the activated $S_2O_8^{2-}$ system. Furthermore, Buxton et al. [54] suggested that the electron transfer from Fe^{2+} and Mn^{2+} to $SO_4^{-\bullet}$ is an outer sphere reaction mechanism.

The electron transfer in BZVN activated HSO_5^- and $S_2O_8^{2-}$ is likely to occur by an outer sphere electron transfer mechanism in which no bonds are formed or broken during the electron transfer, thus the rate of free radical generation is fast, causing a higher TCE degradation rate compared to BZVN activated H_2O_2. As we found in sections 3.1 – 3.3, TCE degradation was achieved in few minutes by BZVN activated $S_2O_8^{2-}$ and HSO_5^- systems compared to several hours for TCE degradation by BZVN activated H_2O_2 system.

Although the outer sphere electron transfer reaction provides us with a plausible explanation for the high reaction rate for the activated HSO_5^- and $S_2O_8^{2-}$ systems, further investigations are

needed to study the chemistry of persulfate and peroxymonosulfate and the behavior of their active intermediates and free radicals.

3.4.3. Kinetic Model for BZVN Activated Hydrogen Peroxide

The data for TCE oxidation by the activated H_2O_2 system can be fitted to a pseudo first-order kinetic model as follows:

$$-d[TCE]/dt = k\,[TCE] \tag{3.18}$$

The rate constant of the pseudo first-order reaction can be obtained by plotting $-\ln [TCE]_t/[TCE]_0$ against the reaction time as presented in Figure 3.4 (d), (e), and (f).

$$k = -(\ln[TCE]_t/[TCE]_0)/t \tag{3.19}$$

In this case, k is the rate constant of the pseudo first-order reaction, $[TCE]_0$ is the initial concentration of TCE, and $[TCE]_t$ is the concentration of TCE at time t.

Generally, the oxidation of organic compounds by the activated H_2O_2 system, regardless of the type of activators or activation methods used, can be fitted to a pseudo first-order kinetic model [28, 35]. The TCE reaction rate constant (Table 3.2) using nano-Ag-Fe^0 activated H_2O_2 is higher than that of nano-Fe^0 activated H_2O_2 by 9- to 18-fold, indicating that nano-Ag-Fe^0 is the more promising activator compared to nano-Fe^0. In general, BZVNs as activators for H_2O_2 increase the TCE reaction rate constant by 4.5- to 9-fold compared to the mono-metallic zero valent nanoparticles.

A higher dosage of nano-activators and H_2O_2 results in a higher TCE oxidation rate, which fits a linear relationship (r^2= 0.99 and 0.97) between the dosage of nano- Fe^0 (or nano-Ag-Fe^0) and the TCE reaction rate constant (Figure 3.5). This is in agreement with the findings of Hoag et al. [55] who observed a linear relationship between the bromothymol blue (a dye) reaction rate constants and the dosage of the nano-Fe^0 activated H_2O_2 system.

3.4.4. The Effect of the Bimetallic System

In terms of TCE oxidation by peroxygens activated by mono- and bi-metallic zero valent nanoparticles, we concluded (as discussed in the previous sections) that the bimetallic system is more promising than the monometallic system for the various peroxygen systems explored. There is a consensus in the peer-reviewed literature that metal additives enhance the reactivity of zero valent iron when chemical reduction is the desired pathway in the absence of peroxygens. Four theories or mechanisms were proposed to illustrate the enhancement of degradation by a bimetallic system: (1) the metal additives (e.g., Pd, Ag) serve as an additional electron donor [56]; (2) the metal additives increase the surface area of zero valent iron nanoparticles by depositing a non-uniform layer of metal additives on the surface of the nanoparticles, which enhances the catalytic ability of the nanoparticles [16]; (3) the metal additives may prevent or delay the formation of an iron oxide shell, which maintains the catalytic ability of zero valent iron nanoparticles for a longer time [16-17]; and (4) the metal additives can form a galvanic corrosion system on the surface of zero valent iron nanoparticles, in which the metal additives act as catalysts (cathode) while the zero valent iron nanoparticles act as an electron donor (anode) [9, 57]. The forth mechanism is the most accepted explanation of how the second metal helps to increase the ability of zero valent iron nanoparticles. The first two mechanisms are also possible but unlikely to be counted as the main mechanisms. For the third mechanism, the second metal (e.g., Pd) on the surface of nano-Fe^0 most likely acts as a temporary factor to delay the passivation on the surfaces, and that is also a possible cause of the increasing TCE oxidation by BZVN activated $S_2O_8^{2-}$ compared to nano-Fe^0 activated $S_2O_8^{2-}$.

XPS analyses (data not shown) showed that the mono- and the bi-metallic zero valent nanoparticles were deactivated after exposure to $S_2O_8^{2-}$, forming an iron sulfate complex as

found by Al-Shamsi and Thomson [3]. Surprisingly the elemental spectra for both the mono- and bi-metallic zero valent nanoparticles were exactly the same after exposure to $S_2O_8^{2-}$.

3.4.5. The Effect of the Type of the Second Metal

In the investigation of nine different BZVNs, each BZVN was found to have a different ability to activate various peroxygens. For instance, the highest TCE oxidation was achieved by nano-Pd-Fe^0 and nano-Zn-Fe^0 in the activated $S_2O_8^{2-}$ system, nano-Co-Fe^0 in the activated HSO_5^- system, and nano-Ag-Fe^0 in the activated H_2O_2 system. These results are consistent with those who used various BZVNs to treat organic compounds directly in a chemical reduction treatment system [9, 16, 58-60].

Although the consistency in the peer-reviewed literature concerning the differences in the activation abilities of different BZVNs is apparent, the differences in the effects of the different BZVNs are not fully understood. Chun et al. [9] suggested that the structural properties of the different metal additives on the zero valent iron nanoparticles cause the main differences in their reactivity. Specifically, they found that the different metal additives can be distributed heterogeneously on the surface of the zero valent iron nanoparticles, and the size of the different metal additives, which ranged from 5 to 20 nm, are also different. This suggests that the differences in the size and distribution are a plausible explanation for the differences in their reactivity. In addition, they suggested that the reaction rate is independent of the type of metal additive.

In our case; however, we found that the highest TCE oxidation in the activated H_2O_2 system was obtained using nano-Ag-Fe^0 as an activator, while the lowest TCE oxidation in the activated $S_2O_8^{2-}$ system was obtained by that same activator. Nano-Ag-Fe^0, which was used to activate H_2O_2 and $S_2O_8^{2-}$, was synthesized the same way and had the same properties, yet it gives very

different rates of reaction with the different peroxygens, suggesting that the difference in the structural properties of the metal additives on the zero valent iron is not the best explanation for this phenomenon, at least in the case of the activated peroxygens.

A caged metal-radical species phenomenon is also a plausible explanation for the differences between the different metal additives. In the case of nano-Ag-Fe^0 activated $S_2O_8^{2-}$, almost no improvement was made in TCE oxidation compared to nano-Fe^0 activated $S_2O_8^{2-}$, suggesting that a caged metal-radical species is formed between the leaching of the metal additives and the generated free radicals. Such a species was suggested by Anipsitakis and Dionysiou [25] in a homogenous system between Ag^+ and $S_2O_8^{2-}$. The authors suggested the formation of a caged metal-radical species $[Ag^{II}(SO_4^{\bullet})]^+$ in which the sulfate free radical is not free to react in the solution with the targeted organic compounds. Numerous articles have indicated the presence of a caged metal-radical species in various metal complexes/peroxygens systems [61-63]. Further studies are needed to illuminate this mysterious phenomenon.

3.5. Summary

In this work, a class of synthesized metal nanoparticles was used to activate three common peroxygens (H_2O_2, $S_2O_8^{2-}$, and HSO_5^-) for the degradation of a model hazardous organic compound (i.e., TCE). Iron-based bimetallic zero valent nanoparticles (BZVNs) were synthesized by a borohydride reduction method. We found that BZVNs are promising activators for peroxygens to treat hazardous organic compounds and they are more promising than the monometallic zero valent nanoparticles. For example, the TCE reaction rate constant by nano-Ag-Fe^0 activated H_2O_2 is 9- to 18-fold higher than that with nano-Fe^0 activated H_2O_2.

The highest TCE oxidation was achieved using nano-Ag-Fe^0 in the activated H_2O_2 system, nano-Pd-Fe^0 in the activated $S_2O_8^{2-}$ system, and nano-Co-Fe^0 in the activated HSO_5^- system. The

ability of the BZVN activated H_2O_2 system to oxidize TCE was less than that of BZVN activated $S_2O_8^{2-}$ and HSO_5^- systems, suggesting a bridged group complex was formed during the electron transfer reaction between the surface of BZVNs and the O-O bond in the H_2O_2 molecule. This bridged group complex is responsible for the lower oxidation rate in the BZVN activated H_2O_2.

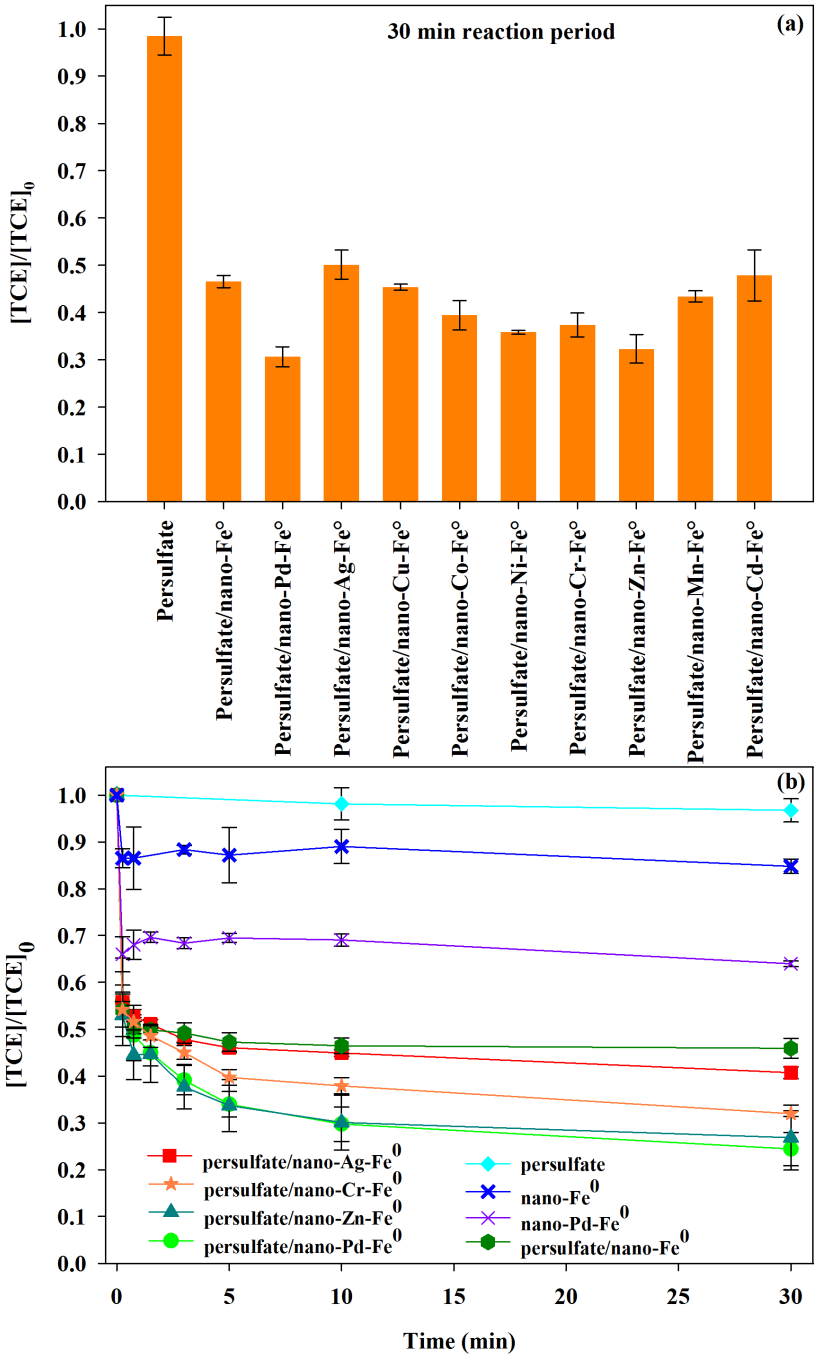

Figure 3.1.9TCE degradation (a) by persulfate with nine different types of bimetallic zero valent nanoparticles and (b) by nano-Fe^0, nano-Pd-Fe^0, non-activated persulfate, and activated persulfate with four different types of bimetallic zero valent nanoparticles. The molar ratio between TCE/persulfate/nano-activator was 1/20/20, and the error bars represent the standard deviation from triplicates.

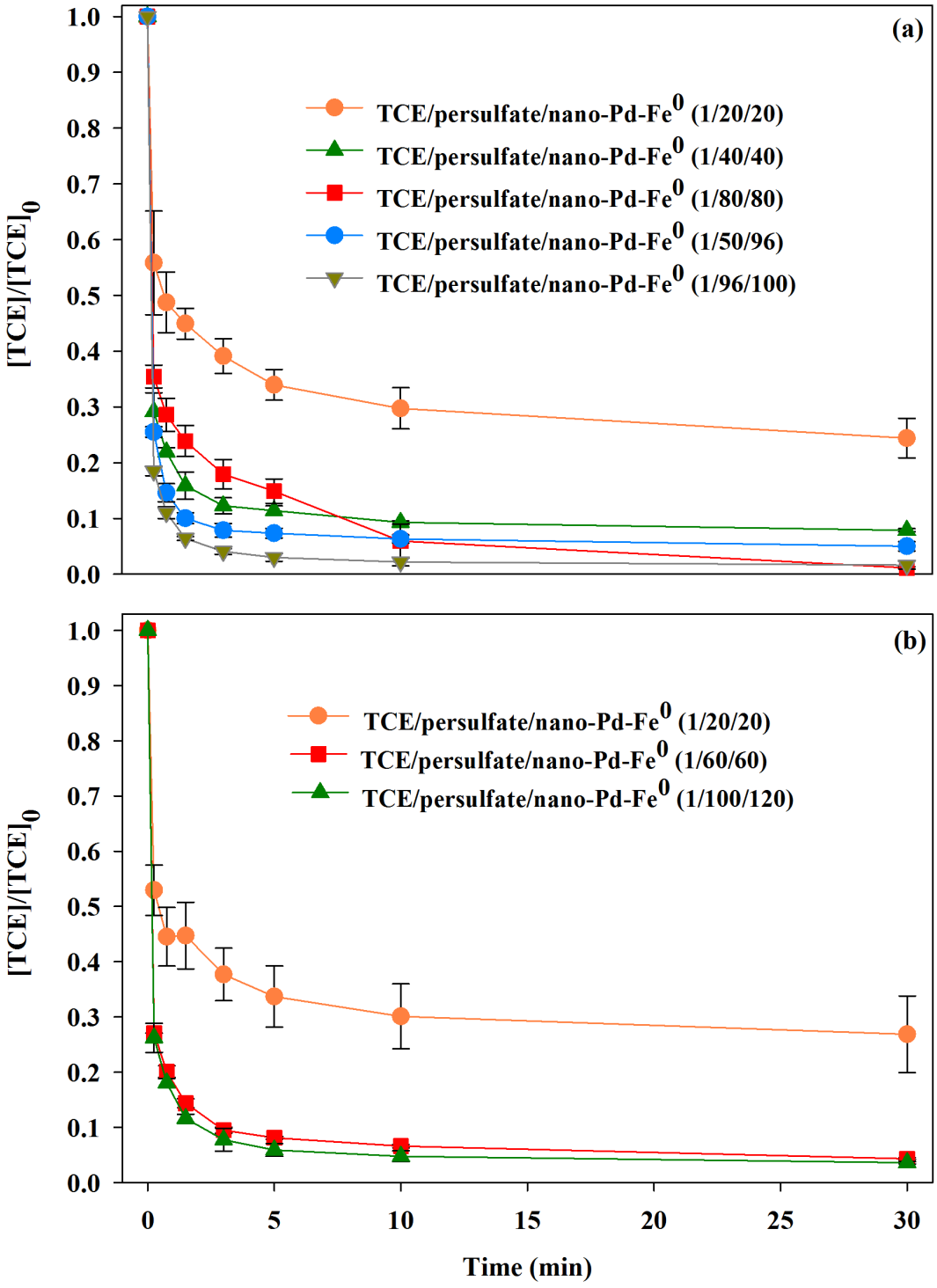

Figure 3.2.10TCE treatment for different molar ratios of (a) nano-Pd-Fe^0 activated persulfate and (b) nano-Zn-Fe^0 activated persulfate. The error bars represent the standard deviation from triplicates.

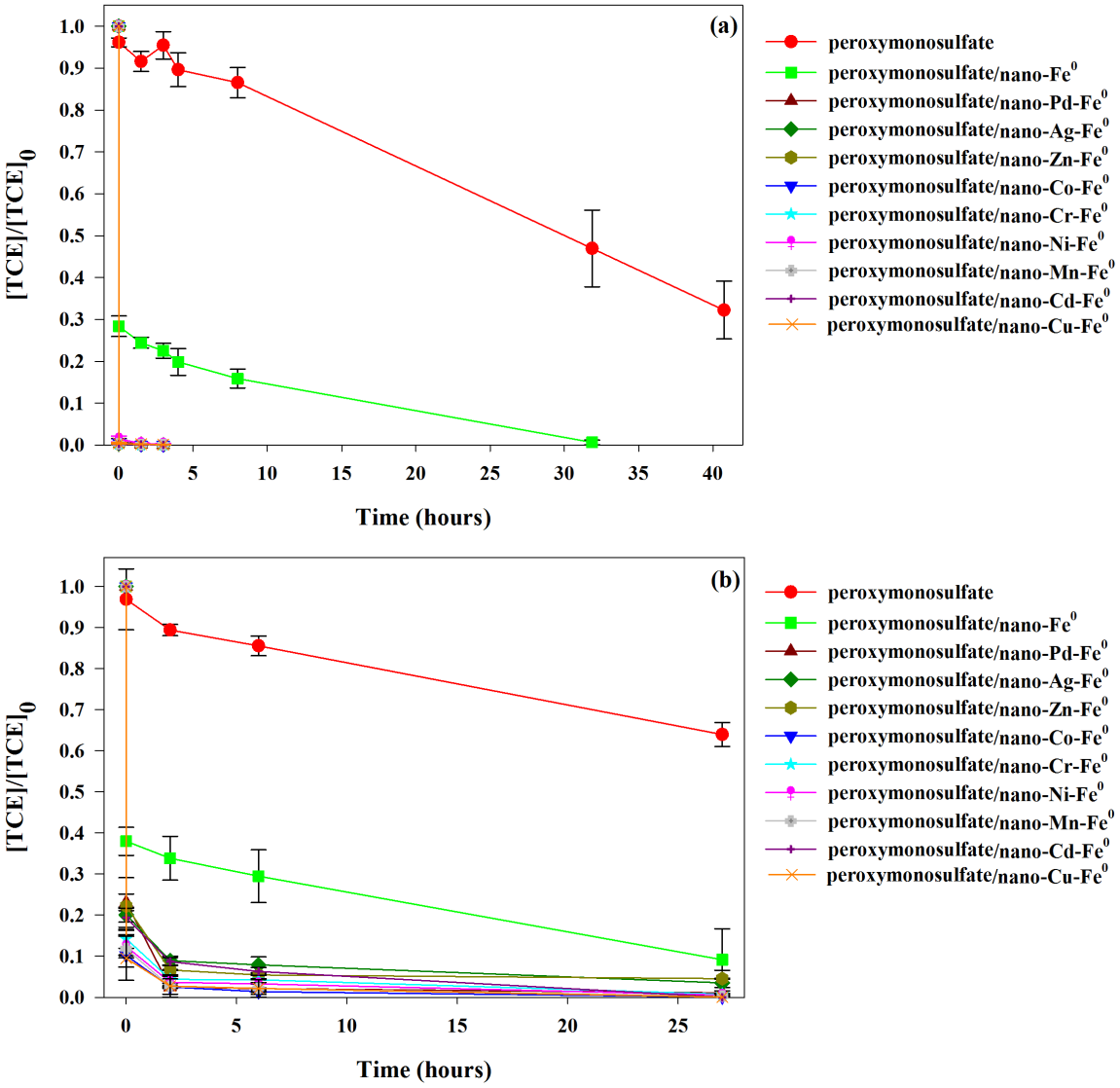

Figure 3.3.11TCE oxidation by various BZVN activated peroxymonosulfate systems at molar ratios of (a) 1/20/20 and (b) 1/10/10 between TCE/peroxymonosulfate/nano-activator. The error bars represent the standard deviation from triplicates.

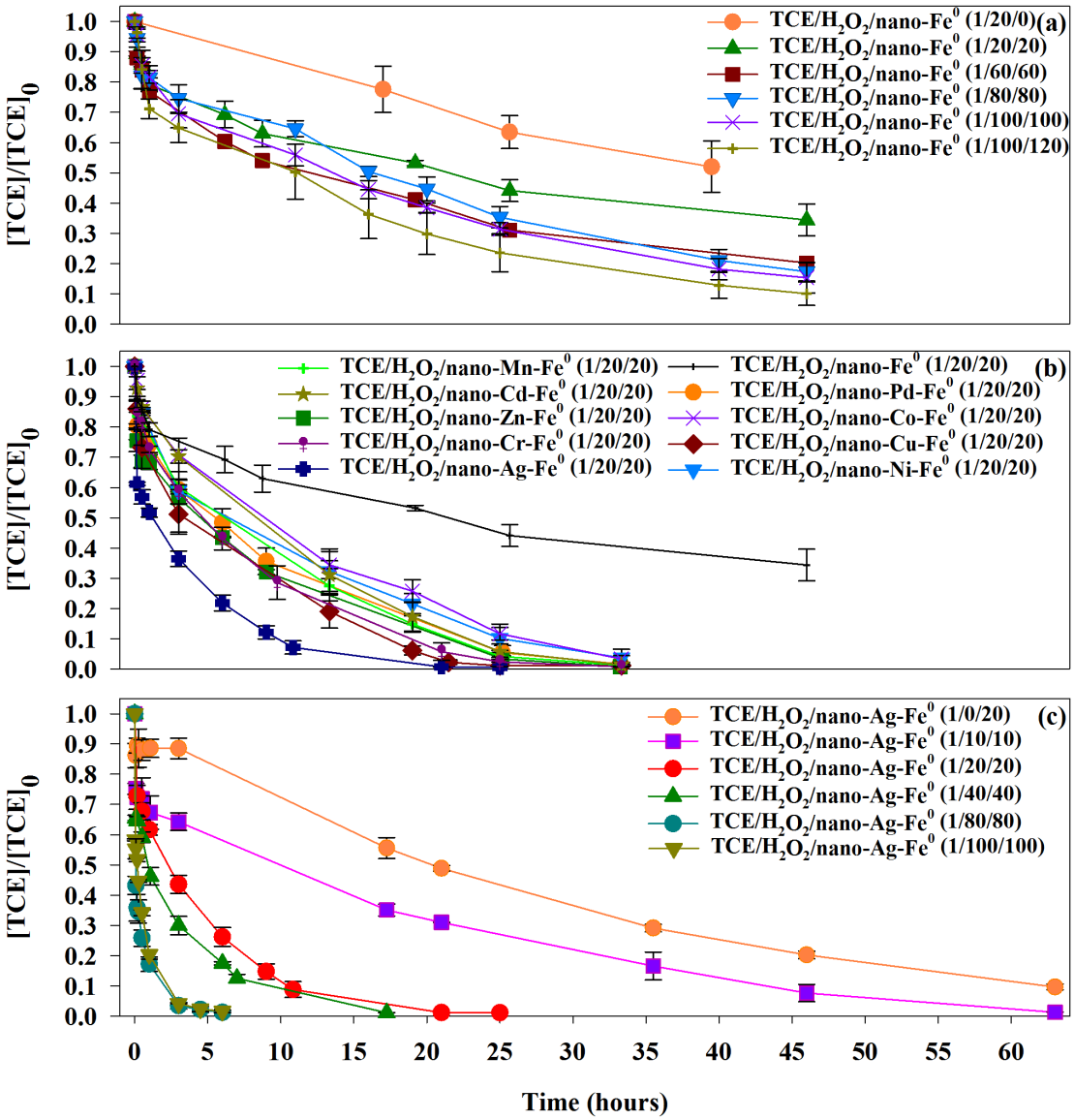
[TCE]/[TCE]0
TCE/H2O2/nano-Fe0 (1/20/0)
TCE/H2O2/nano-Fe0 (1/20/20)
TCE/H2O2/nano-Fe0 (1/60/60)
TCE/H2O2/nano-Fe0 (1/80/80)
TCE/H2O2/nano-Fe0 (1/100/100)
TCE/H2O2/nano-Fe0 (1/100/120)
(a)
TCE/H2O2/nano-Mn-Fe0 (1/20/20)
TCE/H2O2/nano-Cd-Fe0 (1/20/20)
TCE/H2O2/nano-Zn-Fe0 (1/20/20)
TCE/H2O2/nano-Cr-Fe0 (1/20/20)
TCE/H2O2/nano-Ag-Fe0 (1/20/20)
TCE/H2O2/nano-Fe0 (1/20/20)
TCE/H2O2/nano-Pd-Fe0 (1/20/20)
TCE/H2O2/nano-Co-Fe0 (1/20/20)
TCE/H2O2/nano-Cu-Fe0 (1/20/20)
TCE/H2O2/nano-Ni-Fe0 (1/20/20)
(b)
TCE/H2O2/nano-Ag-Fe0 (1/0/20)
TCE/H2O2/nano-Ag-Fe0 (1/10/10)
TCE/H2O2/nano-Ag-Fe0 (1/20/20)
TCE/H2O2/nano-Ag-Fe0 (1/40/40)
TCE/H2O2/nano-Ag-Fe0 (1/80/80)
TCE/H2O2/nano-Ag-Fe0 (1/100/100)
(c)
Time (hours)

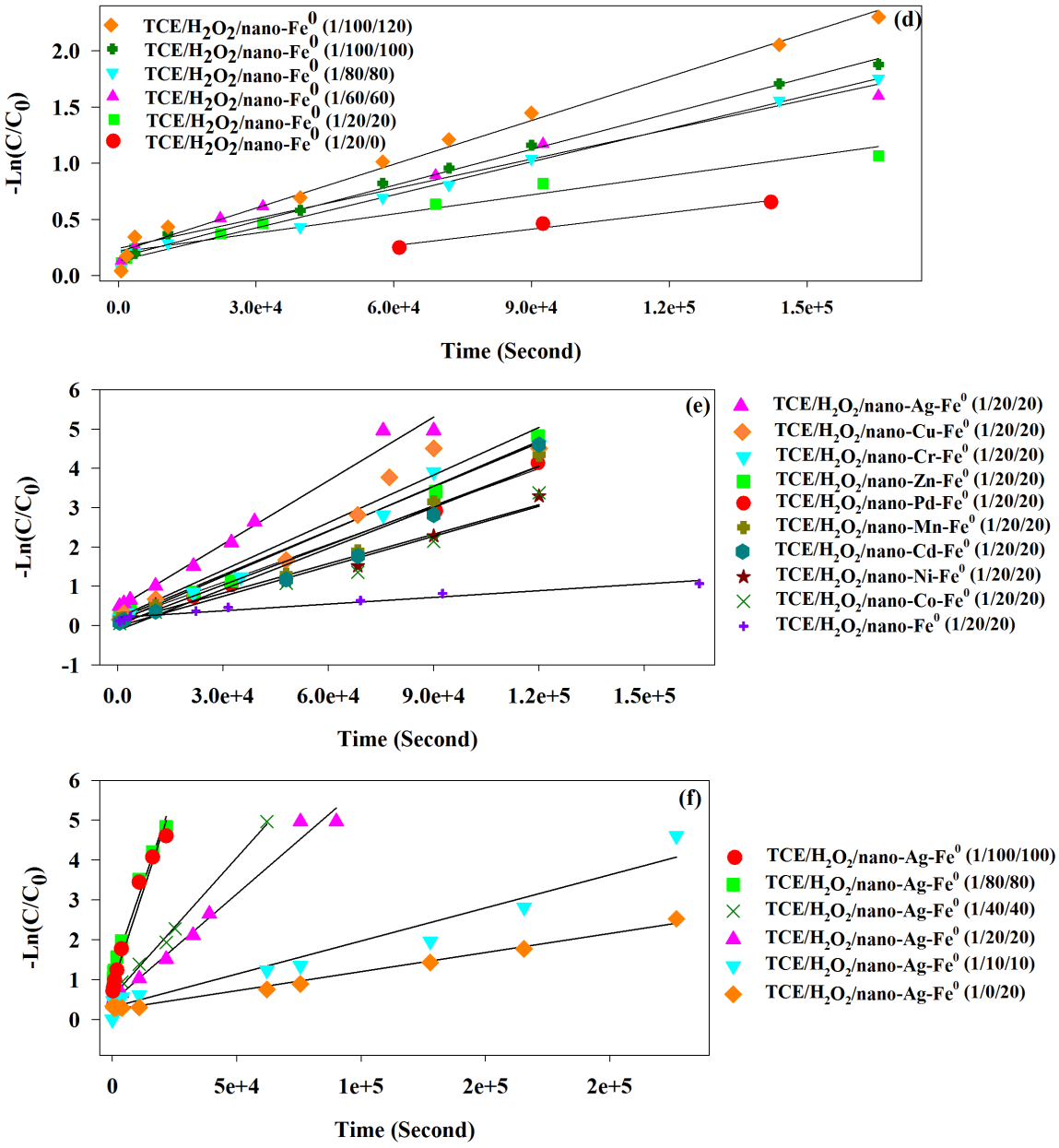

Figure 3.4.12TCE treatment for (a) various TCE/H_2O_2/nano-Fe^0 molar ratios, (b) various BZVN activated H_2O_2 systems, (c) various TCE/H_2O_2/nano-Ag-Fe^0 molar ratios, and a pseudo first-order model of the various systems (d), (e), and (f). The error bars represent the standard deviation from triplicates.

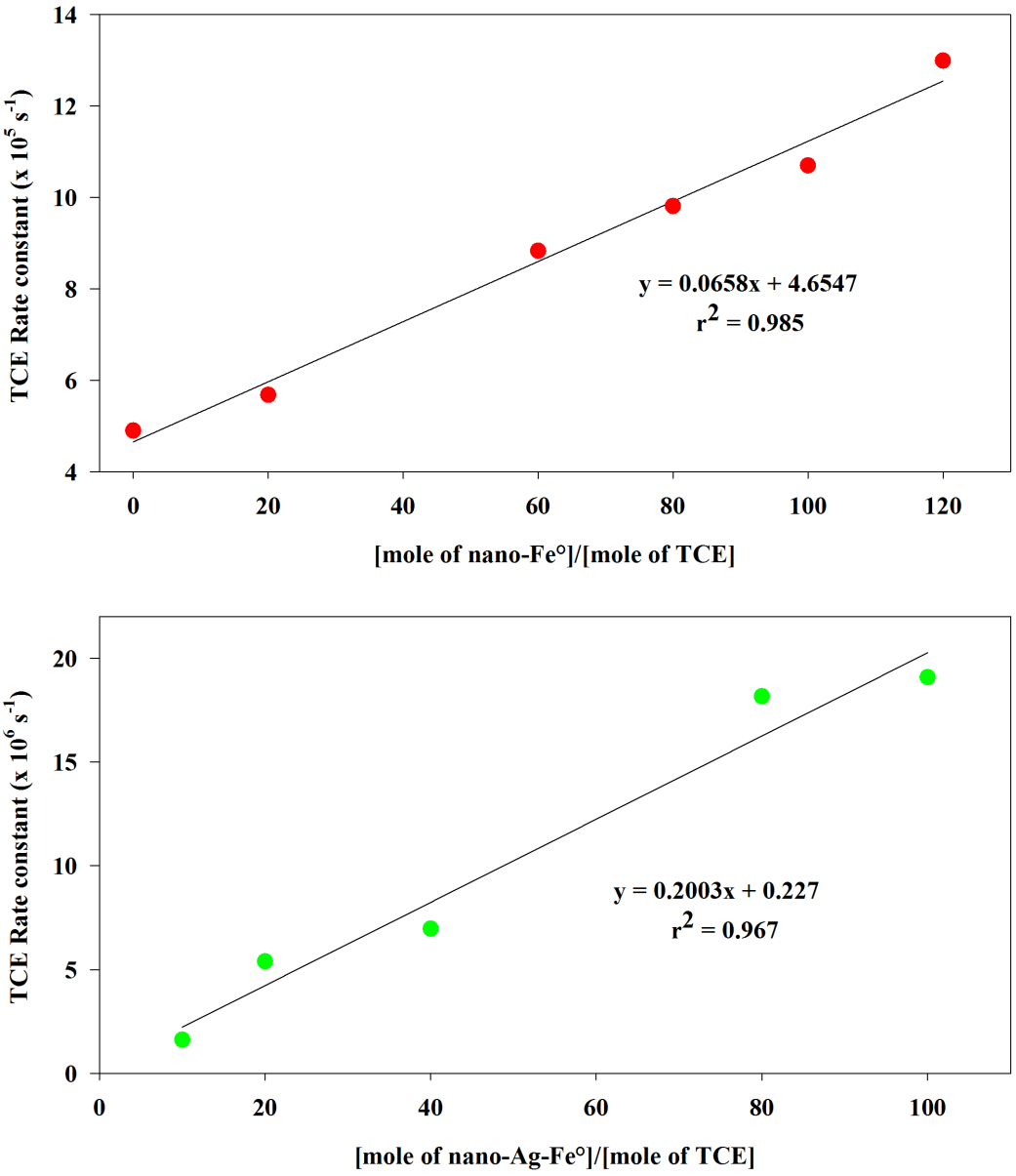

Figure 3.5.13The linear relationship between TCE rate constants and the dosage of (a) nano-Fe^0, and (b) nano-Ag-Fe^0 in the activated H_2O_2 systems.

Table 3.1. The reaction mechanisms of generating free radicals from peroxygens.

No.	Equation	References
(3.1)	$Fe^0 + H_2O_2 \rightarrow Fe^{2+} + 2OH^-$	[18-19]
(3.2)	$Fe^0 + S_2O_8^{2-} \rightarrow Fe^{2+} + 2SO_4^{2-}$	[20-21]
(3.3)	$Fe^0 + \frac{1}{2}O_2 + H_2O \rightarrow Fe^{2+} + 2OH^-$	[22]
(3.4)	$Fe^0 + 2H_2O \rightarrow Fe^{2+} + 2OH^- + H_2$	[20, 22]
(3.5)	$Fe^{2+} + H_2O_2 \rightarrow Fe^{3+} + OH^{\bullet} + OH^-$	[23-24]
(3.6)	$Fe^{2+} + S_2O_8^{2-} \rightarrow Fe^{3+} + SO_4^{2-} + SO_4^{-\bullet}$	[20]
(3.7)	$Fe^{2+} + HSO_5^- \rightarrow Fe^{3+} + HO^- + SO_4^{-\bullet}$	[2]
(3.8)	$Fe^{3+} + HSO_5^- \rightarrow Fe^{2+} + SO_5^{-\bullet} + H^+$	[2, 25]

Table 3.2. Summary of pseudo first-order rate constants for TCE oxidation in the various activated H_2O_2 systems.

No.	Degradation Systems	k (x 10^{-5} s^{-1})	r^2
1	TCE/H_2O_2/nano-Fe^0 (1/20/0)	0.49	0.97
2	TCE/H_2O_2/nano-Fe^0 (1/20/20)	0.57	0.96
3	TCE/H_2O_2/nano-Fe^0 (1/60/60)	0.88	0.97
4	TCE/H_2O_2/nano-Fe^0 (1/80/80)	0.98	0.99
5	TCE/H_2O_2/nano-Fe^0 (1/100/100)	1.07	0.99
6	TCE/H_2O_2/nano-Fe^0 (1/100/120)	1.30	0.98
7	TCE/H_2O_2/nano-Ni-Fe^0 (1/20/20)	2.54	0.97
8	TCE/H_2O_2/nano-Co-Fe^0 (1/20/20)	2.55	0.97
9	TCE/H_2O_2/nano-Pd-Fe^0 (1/20/20)	3.22	1.00
10	TCE/H_2O_2/nano-Mn-Fe^0 (1/20/20)	3.36	0.97
11	TCE/H_2O_2/nano-Cd-Fe^0 (1/20/20)	3.48	0.95
12	TCE/H_2O_2/nano-Zn-Fe^0 (1/20/20)	3.74	0.99
13	TCE/H_2O_2/nano-Cr-Fe^0 (1/20/20)	3.83	0.99
14	TCE/H_2O_2/nano-Cu-Fe^0 (1/20/20)	4.04	0.95
15	TCE/H_2O_2/nano-Ag-Fe^0 (1/20/20)	5.40	0.99
16	TCE/H_2O_2/nano-Ag-Fe^0 (1/0/20)	0.96	0.99
17	TCE/H_2O_2/nano-Ag-Fe^0 (1/10/10)	1.62	0.95
18	TCE/H_2O_2/nano-Ag-Fe^0 (1/20/20)	5.39	0.99
19	TCE/H_2O_2/nano-Ag-Fe^0 (1/40/40)	6.97	1.00
20	TCE/H_2O_2/nano-Ag-Fe^0 (1/80/80)	18.2	0.98
21	TCE/H_2O_2/nano-Ag-Fe^0 (1/100/100)	19.1	0.97

List of Supplementary Data Figures:

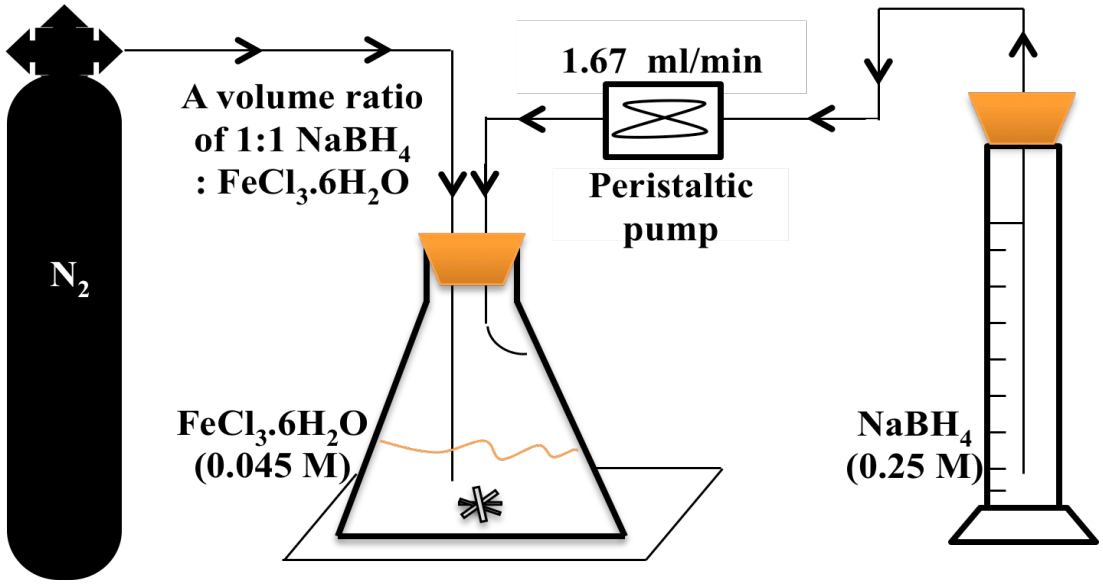

Figure S1.14 Synthesis of zero valent iron nanoparticles.

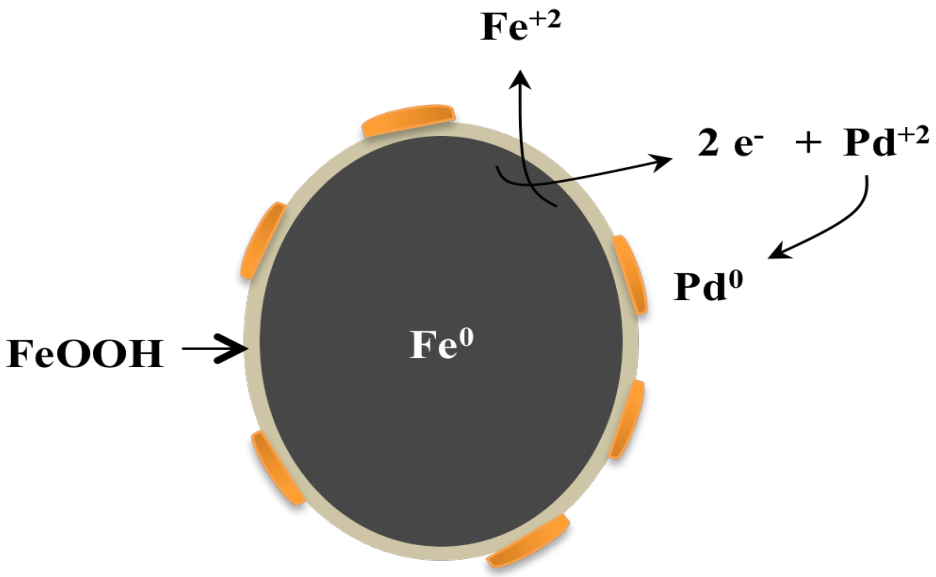

Figure S2.15Schematic of the deposition of palladium (and other metal additives) on the surface of zero valent iron nanoparticles.

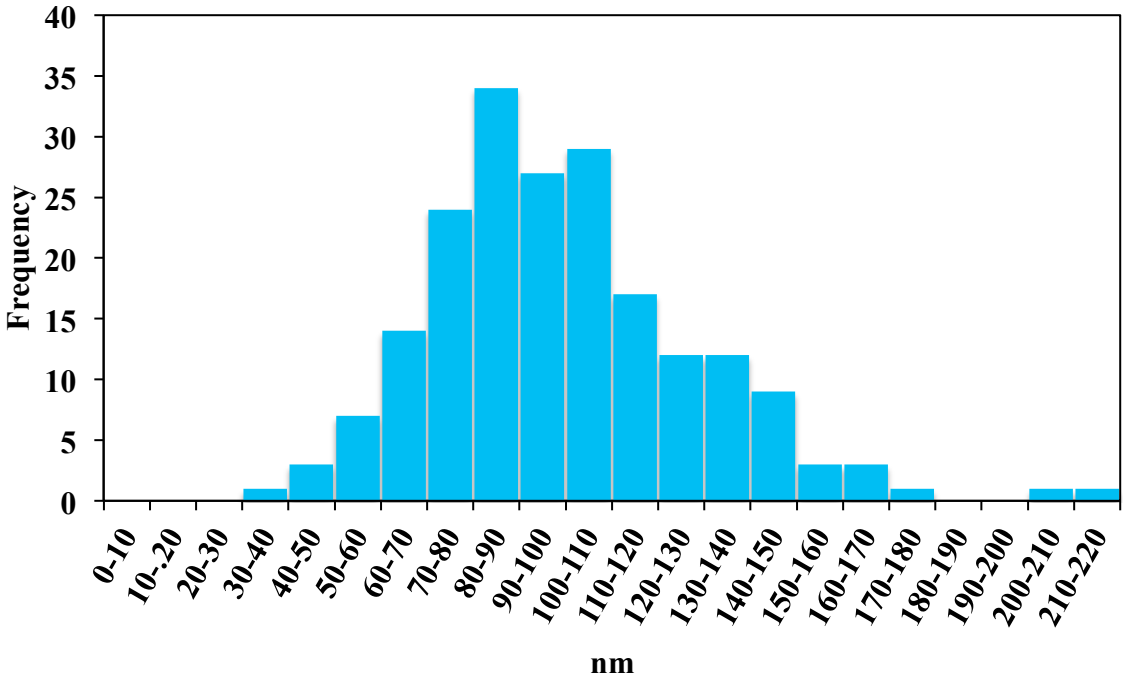

Figure S3.16Size distribution of 198 nanoparticles measured by Image J software from several HR-SEM images.

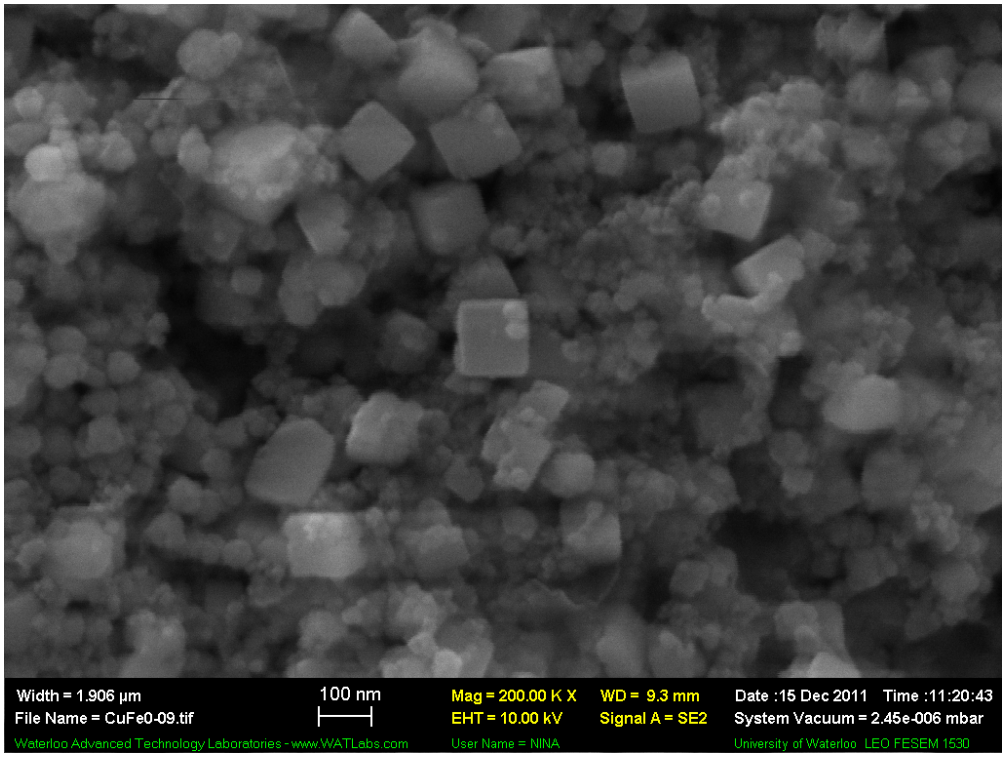

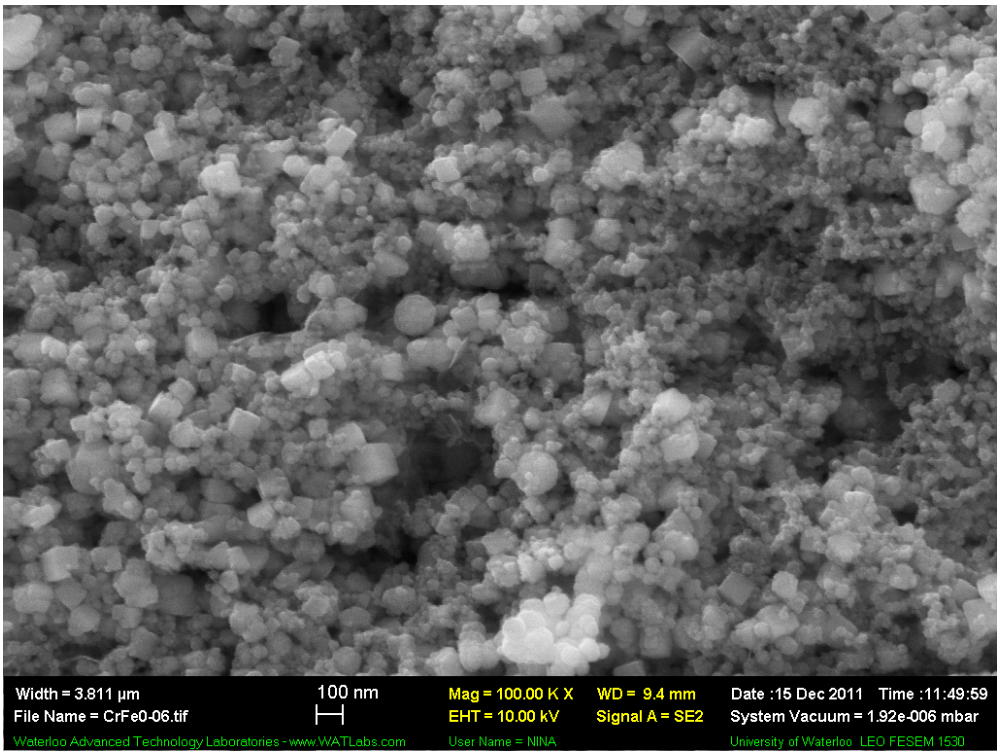

Figure S4.17Selected HR-SEM images for the synthesized bimetallic zero valent nanoparticles.

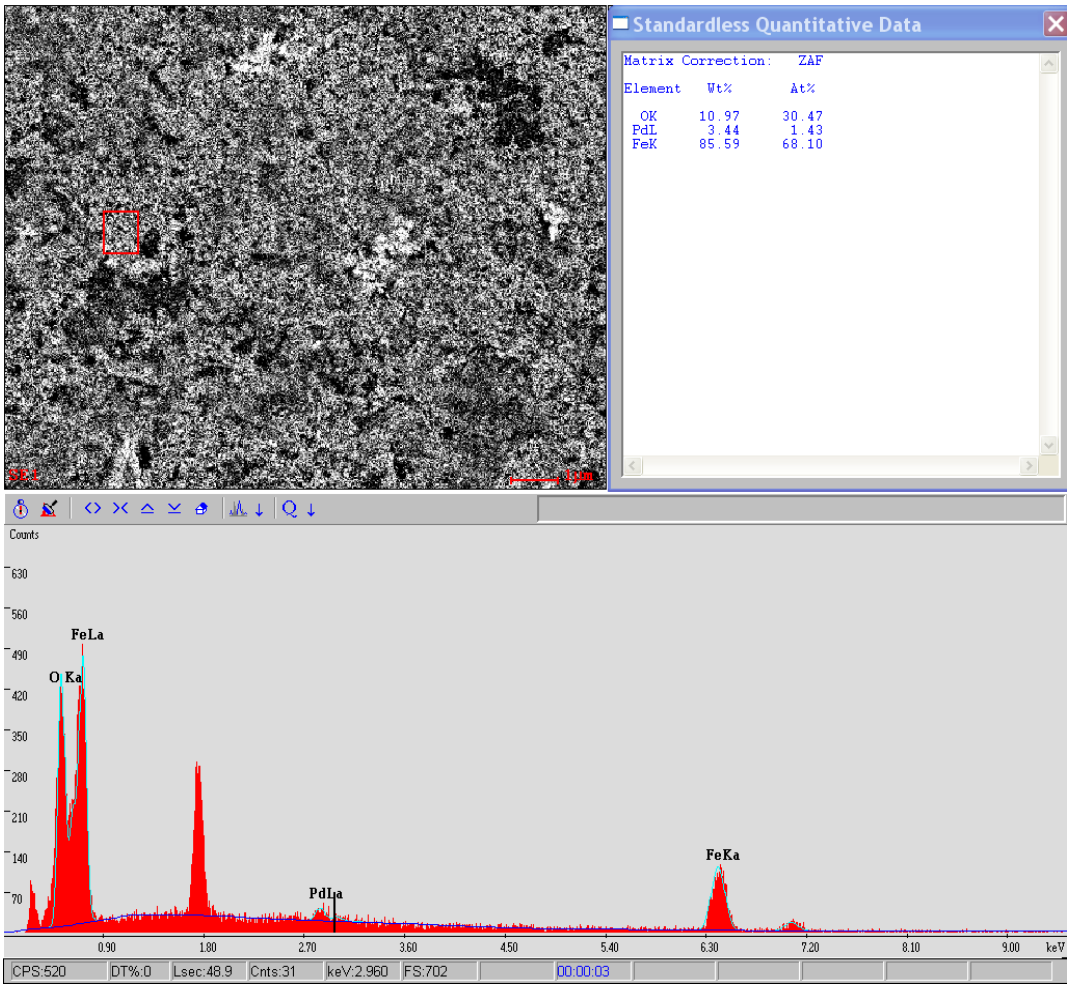

Figure S5.18Elemental analysis of nano-Pd-Fe^0 particles by EDX.

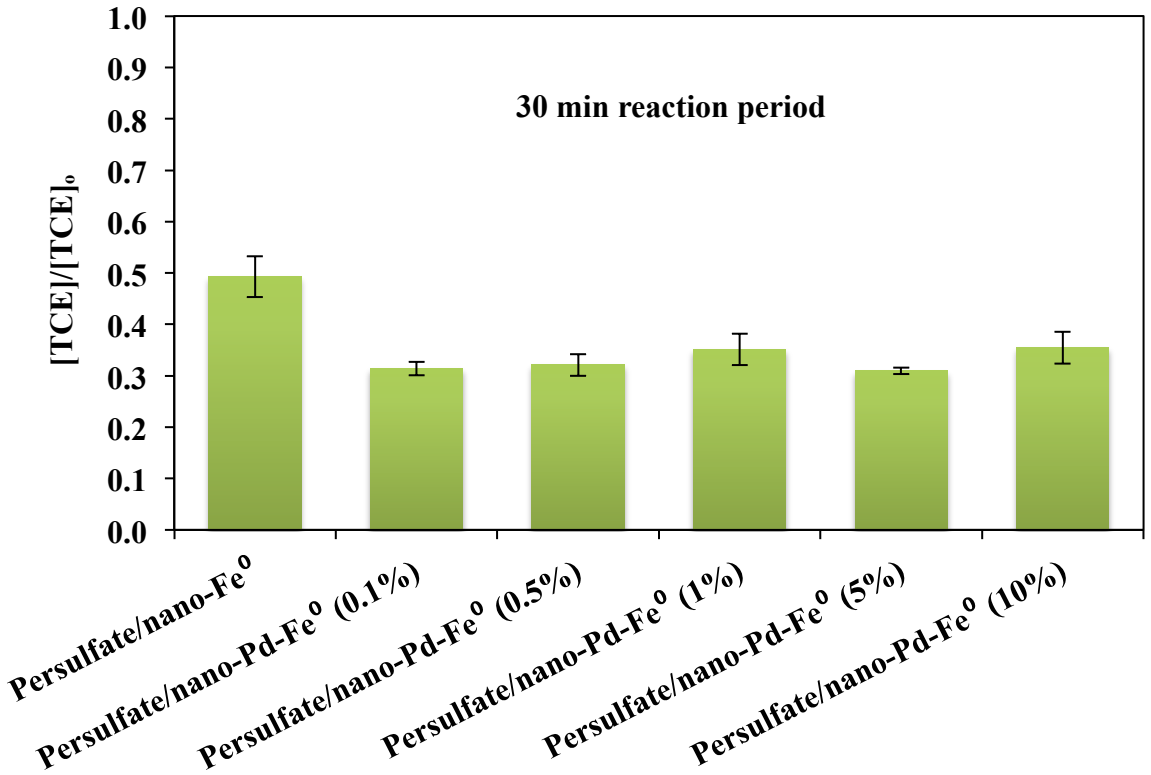

Figure S6.19TCE degradation by nano-Pd-Fe^0 activated persulfate system with a range of palladium loads (wt/wt). The load was added during the synthesizing process of nano-Pd-Fe^0. The error bars represent the standard deviation from triplicates.

Chapter 4

Chapter 4.

Competition by Aquifer Materials in a Bimetallic Nanoparticles/persulfate System for The Treatment of Trichloroethylene

Outline

It has been suggested in the literature that the aquifer materials can compete with the target organic compounds in an activated peroxygen system. In this study, we employed a rapid treatment method using persulfate activated with bimetallic nanoparticles to investigate the competition between aquifer materials and the dissolved phase of the target organic compound. The concentration of dissolved trichloroethylene (TCE) remaining after using the activated persulfate system was two- to three-fold higher in a soil slurry batch system than in an aqueous batch system. For all five aquifer materials investigated, an increase in the mass of the aquifer solids significantly decreased the TCE degradation. A linear relationship was observed between the mass of aquifer materials and the initial TCE degradation rate, suggesting that the organic carbon and/or aquifer material constituents (e.g., carbonates and bicarbonates) compete with TCE treatment.

4.1. Introduction

In the early 1990s, *in situ* chemical oxidation (ISCO) emerged as a promising technique to treat organic compounds in the subsurface. ISCO technology depends on the delivery of a chemical oxidant to the contaminated target zone. However, the successful delivery of a chemical oxidant to the target treatment zone does not guarantee the successful degradation of the target organic compounds.

The organic carbon (OC) content[1-2] and aquifer material constituents (e.g., carbonates and bicarbonates)[3-5], which can vary widely between aquifers due to the heterogeneity of the hydrogeological systems, have a significant effect on the successful implementation of ISCO. Not all organic carbon associated with aquifer materials is readily available, such as organic carbon located within the soil grains[6], or uneasily oxidizable organic carbon (e.g., a low molecular weight of aliphatic carbon, fatty acids, oxalate, and black carbon[7]). However, some organic carbon can be partially oxidized such as humic acids and aromatic hydrocarbons[7]. Those fractions of organic carbon available for chemical oxidation may cause significant drawbacks in the chemical treatment system by competing with the target organic compounds.

Peroxygens have been used since the 1920s as chemical oxidants to estimate the approximate bioavailable fraction of OC in soils[8-9]. However, OC cannot be completely oxidized by peroxygens[10-11]. For example, Cuypers et al.[10] and Martin and Gonzalez-vila[11] indicated that only 10 to 40 % of OC was oxidized by persulfate, whereas, Esterhues et al.[12] found a wider range of oxidation (16.4 to 99.3 %).

A debate has been going on in the peer-reviewed literature[13-15] about the preference of peroxygens (or activated peroxygens) to consume OC rather than attack the target dissolved organic compounds. Weeks et al.[13] suggested that the free radicals that are generated from the

activated peroxygens prefer to oxidize OC rather than the target organic compounds. However, Spencer et al.[14] suggested that OC content has no effect on the degradation of the target organic compounds in the activated peroxygen system.

Aquifer material constituents, such as carbonates and bicarbonates, have a negative effect on the treatment process of the target organic compounds in the activated peroxygen systems[3-5] by two possible mechanisms. First, the aquifer material constituents behave as radical scavenger ions[3, 5, 16-17].

$$HCO_3^- + OH^\bullet \rightarrow H_2O + CO_3^{-\bullet} \qquad K= 8.5 \times 10^6\ M^{-1}\ s^{-1} \qquad (4.1)$$

$$HCO_3^- + SO_4^{-\bullet} \rightarrow SO_4^{2-} + HCO_3^- \qquad K= 1.6 \times 10^6\ M^{-1}\ s^{-1} \qquad (4.2)$$

$$CO_3^{2-} + SO_4^{-\bullet} \rightarrow SO_4^{2-} + CO_3^{-\bullet} \qquad K= 6.1 \times 10^6\ M^{-1}\ s^{-1} \qquad (4.3)$$

Second, the aquifer material constituents can be adsorbed on the surface of the catalysts or activators causing inactivation of catalytic sites[3]. However, Bennedsen et al.[17] and Liang et al.[16] found that, at neutral pH, there is insignificant effect of CO_3^{2-} and HCO_3^- for the iron activated persulfate system.

Therefore, there is a need to better understand the competing role of the aquifer materials with the target organic compounds for the activated peroxygen systems. In this study, soil slurry batch experiments were designed to investigate the potential treatability of the dissolved phase of an organic model compound (i.e., trichloroethylene (TCE)) in the presence of five different selected aquifer materials that contain a wide range of OC content from various sites in North America.

4.2. Materials & Methods

4.2.1. Materials and Chemicals

The following materials were used: ferric chloride hexahydrate (> 99%) from Fluka, Germany; zinc sulfate heptahydrate (> 99.5%) from EM science, Germany; trichloroethylene (99.8%) from BDH, England; and sodium persulfate (≥ 98%), palladium (II) chloride (≥ 99.9%), and sodium borohydride (98%) from Sigma-Aldrich, USA.

Iron-based bimetallic zero valent nanoparticles were synthesized by a borohydride reduction method as previously reported by Al-Shamsi and Thomson [Chapter 3], in which a 1 % wt/wt of palladium or zinc was deposited on the surface of the bare zero valent iron nanoparticles. The average size of the synthesized nanoparticles was 99±30 nm, as measured by high-resolution scanning electron microscopy (HR-SEM). The main structure of the nanoparticles was cubic crystalline as found by HR-SEM. Ferric oxyhydroxide (FeOOH) was present on the surface of the fresh nanoparticles as characterized by X-ray photoelectron spectroscopy (XPS).

Aquifer materials were collected from five different aquifers across North America. The selected physical and chemical properties are presented in Table 4.1 (see Xu[18] for details).

4.2.2. Experimental Procedure & Analytical Methods

Aquifer materials were prepared by drying at 105 °C for a minimum of 24 hours. Only solids that passed through a 2-mm stainless steel sieve were used. Borosilicate glass vials (40-mL) fitted with polytetrafluoroethylene septa were loaded with five different masses of solids (1, 2.5, 5, 10, and 20 g) of each of the aquifer materials. The reactors were added as a sequence that began with the persulfate solution, the dissolved-TCE solution, and the metal nanoparticles. The reactors were manually shaken for 2-3 seconds after adding each component, as shown in the

conceptual model (Figure 4.1). Finally, reactors were filled to a zero head-space with Milli-Q water (resistivity of 18.2 $M\Omega.cm^{-1}$) and were placed in a dark room at 21±3 °C. A 1/20/20 molar ratio of TCE/persulfate/nano-metal activators was used in all the treatment reactors.

Persulfate and the metal nanoparticles were added quickly to minimize TCE loss to the aquifer materials due to sorption. A TCE isotherm study in the presence of 20 g of Borden sand showed that the sorption of TCE on Borden sand over 53 hours resulted in a 12 % loss of TCE concentration (data not shown). The experiment performed in this effort was ~30 hours in duration and loss of TCE to sorption was assumed to be minimal. A minimum of 1-2 days is required for the TCE to reach equilibrium with aquifer materials[19-20].

At the desired reaction time, a 0.7 mL sample was collected through the septa of a reactor and was transferred to a 2-mL vial for gas chromatography (GC) analysis. TCE was analyzed using a head-space solid phase micro-extraction (HS-SPME) method[21] with a GC (HP 6890 series) equipped with a flame ionization detector (FID). The GC was connected to an auto sampler (Varian 8200).

4.3. Results & Discussion

Increasing the mass of the aquifer solids decreased the TCE decomposition by the nano-Pd-Fe^0 activated persulfate system, as shown in Figure 4.2. For example, over a 20-second reaction period, 70 % of the TCE was degraded in the 1 g LC34-USU soil slurry system using nano-Pd-Fe^0 activated persulfate compared with 40 % of the TCE degradation in the 20 g LC34-USU soil slurry system.

The nano-Zn-Fe^0 particles in the presence of LC34-LSU had a similar activation effect compared with nano-Pd-Fe^0 particles on persulfate (Figure 4.3). The same was also observed with the other four aquifer materials (data not shown), indicating that nano-Zn-Fe^0 particles can

be used as an alternative to nano-Pd-Fe^0 particles. The very low price of zinc salts used to synthesize nano-Zn-Fe^0 particles compared with the price of palladium salts makes nano-Zn-Fe^0 particles cost-effective materials [The price ratio of $PdCl_2$ to $ZnCl_2$ is ~ 7].

Treating TCE in an aqueous batch system by nano-Pd-Fe^0 activated persulfate is faster than using a soil slurry batch system (Figure 4.4). For example, over a 10-min reaction period, 85 % of the TCE was degraded in the aqueous system using the nano-Pd-Fe^0 activated persulfate compared with 60 % of the TCE degradation in the soil slurry system. These results are in agreement with Weeks et al.[13], who indicated that TCE decomposition by activated hydrogen peroxide in soil slurry systems was slower than in aqueous systems. Likewise, Liang et al.[22] found that TCE was oxidized in a soil slurry batch system by heat activated persulfate (at 40 °C) in the period of 12.9 hrs compared to 1.4 hrs in an aqueous batch system. Weeks et al.[13] and Liang et al.[22] concluded that the generated free radicals (e.g., $OH^{\bullet}$ and $SO_4^{-\bullet}$) react with the aquifer constituents (e.g., OC). It was also been suggested that, in the activated peroxygen system, the generated free radicals are inhibited by OC[23-26] or by aquifer material constituents (e.g., bicarbonates) [3, 5, 16-17].

We calculated the initial TCE reaction rate based on a reaction period of 20 seconds (Table 4.2). A linear relationship was observed between the mass of aquifer materials and the initial TCE reaction rate by nano-Pd-Fe^0 activated persulfate (Figure 4.5). Adding the same mass of different aquifer materials as expected produced a different TCE degradation behavior since the properties of the aquifer materials used are not the same. Although we have clear evidence of a relationship between aquifer materials and the TCE degradation for the activated persulfate systems explored, we do not have data relating to changes in OC. Attempts to fit a multiple-regression model to the TCE decomposition rate and aquifer constituents were unsuccessful.

However, a linear relationship was observed between the OC content and the initial TCE reaction rate (Figure 4.6), suggesting that OC may compete with the target organic compounds in the activated persulfate system used in this study.

It is unknown whether the generated free radicals degraded the OC content (as expected) or were scavenged by OC as suggested by Lindsey and Tarr[23-24], and Kwan and Voelker[25]. No efforts were made in this study to investigate this issue. It is also likely that the activated peroxygen system can oxidize some of the OC content, as suggested by Mikutta et al.[7].

To scale up the information gathered from this laboratory system (i.e., soil slurry) to *in situ* conditions, it should be noted that the solution-to-solid ratio in the field is less than that in the soil slurry system. For instance, the solution-to-solid ratio in a soil slurry system (1 to 20 g of Borden sand) was, approximately, 0.71-0.98 compared to ~0.33 in the field. Figure 4.7 shows the effect of mass ratio between oxidant and aquifer solid on the initial TCE decomposition rate. Decreasing the mass ratio between the oxidants and the aquifer solids decreases the initial TCE decomposition rate. The mass ratio (oxidant/solid) in the field is approximately 0.001 compared to 0.0038 for 20 g soil slurry batch reactors (i.e., Borden sand), indicating that the mass ratio is decreased by 3.8 times in scaling up from 20 g soil slurry batch reactor to the field. Therefore, soil slurry systems are not accurately representative to the field, and the solution-to-solid ratio is the main concern.

4.4. Conclusion

The dissolved TCE concentration remaining after using the activated persulfate system was two- to three-fold higher in the soil slurry batch system than that in the aqueous batch system. For five different aquifer materials explored, an increase in the mass of the aquifer solids significantly decreased the TCE degradation by the nano-Pd-Fe^0 activated persulfate system. A

linear relationship was observed between the mass of aquifer solids and the initial TCE decomposition rate, suggesting that the OC and/or the aquifer material constituents (e.g., carbonates and bicarbonates) compete with TCE treatment in the activated persulfate system. We also observed that adding the same mass of different aquifer materials produced a different TCE degradation behavior since the properties of the aquifer materials (e.g., OC) used are not the same. Although there is no direct evidence to support a relationship between OC with the TCE treatment in the activated persulfate system, we found a linear regression between OC and the initial TCE decomposition rate, indicating that OC may compete with the dissolved phase of the target organic compounds in the activated peroxygen system.

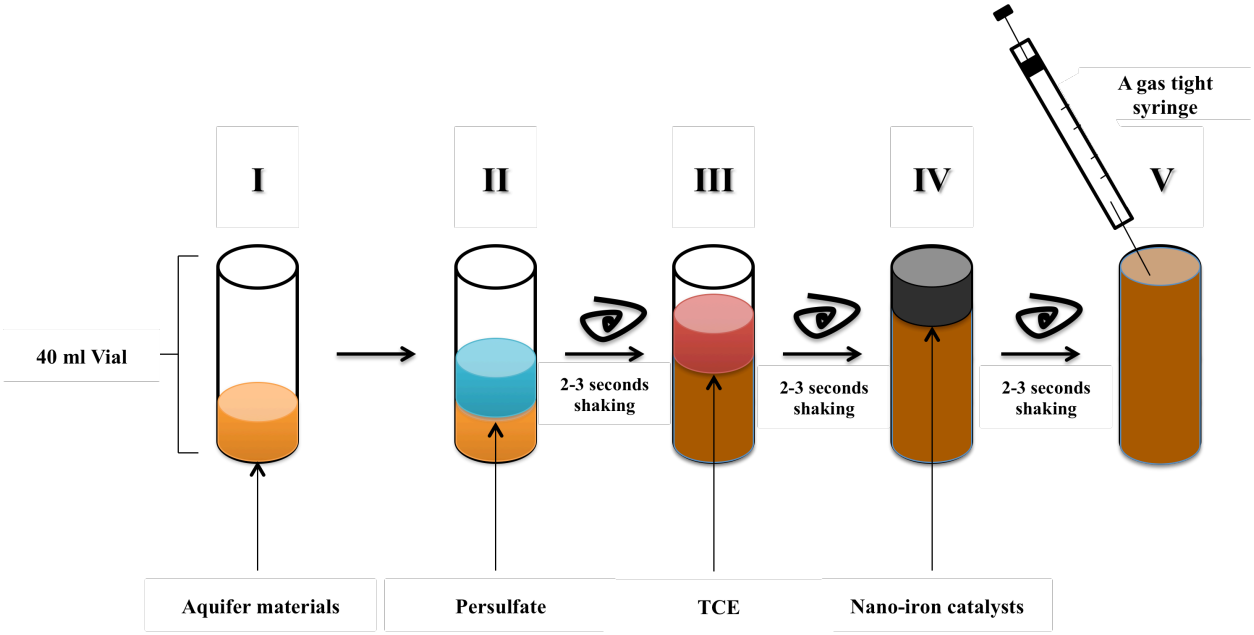

Figure 4.1.20A conceptual model of filling and sampling the soil slurry batch reactors.

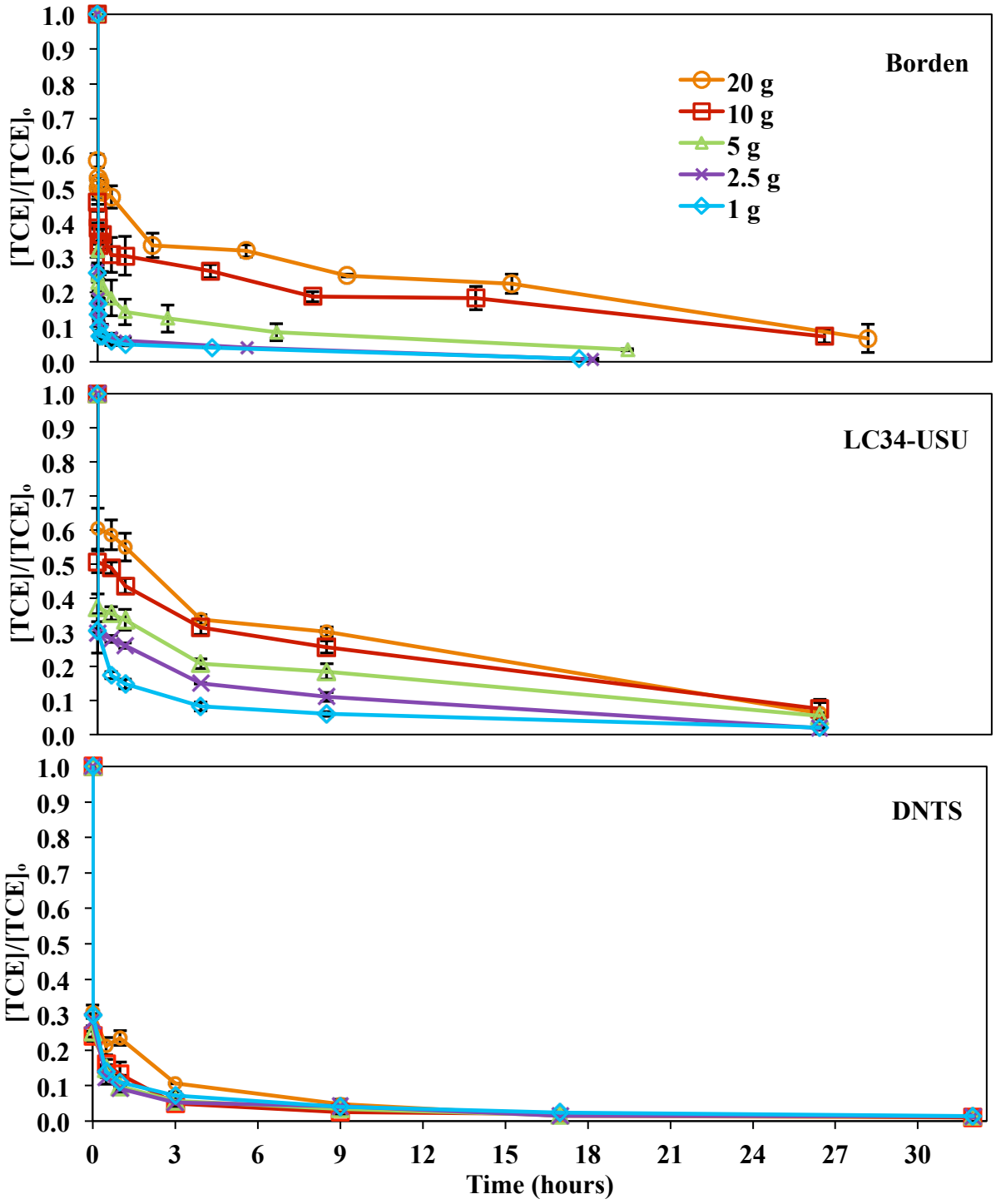

Figure 4.2.21TCE treatment in the presence of various aquifer materials using nano-Pd-Fe^0 activated persulfate (the error bars represent the standard deviation of the triplicates).

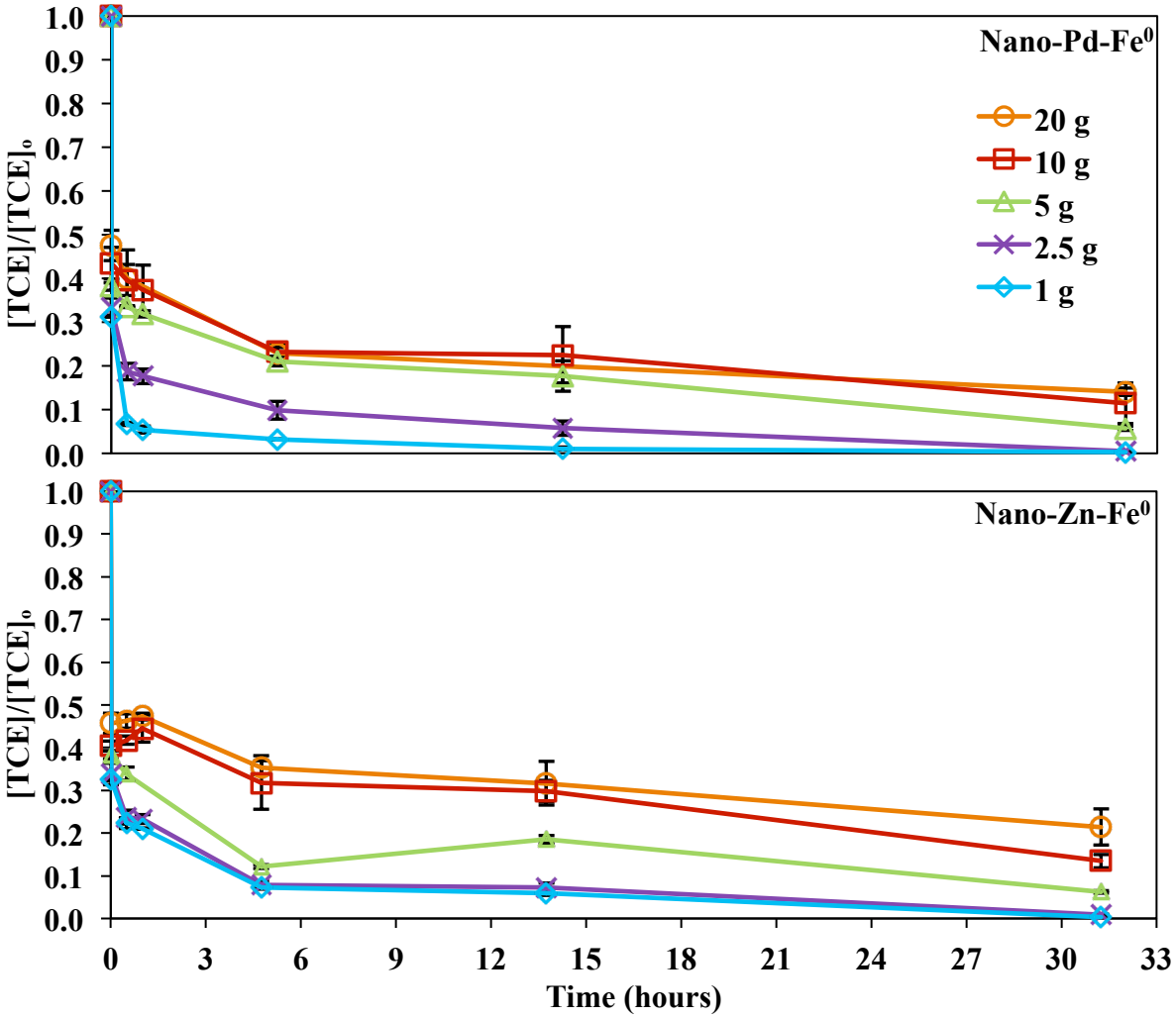

Figure 4.3.22TCE treatment in the presence of LC34-LSU by nano-Pd-Fe^0 and nano-Zn-Fe^0 (the error bars represent the standard deviation of triplicates).

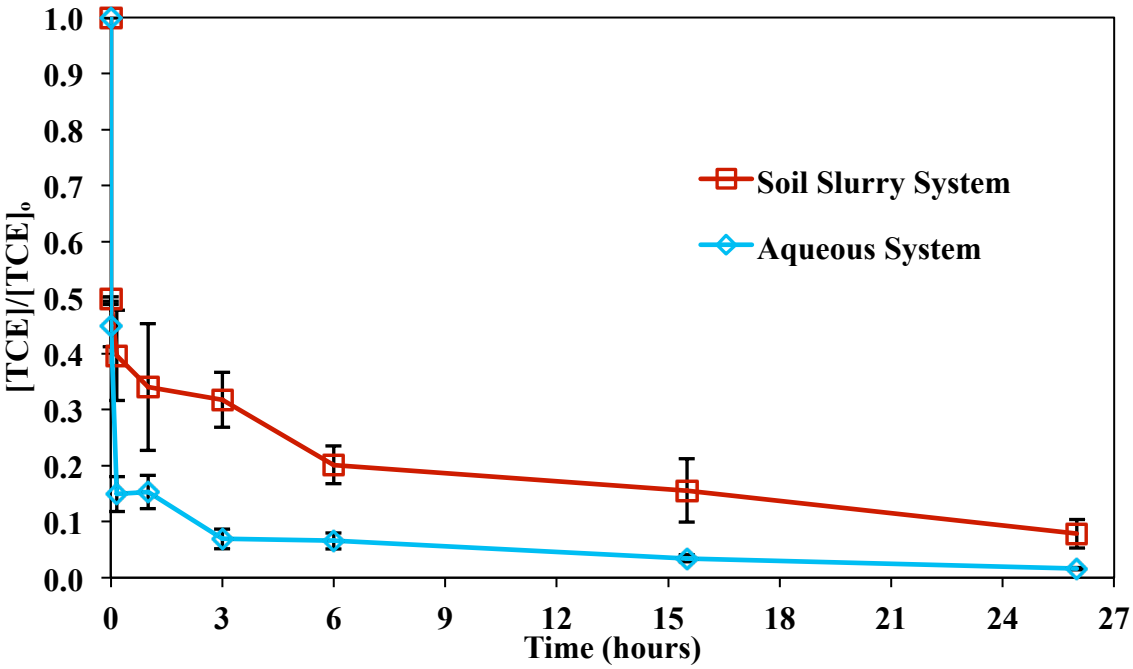

Figure 4.4.23TCE degradation using nano-Pd-Fe^0 activated persulfate in a soil slurry batch system and an aqueous batch system. Twenty grams of Borden sand was added to the soil slurry batch system (the error bars represent the standard deviation of triplicates).

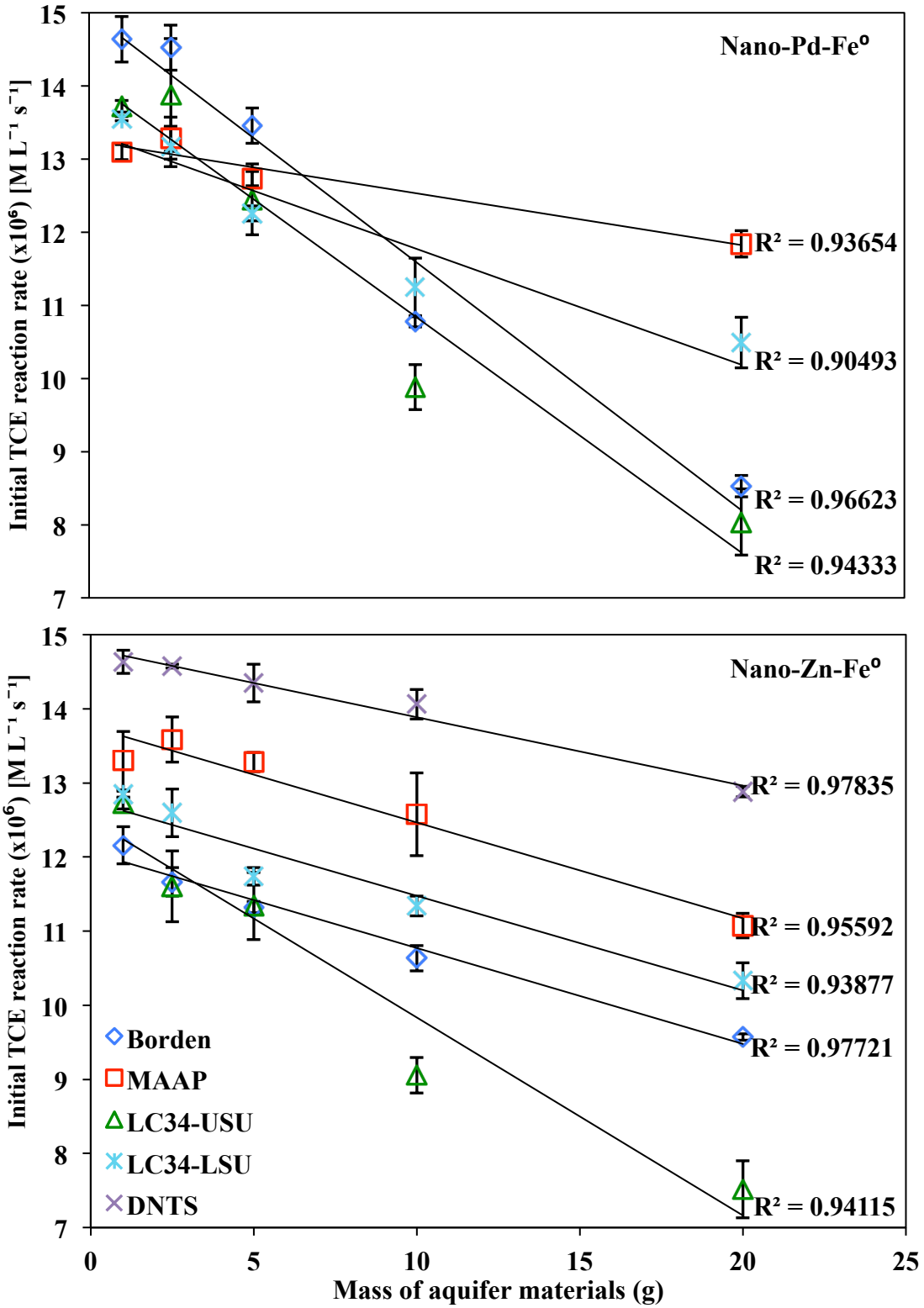

Figure 4.5.24 Initial TCE reaction rates plotted against the mass of various aquifer materials for the nano-Pd-Fe^0 activated persulfate system (the error bars represent the standard deviation of triplicate reactors).

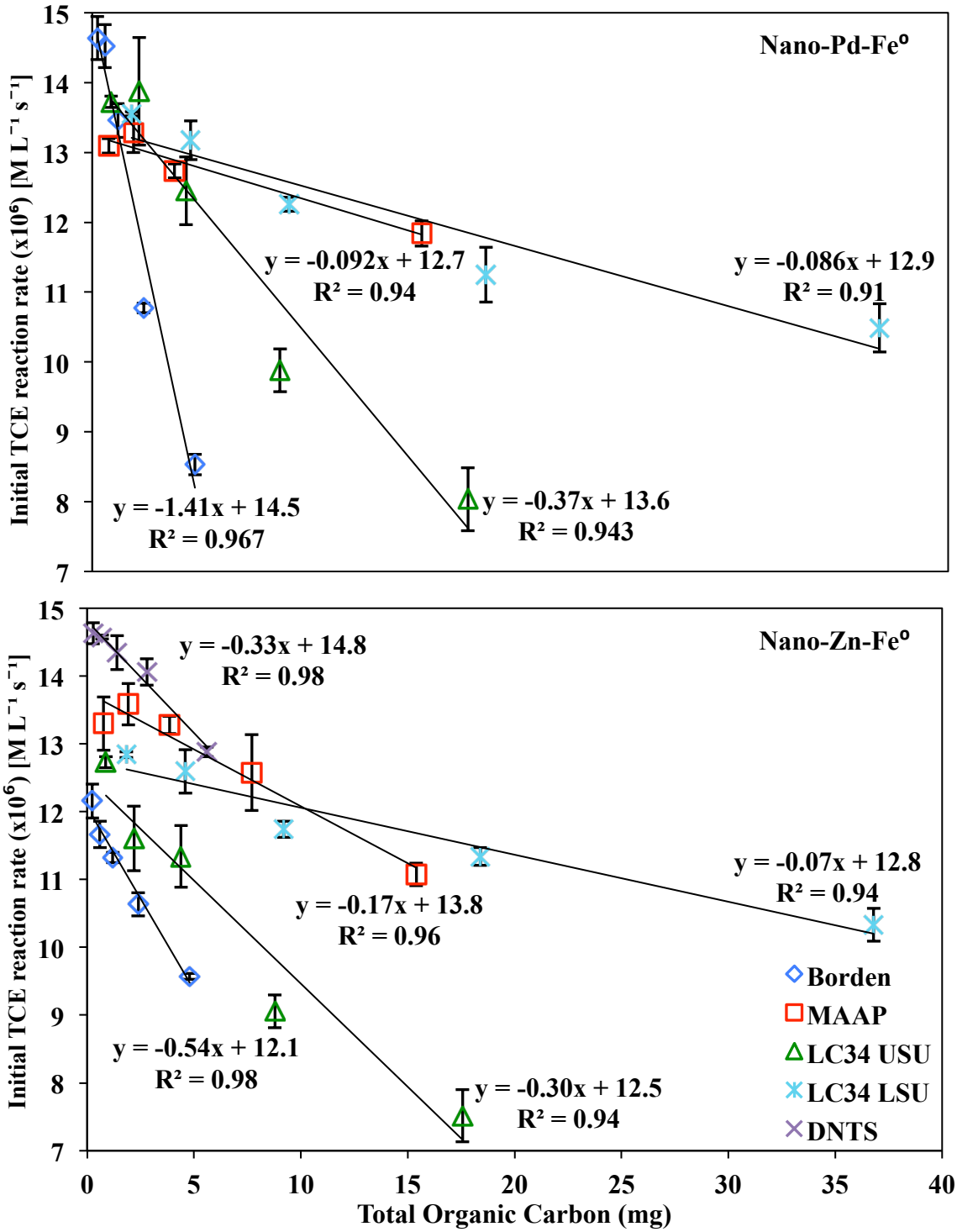

Figure 4.6.25The initial TCE reaction rates plotted against the mass of OC of various aquifer materials for (a) nano-Pd-Fe^0 activated persulfate and (b) nano-Zn-Fe^0 activated persulfate (the error bars represent the standard deviation of triplicate reactors).

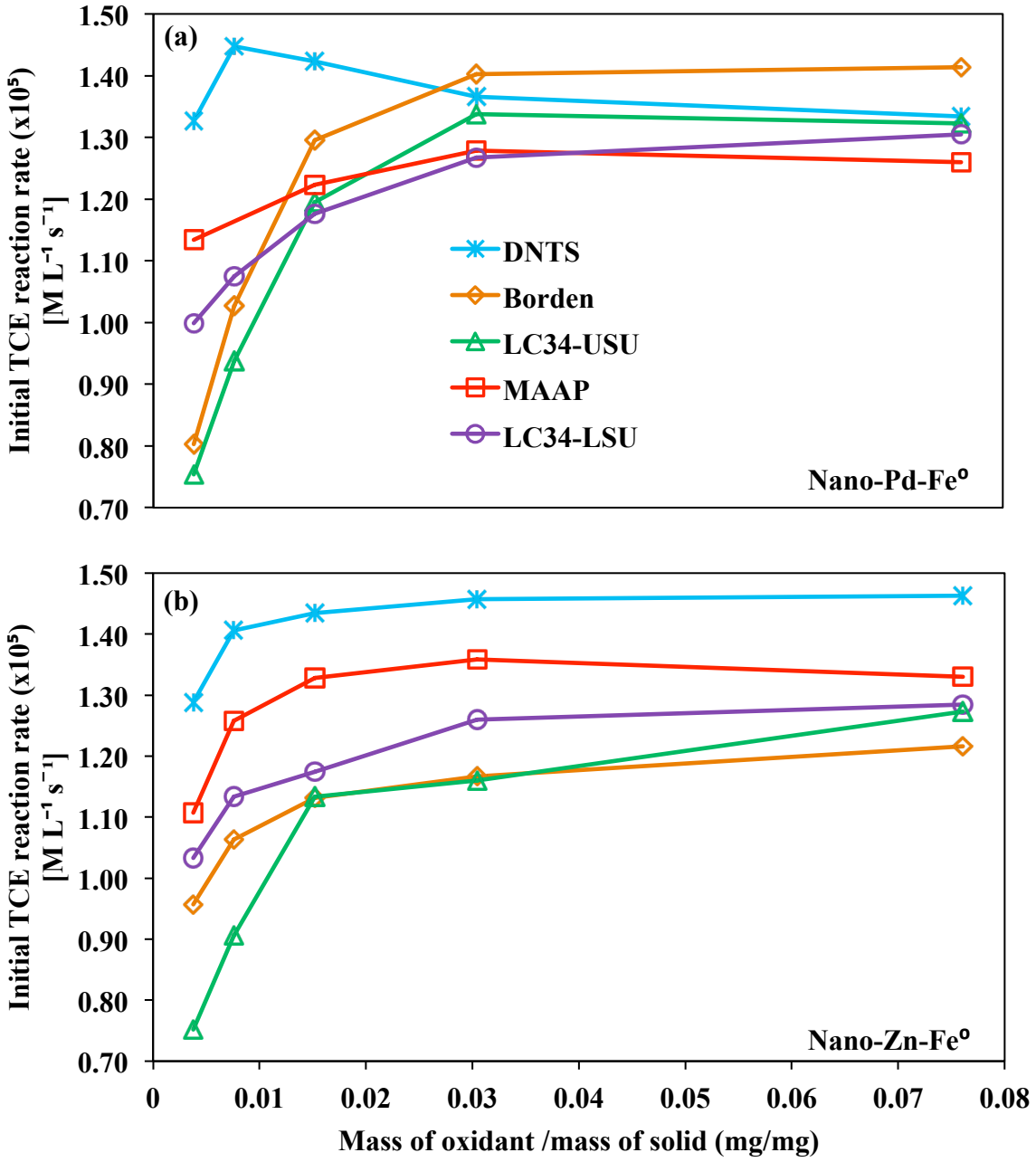

Figure 4.7.26The initial TCE reaction rates plotted against the mass ratio (oxidant/solid) of various aquifer materials for the nano-Pd-Fe^0 (or nano-Zn-Fe^0) activated persulfate system.

Table 4.1. Aquifer material properties.

	Borden	MAAP	LC34-USU	LC34-LSU	DNTS
Site	CFB Borden, ON Canada	Milan Army Ammunition Plant, TN	Launch Complex 34, Cape Canaveral AFS, FL	Launch Complex 34, Cape Canaveral AFS, FL	National Test Site, Dover AFB, DE
Description	Fine/medium sand	Sand	Sand and silty sand	Sand and silty sand	Fine/medium silty sand
pH	8.4	7	8.6	8.8	6.1
CEC[1] (Cmol/kg)	3.5	0.9	8.3	12.8	2.6
% Total Carbon	1.58	0.01	3.15	4.15	0.14
% Total Organic Carbon	0.024	0.077	0.0878	0.184	0.028
Total Fe (mg/kg)	17,500	867	3,700	6,100	63,800
Amorphous Fe (mg/kg)	300	40	410	500	360
Total Mn (mg/kg)	421	25	98	68	154
Amorphous Mn (mg/kg)	4	8	2	2	2

[1] Cation exchange capacity.

Table 4.2. The initial TCE reaction rate for the nano-metal activated persulfate systems in the presence of various aquifer materials (M L^{-1} s^{-1}).

Type of activator	g of aquifer materials	Borden	MAAP	LC34-USU	LC34-LSU	DNTS
Nano-Pd-Fe^0	1	$1.41x10^{-5}$	$1.26x10^{-5}$	1.32E-05	$1.31x10^{-5}$	$1.33x10^{-5}$
Nano-Pd-Fe^0	2.5	$1.40x10^{-5}$	$1.28x10^{-5}$	1.34E-05	$1.27x10^{-5}$	$1.37x10^{-5}$
Nano-Pd-Fe^0	5	$1.30x10^{-5}$	$1.22x10^{-5}$	1.19E-05	$1.18x10^{-5}$	$1.42x10^{-5}$
Nano-Pd-Fe^0	10	$1.03x10^{-5}$	--	$9.38x10^{-6}$	$1.07x10^{-5}$	$1.45x10^{-5}$
Nano-Pd-Fe^0	20	$8.03x10^{-6}$	$1.13x10^{-5}$	$7.53x10^{-6}$	$9.99x10^{-6}$	$1.33x10^{-5}$
Nano-Zn-Fe^0	1	$1.22x10^{-5}$	$1.33x10^{-5}$	$1.27x10^{-5}$	$1.28x10^{-5}$	$1.46x10^{-5}$
Nano-Zn-Fe^0	2.5	$1.17x10^{-5}$	$1.36x10^{-5}$	$1.16x10^{-5}$	$1.26x10^{-5}$	$1.46x10^{-5}$
Nano-Zn-Fe^0	5	$1.13x10^{-5}$	$1.33x10^{-5}$	$1.13x10^{-5}$	$1.17x10^{-5}$	$1.43x10^{-5}$
Nano-Zn-Fe^0	10	$1.06x10^{-5}$	$1.26x10^{-5}$	$9.06x10^{-6}$	$1.13x10^{-5}$	$1.41x10^{-5}$
Nano-Zn-Fe^0	20	$9.57x10^{-6}$	$1.11x10^{-5}$	$7.52x10^{-6}$	$1.03x10^{-5}$	$1.29x10^{-5}$

Chapter 5

Chapter 5.

Treatment of a Trichloroethylene Source Zone Using Persulfate Activated by an Emplaced Nano-Pd-Fe^0 Zone

Outline

Recently, metal nanoparticles have attracted attention as promising peroxygen activators for the rapid and effective remediation of organic contaminants. In this work, a one-dimensional physical model experiment was designed to investigate the mobility of the metal nanoparticles in porous media, and the potential subsurface application of the metal nanoparticles as peroxygen activators for the treatment of a TCE source zone. We found that nano-Pd-Fe^0 particles were mobile in a non-geological porous medium and relatively immobile in a geological porous medium. In addition, we found that iron-based bimetallic nanoparticles have a much longer suspension (>6 weeks) in aqueous systems than iron-based monometallic nanoparticles (<1 hour). To overcome the delivery issue for nano-Pd-Fe^0 particles in geological porous media, an activation zone approach was adopted. Nano-Pd-Fe^0 particles were injected as a zone to activate persulfate for the treatment of a TCE source zone. The TCE mass destruction was only 9 % higher in the nano-Pd-Fe^0 activated $S_2O_8^{2-}$ system compared to the non-activated $S_2O_8^{2-}$ system as revealed by a short duration chloride concentration spike in the effluent. In addition, the activation zone of nano-Pd-Fe^0 was rapidly deactivated after exposed to persulfate as visually observed by color change, indicating that the longevity of the activation zone is limited.

5.1. Introduction

Groundwater is a source of drinking water for more than a third of the world's population. Groundwater can be contaminated with chlorinated solvents from many sources, such as accidental spills, leaking underground storage tanks (USTs), and industrial landfill leachate. Groundwater that has been contaminated by chlorinated solvents has become a global public health threat.

One of the most common chlorinated solvents is trichloroethylene (TCE). TCE has been widely used as an extraction agent, heat transfer agent, and solvent in dry cleaning, paint removal, and textile manufacturing (Wong, 2004). In the 1960s, TCE was the most popular degreasing solvent (Armstrong and Green, 2004). At high exposure level, TCE has been linked to the development of tumors and cancers (e.g., kidney, liver, and lung) in laboratory animals (i.e., rodents) and is classified by the USEPA as a high-potential human carcinogenic (Kester and Clewell, 2004; Wernke and Schell, 2004). In addition, the Agency of Toxic Substances and Disease Registry (ATSDR) selected TCE as a primary contaminant in 1988 (Kester and Clewell, 2004).

In 1997, TCE was observed to be present at 861 of 1428 sites within the USEPA Superfund program (USEPA, 2009). The USEPA indicates that ≥ 30% of water supplies in the U.S. are contaminated with TCE (Wong, 2004). Its high volatility (vapor pressure of 56 mm Hg at 20 °C), high density (1.46 g/mL at 20 °C), and low water solubility (1070 mg/L at 20 °C) suggest that TCE is a hazardous substance in all environmental compartments (air, soil, and water) (Armstrong and Green, 2004).

The limitations of the conventional remediation technologies (e.g., soil excavation and the pump-and-treat technologies) urged regulators and practitioners to seek more effective and less

expensive technologies. As a result, novel subsurface remediation technologies have been developed and tested (Huling and Pivetz, 2006; NRC, 1999; Siegrist et al., 2011).

Permeable reactive barrier (PRB) technology is a promising *in situ* method to treat TCE and other chlorinated solvents by the construction of a porous wall of granular zero valent iron (Fe^0), which is usually installed by soil excavation (Thiruvenkatachari et al., 2008). However, the effectiveness of PRB technology is limited by the aquifer depth and the cost of the installation. In addition, PRB technology is designed to treat the dissolved plume and not the source zone (NRC, 1999).

As an alternative technique, smaller Fe^0 particles such as nanoparticles have been used to treat the source zone. Fe^0 nanoparticles stabilized by polymer coatings or metal additives might be injected directly into the source zone (Elliott and Zhang, 2001; He et al., 2010). Several authors have reported the poor mobility of Fe^0 nanoparticles and the resultant transport difficulties (delivery issues) in the subsurface, even with stabilizing agents (O'Carroll et al., 2012), while others have reported some degree of success. Successful injections of iron nanoparticles in the field have used either a very high-pressure (~5 psi / 34.5 kPa) (He et al., 2010) or very high flow rates (3,700 - 20,000 mL/min) (Bennett et al., 2010; Elliott and Zhang, 2001; Wei et al., 2010). The successful injection of iron nanoparticles in laboratory physical models (i.e., column or box models) have used very short columns (4.5 - 12.5 cm) (Kanel et al., 2007a; Lin et al., 2010; Raychoudhury et al., 2010; Saleh et al., 2007; Zhan et al., 2008), glass burets as columns (Schrick et al., 2004), glass beads as the medium (Kanel et al., 2007b; Lin et al., 2010), or industrial sands (e.g., standard Ottawa sand or silica sand) (Jiemvarangkul et al., 2011; Phenrat et al., 2009; Saleh et al., 2008; Saleh et al., 2007).

Recently, Fe^0 nanoparticles and iron-based bimetallic nanoparticles have shown promising results as activators for peroxygens in aqueous solution (Chapter 2 and 3) (Choi and Lee, 2012; Shafieiyoun, 2012; Shu et al., 2009; Xu and Wang, 2011) and soil slurry systems (Chapter 4) (Liao et al., 2007), and are perhaps better than the conventional iron activators (e.g., Fe^{2+} and granular-Fe^0) (Chapter 2 and 3).

The application of Fe^0 nanoparticles to activate peroxygens *in situ*, requires the Fe^0 nanoparticles to be delivered along with peroxygens to the target treatment zone. However, the poor mobility and transport difficulties of Fe^0 nanoparticles have motivated us to use a different approach where Fe^0 nanoparticles are injected into the subsurface to create a zone to activate peroxygens as shown in the conceptual model (Figure 5.1). In this context, the Fe^0 nanoparticles are used as an activation tool for peroxygens, and the activated peroxygens (suite of reactive species) then migrate into the source zone to degrade the target soluble compounds. In this activation zone approach, we are not concerned about the Fe^0 nanoparticles being mobile but rather require the Fe^0 nanoparticles to be injected. This approach simulates a catalytic wall reactor system, in which the reaction occurs on a film of porous catalyst coating (Schmidt, 2004). Following the injection, the Fe^0 nanoparticles are heterogeneously attached on aquifer material grains in the vicinity of the injection wells. This results in a porous film of Fe^0 coated on aquifer material grains (Figure 5.1).

In the Fe^0 activated peroxygen system, the generated free radicals (e.g., the hydroxyl free radical ($OH^{\bullet}$) and the sulfate free radical ($SO_4^{-\bullet}$)) can oxidize organic compounds much faster than direct oxidation using a non-activated peroxygen system (Chapter 2). Fe^{2+} released from Fe^0 (Eqs 5.1-3) can cleave the oxygen-oxygen bond in peroxygen (e.g., persulfate) and generate highly reactive free radicals (Eqs 5.4-6):

$$Fe^0 + S_2O_8^{2-} \rightarrow Fe^{2+} + 2SO_4^{2-} \quad (5.1)$$

(Liang and Lai, 2008; Oh et al., 2010)

$$Fe^0 + \tfrac{1}{2}O_2 + H_2O \rightarrow Fe^{2+} + 2OH^- \quad (5.2)$$

(Furukawa et al., 2002)

$$Fe^0 + 2H_2O \rightarrow Fe^{2+} + 2OH^- + H_2 \quad (5.3)$$

(Furukawa et al., 2002; Liang and Lai, 2008)

$$Fe^{+2} + S_2O_8^{-2} \rightarrow Fe^{3+} + SO_4^{2-} + SO_4^{-\bullet} \qquad K = 2 \times 10^1\ M^{-1}\ s^{-1} \quad (5.4)$$

(Liang and Lai, 2008)

$$SO_4^{-\bullet} + H_2O \rightarrow SO_4^{2-} + H^+ + OH^\bullet \quad (5.5)$$

(Liang et al., 2009; Norman et al., 1970)

$$SO_4^{-\bullet} + OH^- \rightarrow SO_4^{2-} + OH^\bullet \quad (5.6)$$

(Liang et al., 2007; Norman et al., 1970)

Electrophilic free radicals (e.g., $OH^\bullet$) attack the electron-rich double bond in TCE molecules to form a series of unstable intermediates, followed by the formation of CO_2 and HCl as final products (Li et al., 2007; Pignatello et al., 1999; Qiang et al., 2008).

In this study, a one-dimensional physical model was designed to investigate (1) the potential mobility of bimetallic nanoparticles in geological and non-geological porous media, and (2) the potential treatability of a TCE source zone by persulfate supported with an activation zone of bimetallic nanoparticles.

5.2. Materials & Methods

5.2.1. Materials and Chemicals

The following chemicals were used: ferric chloride hexahydrate (> 99%) from Fluka, Germany; trichloroethylene (99.8%) from BDH, England; sodium persulfate (≥ 98%), palladium (II) chloride (≥ 99.9%), sodium borohydride (98%), sodium bicarbonate (99.5%), Sudan IV (≥ 80%), mercuric thiocyanate solution, and ferric ion solution (Hach kits) from Sigma-Aldrich, USA; and potassium iodide (> 99%) and hydrochloric acid (34-37%) from EMD Chemicals Inc., Germany. All chemicals were reagent grade and used as received.

Nano-Pd-Fe^0 particles were synthesized using a reduction method with sodium borohydride ($NaBH_4$) as previously reported by Al-Shamsi and Thomson [Chapter 3] in which 1 % wt/wt palladium was deposited onto the nano-Fe^0 surfaces. The average size of the synthesized nanoparticles was 99±30 nm as measured by high-resolution scanning electron microscopy (HR-SEM) (Leo 1530, Zeiss, Germany). The morphology of the synthesized nanoparticles was cubic crystalline. Ferric oxyhydroxide (FeOOH) was observed on the surface of the fresh nanoparticles using by X-ray photoelectron spectroscopy (XPS) (Thermo-VG Scientific ESCALab 250, USA).

Uncontaminated core samples of aquifer materials were collected from the Canadian Force Base (CFB) Borden located near Alliston, ON. The aquifer materials were prepared by drying at 85 °C for at least 24 hours. Only materials that passed through a 2-mm stainless steel sieve were used. This aquifer material is a fine to medium sand, with a pH of 8.4, total organic carbon content of 240 mg/kg, and a total iron content of 17,500 mg/kg (Xu, 2006). Glass beads (soda-lime silica glass, 2 mm, Potters Industries Inc., USA) were used in this study as the non-geological porous medium.

5.2.2. Experimental Design and Procedure

Prior to testing the mobility of the bimetallic nanoparticles in porous media, a dispersion test was conducted to evaluate the suspension of nanoparticles in an aqueous system. It is believed that the functionality and performance (e.g., mobility) of nanoparticles are influenced by the dispersion ability of particles. In the dispersion tests, the freshly produced nanoparticles (nano-Fe^0, nano-Pd-Fe^0, nano-Co-Fe^0, nano-Mn-Fe^0, nano-Cd-Fe^0, nano-Ni-Fe^0, nano-Cr-Fe^0, nano-Zn-Fe^0, nano-Cu-Fe^0, and nano-Ag-Fe^0) were dispersed into deoxygenated ultra-pure water (Milli-Q water (resistivity of 18.2 MΩ cm^{-1}) that was prepared by sparging nitrogen gas into the solution for a minimum of two hours) and shaken (vortexer, VWR Science) for 60 seconds. Then the slurry solution of nanoparticles was left undisturbed at a room temperature. Observations were taken daily to check the dispersion ability of nanoparticles.

To investigate the mobility of bimetallic nanoparticles in non-geological porous medium, a plexiglas column (40 cm length x 3.8 cm inner diameter) was packed with glass beads (soda-lime silica glass, 2 mm, Potters Industries Inc., USA). A peristaltic pump (Servodyne controller, Cole-Parmer) was used to flush the nanoparticle solution into the column at a flow rate of 9.6 mL/min (velocity of ~37 m/day). To investigate the mobility of bimetallic nanoparticles in a geological porous medium, the plexiglas column (40 x 3.8 cm) was packed with CFB Borden sand. Each end of the column contained a stainless steel mesh and glass beads to retain the aquifer material in the column and distribute flow. The nanoparticle solution was flushed into the column using a peristaltic pump. The experiments were conducted at different conditions as presented in Table 5.1, and samples were collected from the outlet.

A laboratory experiment was designed to investigate the activation zone approach using a one-dimensional column packed with sand (Figure 5.2). This design is consistent with the

conceptual model (Figure 5.1) to create an activation zone of nano-Pd-Fe^0 particles to activate peroxygen for the treatment of a source zone.

A plexiglas column (40 x 3.8 cm) was used. Each end of the column contained a stainless steel mesh, a layer of glass wool, and glass beads (~1-2 cm thick) to retain the aquifer material in the column and distribute flow. The source zone consisted of 20 g of aquifer material mixed with 0.0752 mL of TCE (99.8% pure) dyed red (Sudan IV) which was allowed to sit for 48 hours in the dark at room temperature, to yield 2% saturation. This source zone mixture was placed into the column ~13 cm from the inlet. A peristaltic pump (Servodyne controller, Cole-Parmer) was used to flush various solutions through the column.

Milli-Q water (18.2 MΩ cm^{-1}) was flushed through the column to establish baseline conditions. Next, nano-Pd-Fe^0 particles (45-70.1 mg) were injected manually using a syringe (1 mL, 1001 Hamilton syringe series, Sigma-Aldrich, USA) into a port located 10 cm from the inlet to create the activation zone (Figure 5.2). Finally, a persulfate solution was flushed through the column. Aqueous samples were collected from the outlet of the column, and analyzed immediately to determine the total iron, persulfate, chloride, aqueous pH, dissolved oxygen (DO), and electrical conductivity (EC). The chloride released by the cleavage of the Cl-C bond in the TCE molecules was used as an indicator of TCE treatment (Liang et al., 2008b; Ravikumar and Gurol, 1994; Schroth et al., 2001).

Two trials were conducted (I and II) using a different: persulfate concentration, mass of nano-iron, flow rate, and treatment duration (Table 5.2). In Trial I, sufficient persulfate mass (598 mg) was injected based on the following stoichiometry:

$$3Na_2S_2O_8 + C_2HCl_3 + 4H_2O \rightarrow 2CO_2 + 9H^+ + 3Cl^- + 6Na^+ + 6SO_4^{2-} \qquad (5.7)$$

and 70.1 mg of nano-Pd-Fe^0 particles (the mass needed to activate persulfate based on the stoichiometry given in Eqs. 5.1 and 5.4) was injected into the activation zone. In Trial II, the mass of persulfate injected was ~70 times in excess of the stoichiometric amount needed to treat TCE. A lower injection flow rate was used (0.10 mL/min [velocity of 0.4 m/day] instead of 0.26 mL/min [velocity of 1 m/day]).

Controls were performed at the same time with the same experimental conditions but without the activation zone of bimetallic nanoparticles. At the end of the experiments, the columns were taken apart to be inspected.

5.2.3. Analytical Methods

Aqueous samples (0.7 mL) were collected from the outlet of the column and transferred into 2-mL vials for gas chromatography (GC) analysis. TCE was analyzed by a head-space solid phase micro-extraction (HS-SPME) method (ASTM-D6889-03, 2003) using an HP 6890 series GC equipped with a flame ionization detector (FID). The GC was connected to an auto sampler (Varian 8200). The method detection limit was 1.6 μg/L.

Total iron, persulfate, and chloride concentration were analyzed using a spectrophotometer (DR/2010, HACH). Persulfate was determined using the method of Liang et al. (2008a) with slight modifications (Chapter 2). The total iron was determined using a standard method with 1,10-phenanthroline monohydrate (APHA, 1989). Chloride was determined by the mercuric thiocyanate method (HACH kits). The aqueous pH, dissolved oxygen (DO), and electrical conductivity (EC) were determined using a pH/ISE meter (Orion 4 star, Thermo Electron Corporation), DO meter (SP70D, VWR SympHony), and conductivity meter (Multi 350i, WTW), respectively.

5.3. Results and Discussion

5.3.1. Suspension of Bimetallic Nanoparticles in an Aqueous System

Iron-based bimetallic nanoparticles have a much longer suspension in aqueous systems than iron-based monometallic nanoparticles (Figure 5.3). For example, the slurry solution of nano-Pd-Fe^0 particles was well dispersed in an aqueous system, even after 6 weeks (data not shown), whereas the suspension of the slurry solution of nano-Fe^0 particles lasted for less than an hour. Nano-Fe^0 particles are rapidly aggregated and agglomerated due to the attractive forces between nanoparticles (e.g., van der Waals and electrostatic forces). As a result, the agglomerated nanoparticles are precipitated by gravitational forces (Phenrat et al., 2010; Phenrat et al., 2009). Nano-Pd-Fe^0 particles showed the greatest suspension compared to the other eight bimetallic systems (nano-Co-Fe^0, nano-Mn-Fe^0, nano-Cd-Fe^0, nano-Ni-Fe^0, nano-Cr-Fe^0, nano-Zn-Fe^0, nano-Cu-Fe^0, and nano-Ag-Fe^0).

5.3.2. Mobility of Bimetallic Nanoparticles

The results from mobility experiments using glass beads showed that the effluent iron concentration was <6 % of the influent iron concentration after the 9 PVs for the nano-Fe^0 particles, while it was between 90 and 100 % for the nano-Pd-Fe^0 particles (Figure 5.4). Nano-Fe^0 particles are effectively filtered by the glass beads because of the large size of the aggregated and agglomerated particles (Bennett et al., 2010), whereas the nano-Pd-Fe^0 particles, are less agglomerated. However, the retardation factor for the nano-Pd-Fe^0 particles in glass beads was 4.9, indicating that the mobility of nano-Pd-Fe^0 particles through glass beads is relatively poor. Three mechanisms are responsible for the filtration of nanoparticles in porous media: Brownian diffusion, interception, and sedimentation (Schrick et al., 2004). Brownian diffusion is the main

process causing the retention of nanoparticles in porous media (Bennett et al., 2010; Schrick et al., 2004).

In the geological porous medium, based on visual inspection, nano-Pd-Fe^0 particles could not travel more than a few centimeters from the inlet into columns packed with CFB Borden sand. The peer-reviewed literature indicates that the mobility of nano-Fe^0 can be improved using lower iron concentrations and using higher water flow rates (Cantrell and Kaplan, 1997; Phenrat et al., 2010; Phenrat et al., 2009). However, several experiments were conducted under various conditions without success in detecting iron at the outlet (Table 5.1). For example, a range of iron influent concentrations (100-2,550 mg/L) and injected volumes (2-14 pore volumes) were used. Furthermore, the experiments were performed at different flow rates (2.9-9.6 mL/min) and different flow directions. These observations support the findings in the literature about the poor mobility of Fe^0 nanoparticles in geological porous media.

5.3.3. TCE Treatability Study

In Trial I, the effluent TCE concentration decreased with time when using either the non-activated persulfate or nano-Pd-Fe^0 activated persulfate systems (Figure 5.5 (a.)); however, the degree of treatment for both systems was not sufficient to degrade the TCE, suggesting that the mass of persulfate or nano-Pd-Fe^0 particles should be much greater than used. Reasons for this poor treatment are not clear; however, aquifer material constituents (e.g., organic carbon content and native metals) are probably responsible for the poor treatment (Cuypers et al., 2000; Siegrist et al., 2011; Sra et al., 2010). It could be also that the contact time of persulfate with the TCE source zone was limited by the injection flow rate (0.26 mL/min).

In Trial II, the effluent TCE concentration was gradually decreased when using nano-Pd-Fe^0 activated persulfate system to below the method detection limit (1.6 µg/L); however, in the post-

treatment period, the TCE concentration fluctuated above and below the method detection limit (Figure 5.6 (a)). Unfortunately, problems with the samples collected for TCE analysis prevented the effluent TCE concentration for the Trial II control (for the non-activated persulfate system) from being qualified.

In Trial I, a chloride peak was observed in the nano-Pd-Fe^0/persulfate system, whereas no chloride peak was observed in the non-activated persulfate system (Figure 5.5 (b) and (c)), indicating that the activation zone of nano-Pd-Fe^0 particles slightly enhanced the treatment of TCE. The TCE mass destruction was only ~9 % as revealed by the effluent chloride concentration. Similar to Trial I, we found the same chloride peak in the nano-Pd-Fe^0 activated persulfate system (Trial II) (Figure 5.6 (b) and (c)). It should be noted in the effluent concentration of chloride (Trial I and II) that after the deactivation of the nano-Pd-Fe^0 particles in the activation zone, the effluent chloride concentration was similar to the non-activated persulfate system (Figure 5.5 (b) and Figure 5.6 (b)).

In the non-activated persulfate system (Trial I and II), the effluent chloride concentration was similar to that of the chloride baseline concentration. The same observation was made by Liang et al. (2008b), who could not distinguish between the chloride baseline concentration and that produced by the cleavage of TCE molecules in the non-activated persulfate system.

In the nano-Pd-Fe^0 activated persulfate system (Trial I and II), the activation zone of nano-Pd-Fe^0 was rapidly deactivated after exposure to persulfate, as visually observed (Figure 5.7) by the color change [from black (for fresh nanparticles) to orange-brown (for the deactivated nanoparticles)], indicating that the longevity of the activation zone is limited.

Al-Shamsi and Thomson (Chapter 2) extensively studied the deactivation of nano-Fe^0 particles by persulfate in aqueous systems and noted a formation of an iron-sulfate complex on the surfaces of the deactivated iron nanoparticles in the accordance with the following:

$$Fe^0 + SO_4^{2-} + 2H_2O \rightarrow FeSO_4 + H_2 + 2OH^- \quad (5.8)$$

In the nano-Pd-Fe^0 activated persulfate system (Trial I), almost 35 % of the persulfate was consumed during the transport through the sand-packed column compared to ~10 % persulfate consumption for the non-activated persulfate system (Figure 5.5 (b) and (c)), indicating that ~25 % of the persulfate was consumed as a consequence of the interaction between persulfate and the activation zone of nano-Pd-Fe^0 particles. In the non-activated persulfate system, it is possible that the presence of the organic carbon and the native metals were responsible for the decomposition of persulfate (Cuypers et al., 2000; Sra et al., 2010).

In the nano-Pd-Fe^0 activated persulfate system (Trial II), the effluent persulfate concentration was similar to the influent persulfate concentration except for the first pore volume, in which 35 % of persulfate concentration was reduced (Figure 5.6 (b) and (c)). Unlike Trial I, as a result of the high persulfate concentration used (i.e., 30 g/L), minimal persulfate mass was lost to interactions with aquifer material constituents (e.g., organic carbon, native metals).

Furthermore, several parameters were estimated to evaluate the changes in this treatment system including the effluent concentrations of dissolved oxygen (DO), electrical conductivity (EC), and pH. However, in the parameters, there was no significant differences between the nano-Pd-Fe^0 activated persulfate and the non-activated persulfate systems (Figure S.5.1 and S.5.2) (in the supplementary information data).

5.3. Summary

The delivery of iron nanoparticles in the subsurface is necessary for the successful implication of the metal nanoparticles/persulfate system for the remediation of organic contaminants. We found that iron-based bimetallic nanoparticles have a much longer suspension (>6 weeks) in aqueous systems than iron-based monometallic nanoparticles (<1 hour). In a glass-bead-packed column, the effluent concentration of nano-Fe^0 particles was only 6 % of the influent concentration compared to 100 % with nano-Pd-Fe^0 particles. Although the iron-based bimetallic nanoparticles are mobile in non-geological porous media, they are relatively immobile in geological porous media. To overcome the delivery issue in geological porous media, nano-Pd-Fe^0 particles were injected as an activation zone (from a port in a physical model) to activate persulfate for the treatment of the TCE source zone. The TCE mass destruction was only 9 % higher in the nano-Pd-Fe^0 activated $S_2O_8^{2-}$ system compared to the non-activated $S_2O_8^{2-}$ system as revealed by a short duration chloride spike in the effluent chloride concentration. In addition, the activation zone of nano-Pd-Fe^0 was rapidly deactivated after exposure to persulfate, as visually observed.

If the issues that we faced in the physical model are resolved, the technique may be applicable in the field. To scale up this technique from a laboratory to a field, three main limitations should be considered. First, the procedure of injecting the iron nanoparticles in the subsurface to create an activation zone is necessary. It should be noted that, in the physical model, the activation zone of iron nanoparticles was created in a column with a small diameter (3.8 cm). In addition, the syringe, which was used to inject the nanoparticles, was able to extend from the opening of the port to the other edge of the column. These semi-ideal conditions may not be available in the field. Second, finding a potential solution of the deactivated phenomenon such as the

depassivation of the iron surfaces by an electrical current technique is essential to increase the longevity of the iron nanoparticles. Third, the injected mass of iron nanoparticles should be carefully balanced to prevent clogging of the pores.

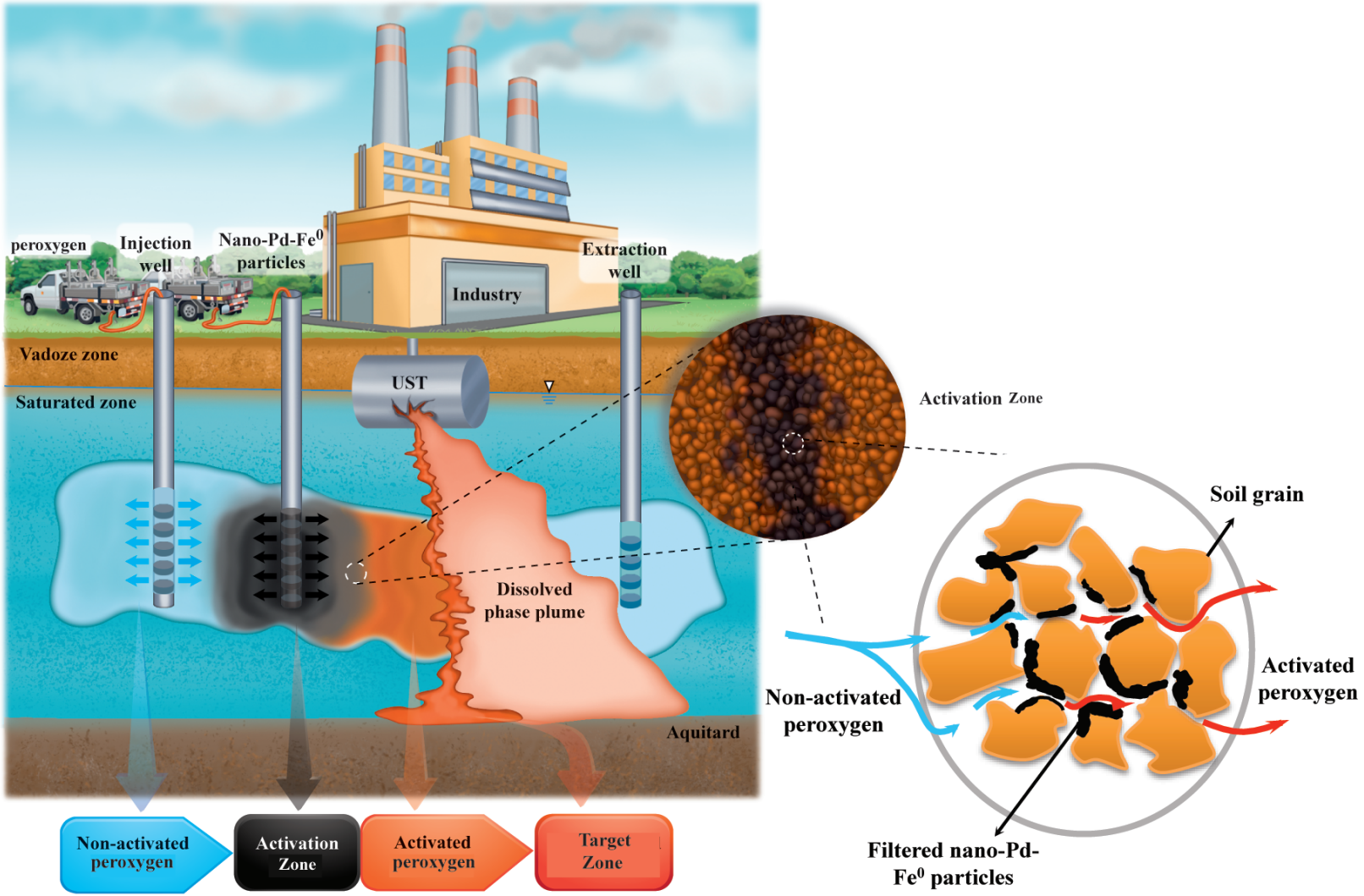

Figure 5.1. Conceptual model of a zone of nano-Pd/Fe^0 particles used to activate persulfate for the treatment of a source zone.

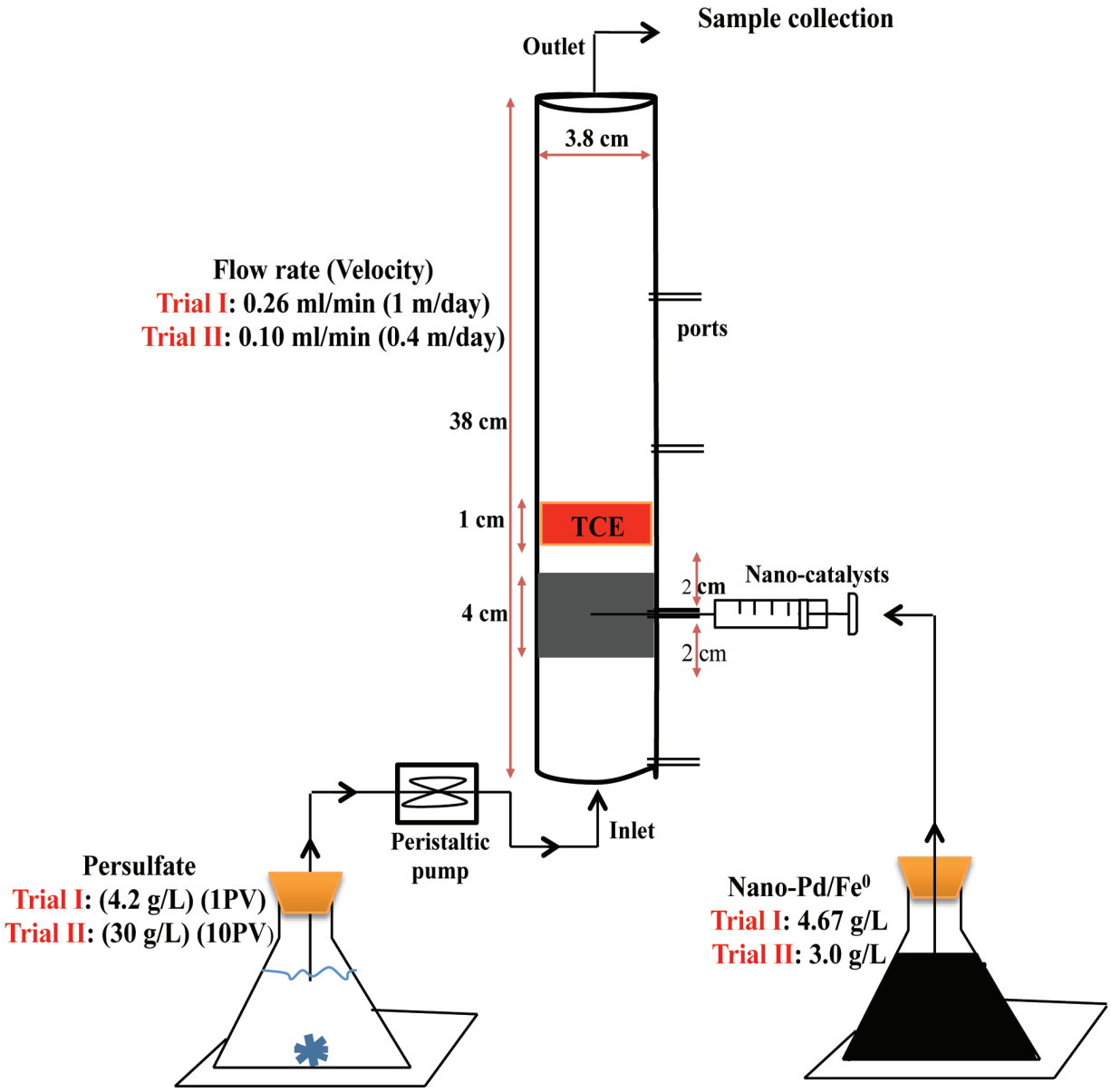

Figure 5.2. Laboratory experimental design for the TCE source zone treatment using the nano-Pd/Fe^0/persulfate system.

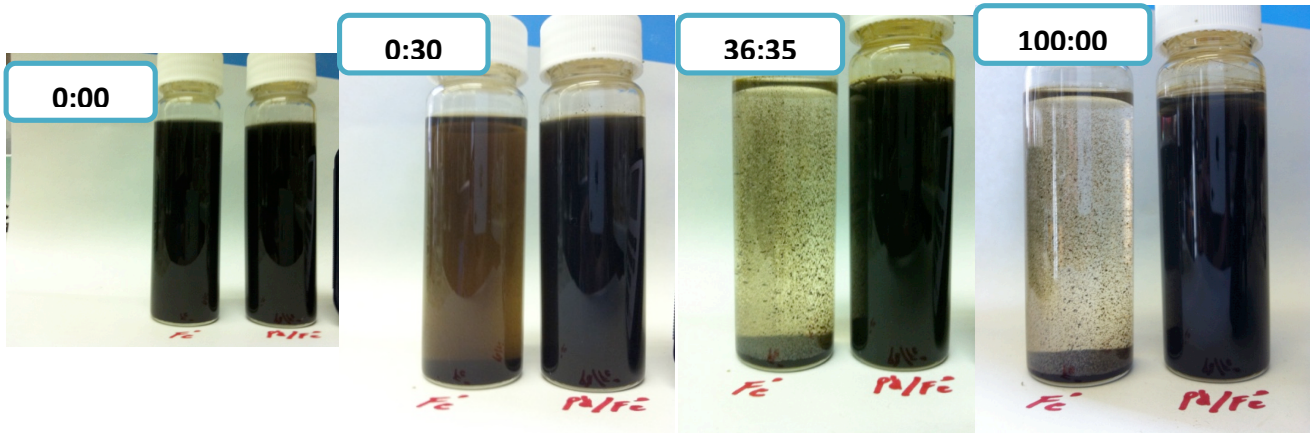

Figure 5.3. The dispersion of nano-Fe^0 and nano-Pd/Fe^0 particles (iron concentration of 425 mg/L) in Milli-Q water.

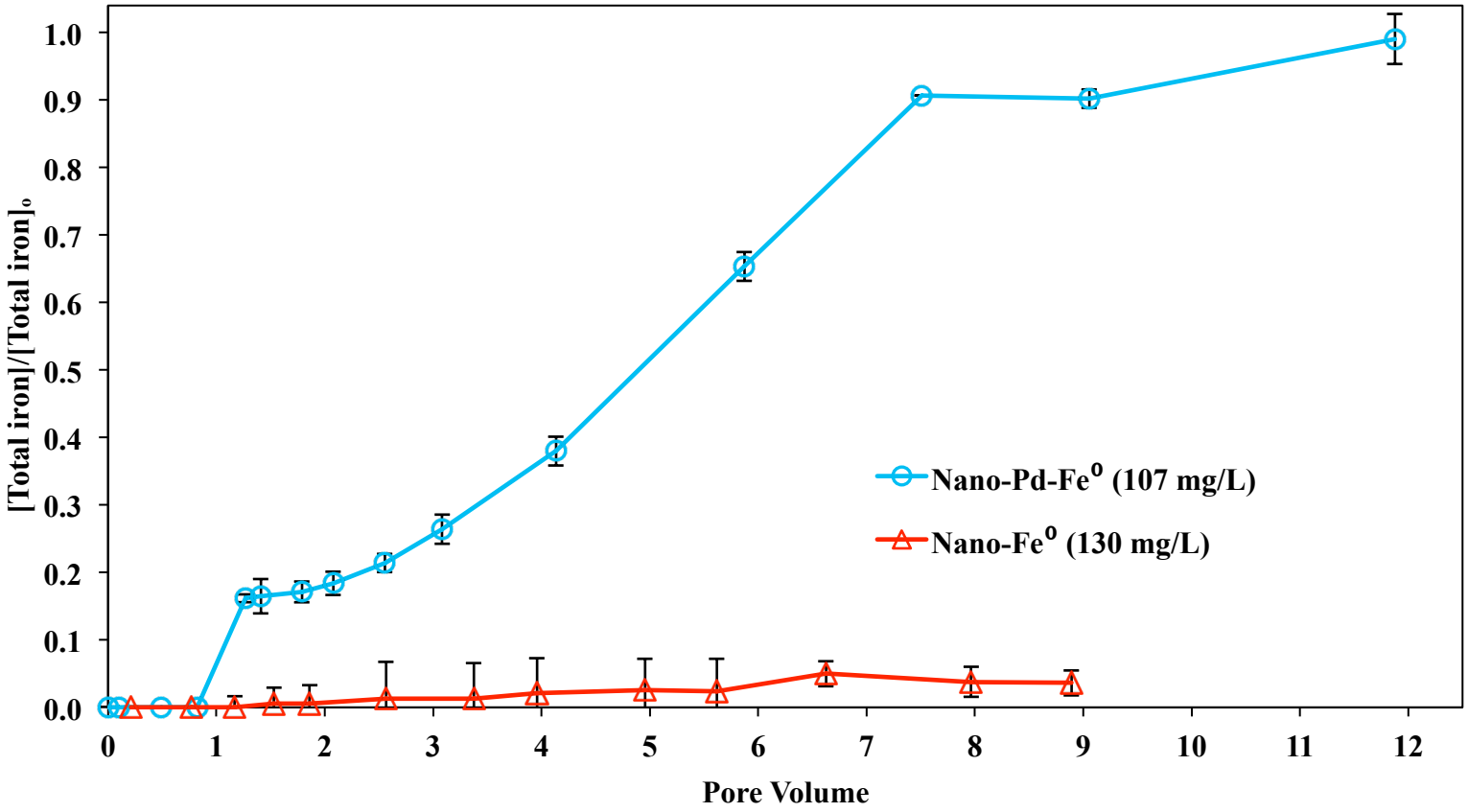

Figure 5.4. The breakthrough of nano-Fe^0 and nano-Pd/Fe^0 particles in a non-geological porous medium (glass beads).

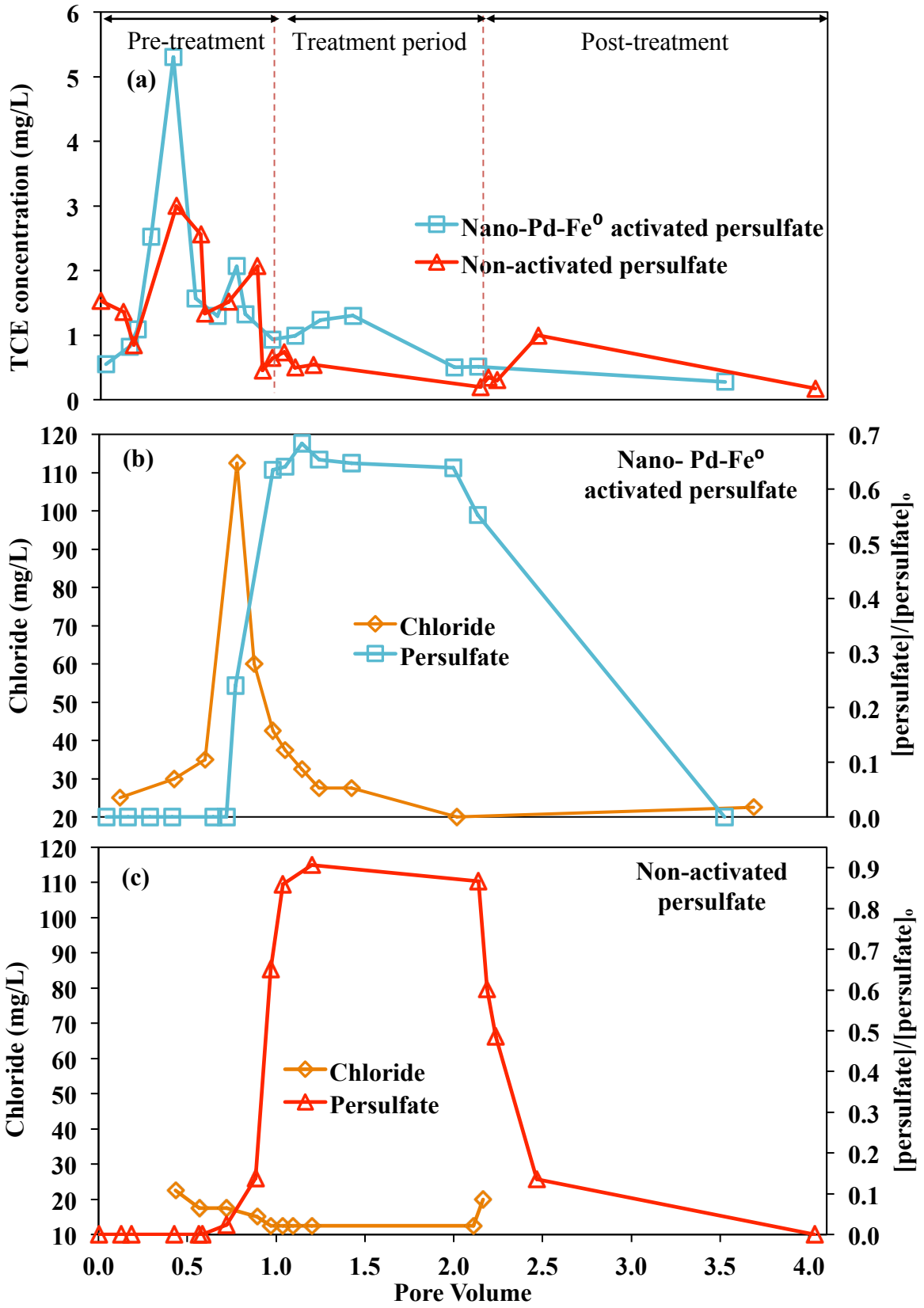

Figure 5.5.31Effluent concentrations of TCE, persulfate, chloride, EC, DO, and pH (Triall I).

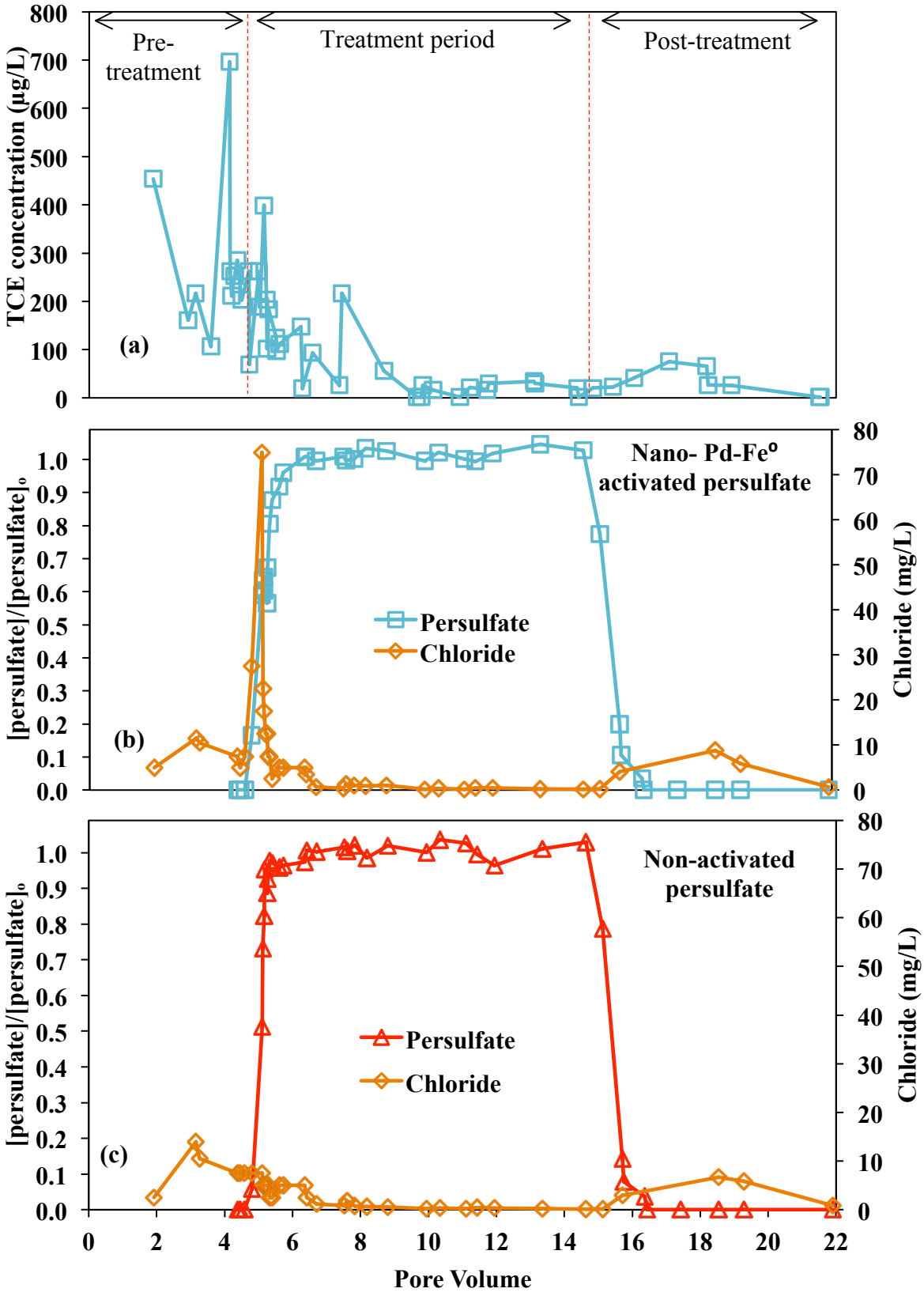

Figure 5.6.32Effluent concentrations of TCE, persulfate, and chloride (Trial II).

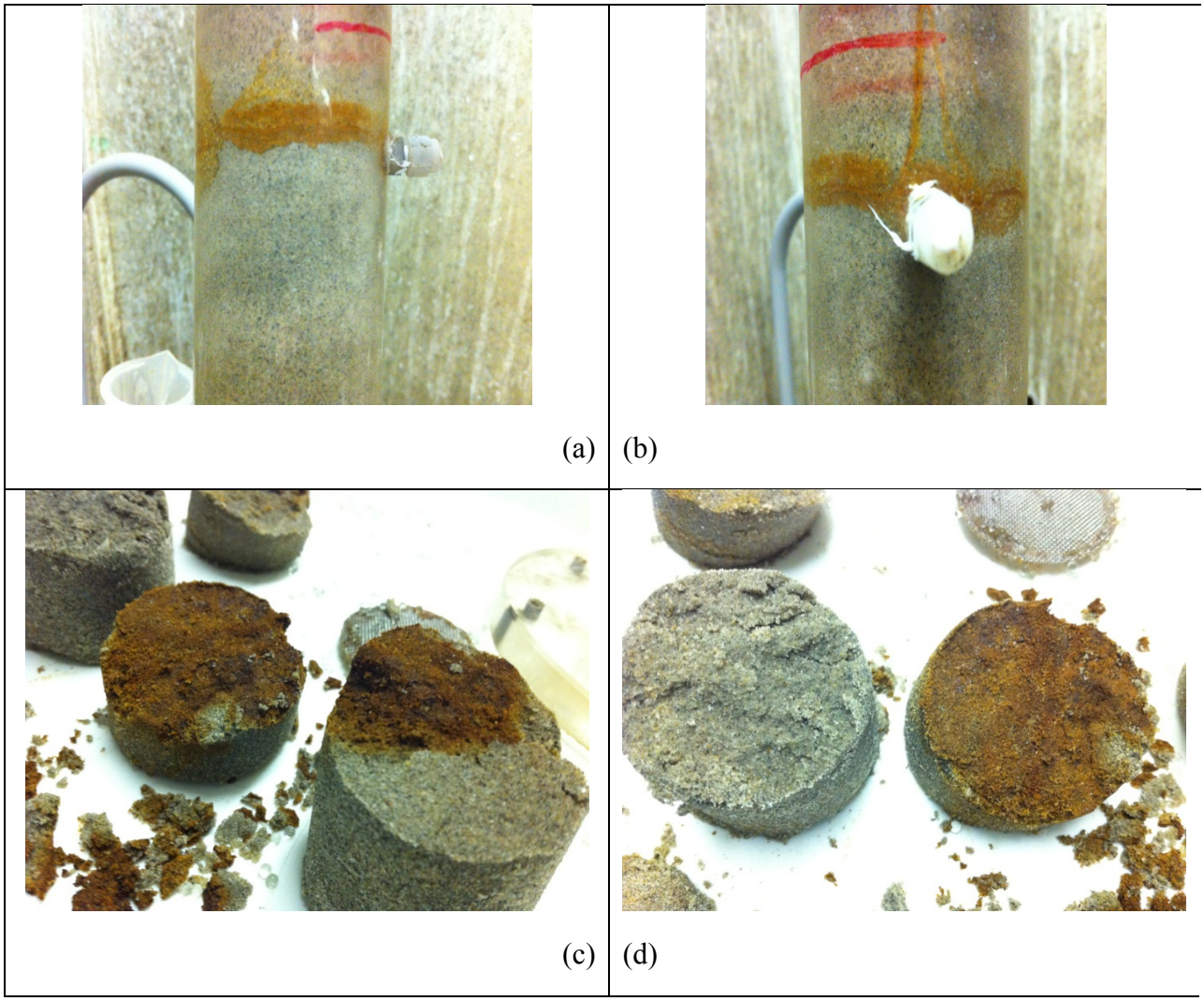

Figure 5.7.33Images of the activation zone of nano-Pd-Fe^0 after exposure to persulfate. (a) a layer of the activation zone in the sand packed column [from the side], (b) a layer of the activation zone in the sand packed column [from the front], (c) and (d) cross-section of the activation zone.

Supplementary information:

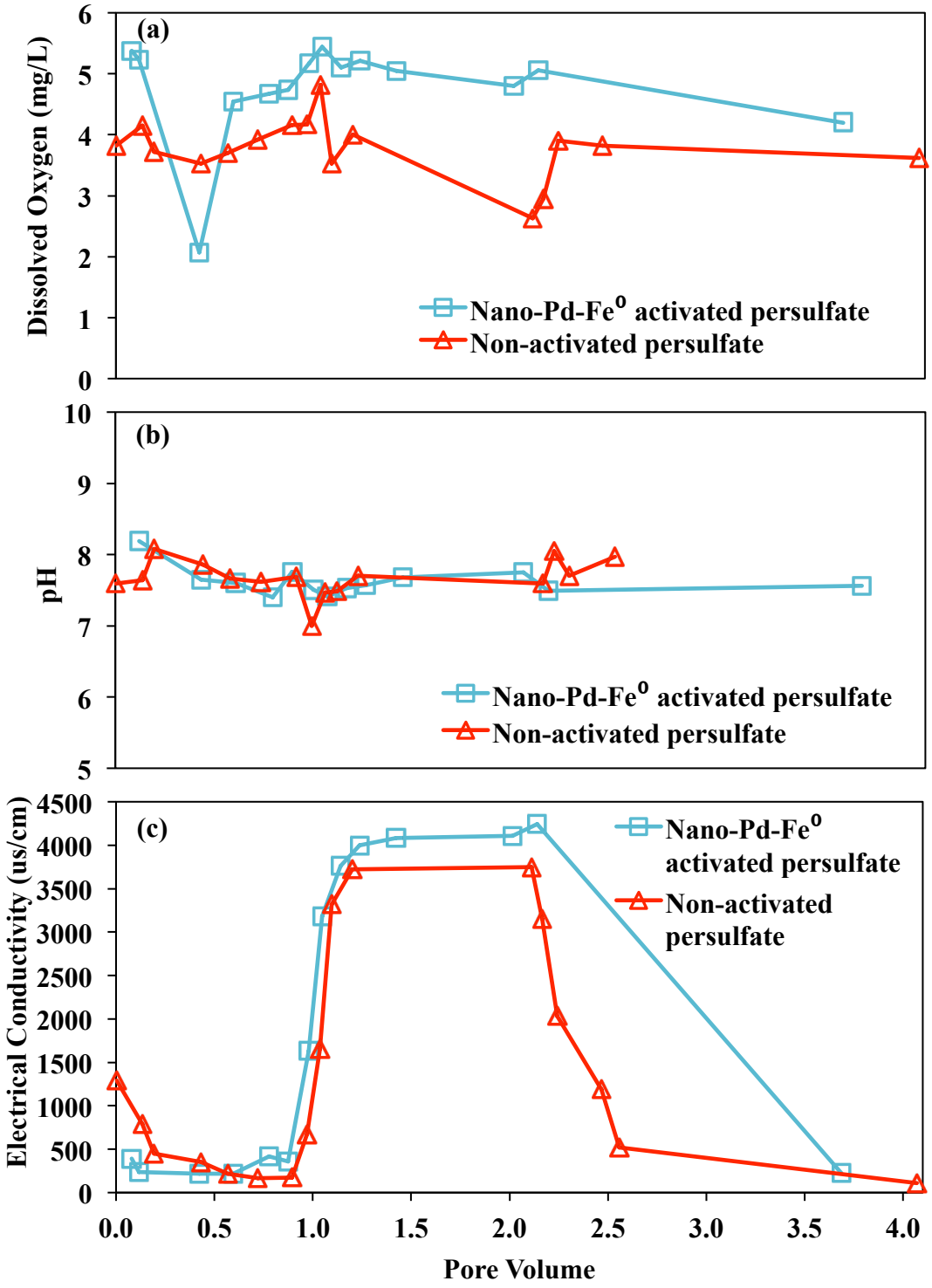

Figure S.5.1.34Effluent concentrations of EC, DO, and pH (Trial I).

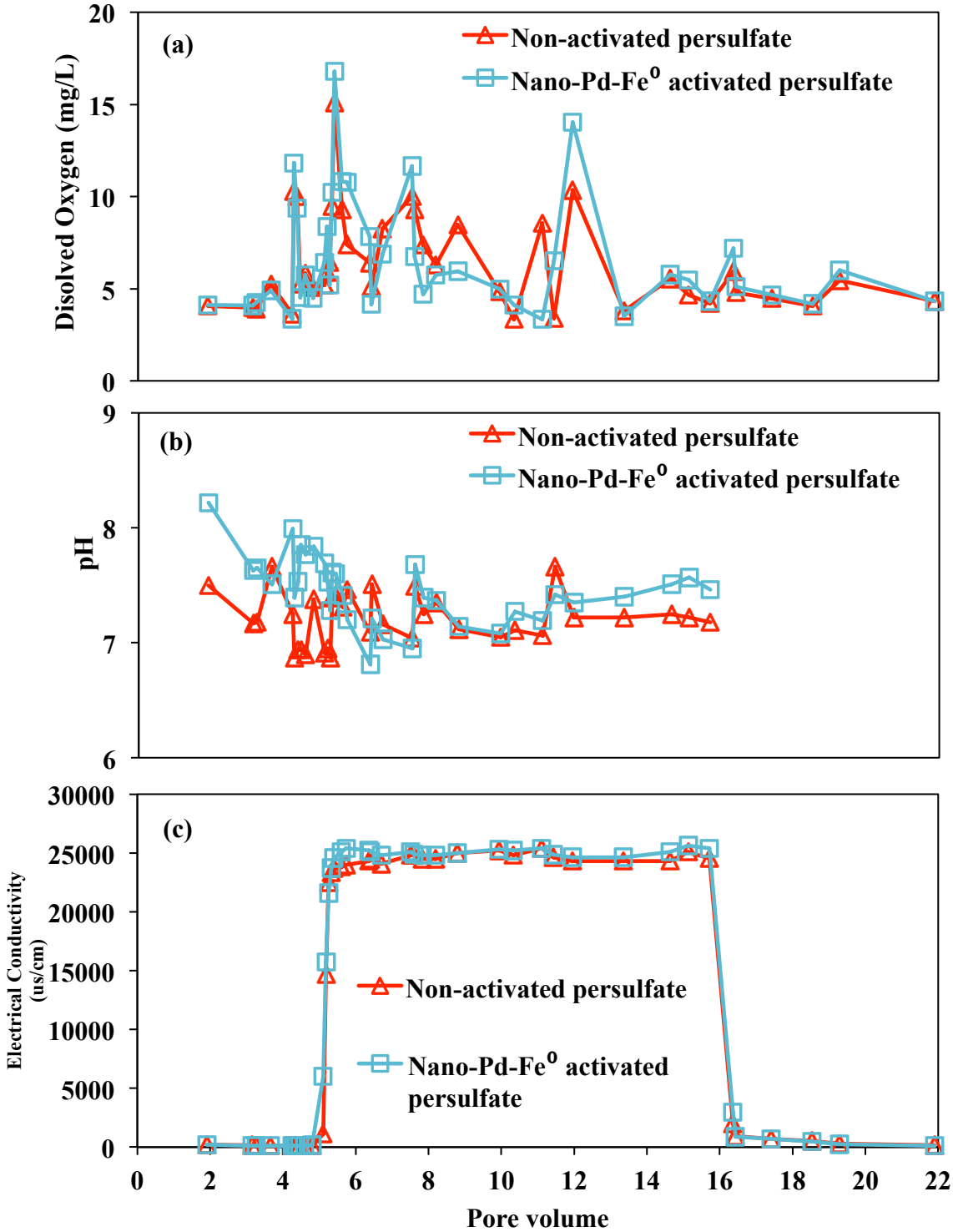

Figure S.5.2.35Effluent concentrations of EC, DO, and pH (Trial II).

Table 5.1. Mobility of nano-Pd/Fe^0 particles in a geological porous medium (CFB Borden sand).

Trial	Iron influent concentration (mg/L)	Injected volume (PV)	Flow rate (mL/min)	Iron effluent concentration (mg/L)	Flow direction
1	100	2	2.89	<MDL[2]	Down-up
2	2,550	4	2.89	<MDL	Down-up
3	2,550	4	9.60	<MDL	Down-up
4	1,000	5	2.89	<MDL	Down-up
5	2,550	14	2.89	<MDL	Up-down

[2] MDL = method detection limit.

Table 5.2. The operation conditions of the sand packed column in the TCE treatability study.

	Flow rate (mL/min) and velocity (m/day)	TCE mass (mg)	Nano-iron mass (mg)	Persulfate		
				Mass (mg)	Concentration (g/L)	Volume (mL)
Trial I	0.26 (1)	110	70	598	4.2	143
Trial II	0.10 (0.4)	110	45	42,750	30	1,425

Chapter 6

Chapter 6.

Conclusions and Recommendations

6.1. Conclusions

The core findings of this research can be summarized as:

- Nano-Fe^0 particles are promising to activate $S_2O_8^{2-}$ to treat hazardous organic compounds (i.e., TCE, MTBE, naphthalene, and chloro-benzene) compared to other conventional activators such as granular-Fe^0 and Fe^{2+}.
- Nano-Fe^0 particles were passivated quickly following exposure to $S_2O_8^{2-}$, causing the reaction rate to reduce to a magnitude representative of an un-activated $S_2O_8^{2-}$ system.
- An iron-sulfate ($FeSO_4$) complex was formed on the surfaces of nano-Fe^0 particles following exposure to $S_2O_8^{2-}$ compared to an iron oxyhydroxide (FeOOH) layer that was present on the surfaces of the fresh nano-Fe^0 particles.
- The treatment of TCE was optimized using a 1 to 1 molar ratio between nano-Fe^0 particles and $S_2O_8^{2-}$.
- Iron-based bimetallic zero valent nanoparticles (BZVNs) are more promising activators for H_2O_2, $S_2O_8^{2-}$, and HSO_5^- to treat TCE than monometallic zero valent nanoparticles. For example, the TCE reaction rate constant by nano-Ag-Fe^0 activated H_2O_2 is 9- to 18-fold higher than that with nano-Fe^0 activated H_2O_2.
- The response of peroxygens for the various activators are not the same. In the investigation of nine different BZVNs as activators, the highest TCE oxidation was achieved by nano-Pd-Fe^0 and nano-Zn-Fe^0 in the activated $S_2O_8^{2-}$ system, nano-Co-Fe^0 in

the activated HSO_5^- system, and nano-Ag-Fe^0 in the activated H_2O_2 system. Although the mechanisms are unknown, the differences are significant.

- In all three peroxygen systems, increasing dosage of nanoparticles and peroxygens increased the oxidation of TCE.
- The BZVNs activated H_2O_2 system showed a much lower TCE treatment rate compared to either the BZVNs activated $S_2O_8^{2-}$ or the BZVNs activated HSO_5^- systems, suggesting that a bridged group complex is formed between the activators and H_2O_2, causing a lower TCE treatment rate.
- In the soil slurry batch system, the remaining concentration of dissolved TCE after using the activated $S_2O_8^{2-}$ system was two- to three-fold higher in a soil slurry batch system than that in an aqueous batch system. In addition, for five different aquifer materials, increasing the mass of the aquifer solids significantly decreased the TCE decomposition by the nano-Pd-Fe^0 activated $S_2O_8^{2-}$ system. A linear relationship was observed between the mass of aquifer solids and the initial TCE decomposition rate, suggesting that the OC and/or the dissolved aquifer material constituents (e.g., carbonates and bicarbonates) compete with TCE treatment in the activated persulfate system.
- The mass ratio (oxidant/solid) in the field is approximately 0.001 compared to 0.0038 for 20 g soil slurry batch reactors (i.e., Borden sand), indicating that the mass ratio is decreased by 3.8 times in scaling up from 20 g soil slurry batch reactor to the field. Therefore, soil slurry systems are not representative of the field.
- In the one-dimensional physical model systems, bimetallic nanoparticles (i.e., nano-Pd-Fe^0 particles) were mobile in non-geological porous media and relatively immobile in geological porous media.

- For the injection of monometallic nanoparticles (i.e., nano-Fe^0 particles) in a glass-bead-packed column, the effluent iron concentration was less than 6 % of the influent iron concentration; in contrast, this value was between 90 and 100 % for the bimetallic nanoparticles (nano-Pd-Fe^0 particles).
- Bimetallic nanoparticles (i.e., nano-Pd-Fe^0 particles) were suspended in aqueous systems for a longer period (> 6 weeks) compared to the monometallic nanoparticles (nano-Fe^0 particles) (<1 hour), indicating that adding metal additives improves the suspension of nanoparticles.
- Nano-Pd-Fe^0 particles were injected as an activation zone to activate $S_2O_8^{2-}$ for the treatment of a TCE source zone. The TCE mass destruction was only 9 % higher in the nano-Pd-Fe^0 activated $S_2O_8^{2-}$ system compared to the non-activated $S_2O_8^{2-}$ system as captured by a short duration chloride spike in the effluent chloride concentration.
- The activation wall of nano-Pd-Fe^0 was rapidly deactivated after exposed to persulfate as visually observed by color change, indicating that the longevity of the activation wall is limited.

6.2. Recommendations

Nanoparticles might be the future activators for some ISCO systems; however, the study in this field is still at an early stage. Two limitations of using nano-activators in ISCO applications have been well characterized and identified in this work: I) the passivation phenomenon of the surfaces of nanoparticles, and II) the difficulties in the subsurface mobility of nanoparticles. Future research is needed to find potential solutions for these problems. Finding such solutions will indeed advance the application of nano-activators for ISCO.

This research was limited by using a certain class of nanoparticles as activators for peroxygens (zero valent iron, and iron-based bimetallic zero valent nanoparticles). Other classes of nanoparticles might be applicable for peroxygens such as nanoparticles with different oxidation states (e.g., nano-Fe_3O_4 and nano-Fe_2O_3), other types of metals (e.g., Au, Ag, and Zn nanoparticles), or other types of materials (e.g., activated carbon nanoparticles). Future research is needed to explore the potential of other classes of nanoparticles in ISCO technology and advanced oxidation technologies (AOTs).

Metal nanoparticles in the persulfate and peroxymonosulfate systems showed greater treatment ability compared to the hydrogen peroxide system. Although the mobility and stability of persulfate in the subsurface have been studied extensively in the recent years, the mobility and stability of peroxymonosulfate have not been studied. Future research should focus on the potential application of peroxymonosulfate in the subsurface.

The evaluation techniques in this study were limited by three stages of laboratory experiments: aqueous batch systems, soil slurry batch systems, and 1-D physical model systems.

The response of the various peroxygens to the various activators is not the same. The mechanisms and pathways behind this phenomenon have not fully understood. It would be a great advancement in the science to discover the key factors for such phenomenon.

Over 95 % of this work was limited by examining the ability of nano-activators and peroxygens to treat a single organic compound (i.e., TCE), and therefore other organic compounds from various classes deserve more study in the future. This work was also limited using a single synthesizing method of nanoparticles (i.e., Borohidride reduction method), other synthesizing methods can produce the same nanoparticles with different properties (e.g., size,

shape, and surface area), so that the activation ability is likely to be different. This deserves more attention in the future.

References

Chapter 2:

(1) Kester, J. E.; Clewell, H. J., The perils and promise of modern risk assessment: the example of trichloroethylene. *Clin Occup Environ Med* **2004,** 4, (3), 497-512.

(2) Wernke, M.; Schell, J., Solvents and malignancy. *Clin Occup Environ Med* **2004,** 4, (3), 513–527.

(3) NTP *Report on carcinogens background document for Methyl Tertiary-Butyl Ether*; National Toxicology programm, U.S. Department of Health and Human services: NC, USA, 1998.

(4) NTP *Report on carcinogens background document for Napthalene*; National Toxicology Programm, U.S. Department of Health and Human Services: NC, USA, 2002.

(5) NTP *Report on carcinogens background document for Chlorobenzene*; National Toxicology Programm, U.S. Department of Health and Human Services: NC, USA, 1985.

(6) Tsai, T. T.; Kao, C. M.; Yeh, T. Y.; Lee, M. S., Chemical oxidation of chlorinated solvents in contaminated groundwater: Review. *Pract. Periodical Hazard., Toxic, Radioact. Waste Manage.* **2008,** 12, (2), 116-126.

(7) Xu, X.; Thomson, N. R., Hydrogen Peroxide Persistence in the Presence of Aquifer Materials. *Soil Sediment Contam* **2010,** 19, (5), 602-616.

(8) Xu, X.; Thomson, N. R., A long-term bench-scale investigation of permanganate consumption by aquifer materials. *J. Contam. Hydrol.* **2009,** 110, (3-4), 73-86.

(9) Russo, L.; Rizzo, L.; Belgiorno, V., PAHs contaminated soils remediation by ozone oxidation. *Desalin Water Treat* **2010,** 23, (1-3), 161-172.

(10) Sra, K. S.; Thomson, N. R.; Barker, J. F., Persistence of Persulfate in Uncontaminated Aquifer Materials. *Environ. Sci. Technol.* **2010,** 44, (8), 3098-3104.

(11) Killian, P. F.; Bruell, C. J.; Liang, C.; Marley, M. C., Iron (II) Activated Persulfate Oxidation of MGP Contaminated Soil. *Soil Sediment Contam* **2007,** 16, (6), 523 - 537.

(12) Liang, C.; Liang, C. P.; Chen, C. C., pH dependence of persulfate activation by EDTA/Fe(III) for degradation of trichloroethylene. *J. Contam. Hydrol.* **2009,** 106, (3-4), 173-182.

(13) Liang, C.; Wang, Z. S.; Bruell, C. J., Influence of pH on persulfate oxidation of TCE at ambient temperatures. *Chemosphere* **2007,** 66, (1), 106-113.

(14) Norman, R. O. C.; Storey, P. M.; West, P. R., Electron spin resonance studies. Part XXV. Reactions of the sulphate radical anion with organic compounds. *J. Chem. Soc. B* **1970**, 1087-1095.

(15) Anbar, M.; Neta, P., A compilation of specific bimolecular rate constants for the reactions of hydrated electrons, hydrogen atoms and hydroxyl radicals with inorganic and organic compounds in aqueous solution. *Int. J. Appl. Radiat. Is.* **1967,** 18, (7), 493-523.

(16) House, D. A., Kinetics and mechanism of oxidations by peroxydisulfate. *Chem. Rev.* **1962,** 62, 185-203.

(17) Pignatello, J. J.; Baehr, K., Ferric complexes as catalysts for Fenton degradation of 2,4-D and metolachlor in soil. *J. Enviro. Qual.* **1994,** 23, (2), 365-370.

(18) Sun, Y.; Pignatello, J. J., Chemical treatment of pesticide wastes. Evaluation of iron(III) chelates for catalytic hydrogen peroxide oxidation of 2,4-D at circumneutral pH. *J. Agric. Food. Chem.* **1992,** 40, (2), 322-327.

(19) Oh, S. Y.; Kim, H. W.; Park, J. M.; Park, H. S.; Yoon, C., Oxidation of polyvinyl alcohol by persulfate activated with heat, Fe2+, and zero-valent iron. *J. Hazard. Mater.* **2009,** 168, (1), 346-351.

(20) Liang, C.; Lai, M. C., Trichloroethylene degradation by zero valent iron activated persulfate oxidation. *Environ. Eng. Sci.* **2008,** 25, (7), 1071-1077.

(21) Oh, S.-Y.; Kang, S.-G.; Chiu, P. C., Degradation of 2,4-dinitrotoluene by persulfate activated with zero-valent iron. *Sci. Total Environ.* **2010,** 408, (16), 3464-3468.

(22) Liang, C.; Guo, Y. Y., Mass Transfer and Chemical Oxidation of Naphthalene Particles with Zerovalent Iron Activated Persulfate. *Environ. Sci. Technol.* **2010,** 44, (21), 8203-8208.

(23) Furukawa, Y.; Kim, J. W.; Watkins, J.; Wilkin, R. T., Formation-of ferrihydrite and associated iron corrosion products in permeable reactive barriers of zero-valent iron. *Environ. Sci. Technol.* **2002,** 36, (24), 5469-5475.

(24) Liang, C.; Su, H.-W., Identification of Sulfate and Hydroxyl Radicals in Thermally Activated Persulfate. *Ind. Eng. Chem. Res.* **2009,** 48, (11), 5558-5562.

(25) ASTM-D6889-03, Standard Practice for Fast Screening for Volatile Organic Compounds in Water Using Solid Phase Microextraction (SPME). West Conshohocken, 2003.

(26) Liang, C.; Huang, C.-F.; Mohanty, N.; Kurakalva, R. M., A rapid spectrophotometric determination of persulfate anion in ISCO. *Chemosphere* **2008,** 73, (9), 1540-1543.

(27) APHA, Standard methods for the examination of water and wastewater 17th ed.; Washington, D. C. , 1989.

(28) Chen, K. F.; Kao, C. M.; Wu, L. C.; Surampalli, R. Y.; Liang, S. H., Methyl Tert-Butyl Ether (MTBE) Degradation by Ferrous Ion-Activated Persulfate Oxidation: Feasibility and Kinetics Studies. *Water Environ. Res* **2009,** 81, 687-694.

(29) Padmanabhan, A. R. Novel Simultaneous Reduction/Oxidation Process for Destroying Organic Solvents. Worcester Polytechnic Institute, 2008.

(30) Levenspiel, O., *Chemical Reaction Engineering*. 3rd ed.; John Wiley & Sons: New York, 1999.

(31) Liang, C.; Bruell, C. J.; Marley, M. C.; Sperry, K. L., Persulfate oxidation for in situ remediation of TCE. I. Activated by ferrous ion with and without a persulfate-thiosulfate redox couple. *Chemosphere* **2004,** 55, (9), 1213-1223.

(32) Li, L.; Fan, M.; Brown, R. C.; Van Leeuwen, J.; Wang, J.; Wang, W.; Song, Y.; Zhang, P., Synthesis, properties, and environmental applications of nanoscale iron-based materials: A review. *Crit. Rev. Environ. Sci. Technol.* **2006,** 36, (5), 405-431.

(33) Li, X. Q.; Cao, J.; Zhang, W. X., Stoichiometry of Cr(VI) immobilization using nanoscale zero valent iron (nZVI): A study with high-resolution X-ray photoelectron spectroscopy (HR-XPS). *Ind. Eng. Chem. Res.* **2008,** 47, (7), 2131-2139.

(34) Sun, Y. P.; Li, X. Q.; Cao, J.; Zhang, W. X.; Wang, H. P., Characterization of zero-valent iron nanoparticles. *Adv. Colloid Interface Sci.* **2006,** 120, (1-3), 47-56.

(35) Haber, J.; Stoch, J.; Ungier, L., X-ray photoelectron spectra of oxygen in oxides of Co, Ni, Fe and Zn. *J. Electron. Spectrosc. Relat. Phenom.* **1976,** 9, (5), 459-467.

(36) Baltrusaitis, J.; Cwiertny, D. M.; Grassian, V. H., Adsorption of sulfur dioxide on hematite and goethite particle surfaces. J. *Phys. Chem. Chem. Phys.* **2007,** 9, (41), 5542-5554.

(37) Legrand, D. L.; Bancroft, G. M.; Nesbitt, H. W., Oxidation/alteration of pentlandite and pyrrhotite surfaces at pH 9.3: Part 1. Assignment of XPS spectra and chemical trends. *Am. Mineral.* **2005,** 90, (7), 1042-1054.

(38) Fu, H.; Wang, X.; Wu, H.; Yin, Y.; Chen, J., Heterogeneous uptake and oxidation of SO2 on iron oxides. *J. Phys. Chem. C* **2007,** 111, (16), 6077-6085.

(39) Grosvenor, A. P.; Kobe, B. A.; Biesinger, M. C.; McIntyre, N. S., Investigation of multiplet splitting of Fe 2p XPS spectra and bonding in iron compounds. *Surf. Interface Anal.* **2004,** 36, 1564-1574.

(40) Frost, D. C.; Leeder, W. R.; Tapping, R. L., X-ray photoelectron spectroscopic investigation of coal. *Fuel* **1974,** 53, (3), 206-211.

(41) Nesbitt, H. W.; Muir, I. J., X-ray photoelectron spectroscopic study of a pristine pyrite surface reacted with water vapour and air. *Geochim. Cosmochim. Acta* **1994,** 58, (21), 4667-4679.

(42) Kelemen, S. R.; George, G. N.; Gorbaty, M. L., Direct determination and quantification of sulphur forms in heavy petroleum and coals. 1. The X-ray photoelectron spectroscopy (XPS) approach. *Fuel* **1990,** 69, (8), 939-944.

(43) Descostes, M.; Mercier, F.; Beaucaire, C.; Zuddas, P.; Trocellier, P., Nature and distribution of chemical species on oxidized pyrite surface: Complementarity of XPS and nuclear microprobe analysis. *Nucl. Instrum. Methods Phys. Res., Sect. B* **2001,** 181, (1-4), 603-609.

(44) Bukhtiyarova, G. A.; Bukhtiyarov, V. I.; Sakaeva, N. S.; Kaichev, V. V.; Zolotovskii, B. P., XPS study of the silica-supported Fe-containing catalysts for deep or partial H2S oxidation. *J. Mol. Catal. A: Chem.* **2000,** 158, (1), 251-255.

(45) Baltrus, J. P.; Diehl, J. R., Surface spectroscopic studies of factors influencing xanthate adsorption on coal pyrite surfaces. *Surf. Interface Anal.* **1997,** 25, (2), 64-70.

(46) Descostes, M.; Mercier, F.; Thromat, N.; Beaucaire, C.; Gautier-Soyer, M., Use of XPS in the determination of chemical environment and oxidation state of iron and sulfur samples: constitution of a data basis in binding energies for Fe and S reference compounds and applications to the evidence of surface species of an oxidized pyrite in a carbonate medium. *Appl. Surf. Sci.* **2000,** 165, (4), 288-302.

(47) Parfitt, R. L.; Smart, R. S. C., the mechanism of sulfate adsorption on iron oxides. *Soil Sci. Soc. Am. J.* **1978,** 42, 48-50.

(48) Parfitt, R. L.; Smart, R. S. C., Infrared spectra from binuclear bridging complexes of sulphate adsorbed on goethite (α-FeOOH). *J. Chem. Soc., Faraday Trans. 1 F* **1977,** 73, 796-802.

(49) Peak, D.; Ford, R. G.; Sparks, D. L., An in situ ATR-FTIR investigation of sulfate bonding mechanisms on goethite. *J. Colloid Interface Sci.* **1999,** 218, (1), 289-299.

(50) Siegal, J.; Rees, A. A.; Eggers, K. W.; Hobbs, R. L., In situ chemical oxidation of residual LNAPL and dissolved-phase fuel hydrocarbons and chlorinated alkenes in groundwater using activated persulfate. *Remediation* **2009,** 19, (2), 19-35.

Chapter 3:

[1] R. Yuan, S.N. Ramjaun, Z. Wang, J. Liu, Effects of chloride ion on degradation of Acid Orange 7 by sulfate radical-based advanced oxidation process: Implications for formation of chlorinated aromatic compounds, J. Hazard. Mater., 196 (2011) 173-179.

[2]A. Rastogi, S.R. Al-Abed, D.D. Dionysiou, Sulfate radical-based ferrous-peroxymonosulfate oxidative system for PCBs degradation in aqueous and sediment systems, Appl Catal B, 85 (2009) 171-179.

[3]M.A. Al-Shamsi, N.R. Thomson, Treatment of Orgainc Compounds by Activated Persulfate using Nano-scale Zero Valent Iron, Ind. Eng. Chem. Res., (2013) "**Submitted Manuscript**."

[4]H. Wei, E. Wang, Fe3O4 Magnetic Nanoparticles as Peroxidase Mimetics and Their Applications in H2O2 and Glucose Detection, Anal. Chem., 80 (2008) 2250-2254.

[5]S.-P. Sun, A.T. Lemley, p-Nitrophenol degradation by a heterogeneous Fenton-like reaction on nano-magnetite: Process optimization, kinetics, and degradation pathways, J. Mol. Catal. A: Chem., 349 (2011) 71-79.

[6]S. Zhang, X. Zhao, H. Niu, Y. Shi, Y. Cai, G. Jiang, Superparamagnetic Fe3O4 nanoparticles as catalysts for the catalytic oxidation of phenolic and aniline compounds, J. Hazard. Mater., 167 (2009) 560-566.

[7]T. Ben-Moshe, I. Dror, B. Berkowitz, Oxidation of organic pollutants in aqueous solutions by nanosized copper oxide catalysts, Appl Catal B, 85 (2009) 207-211.

[8]Q. Yang, H. Choi, S.R. Al-Abed, D.D. Dionysiou, Iron-cobalt mixed oxide nanocatalysts: Heterogeneous peroxymonosulfate activation, cobalt leaching, and ferromagnetic properties for environmental applications, Appl Catal B, 88 (2009) 462-469.

[9]C.L. Chun, D.R. Baer, D.W. Matson, J.E. Amonette, R.L. Penn, Characterization and Reactivity of Iron Nanoparticles prepared with added Cu, Pd, and Ni, Enviro Sci Tech, 44 (2010) 5079-5085.

[10]H.Y. Shu, M.C. Chang, C.C. Chang, Integration of nanosized zero-valent iron particles addition with UV/H2O2 process for purification of azo dye Acid Black 24 solution, J. Hazard. Mater., 167 (2009) 1178-1184.

[11]C.J. Liao, T.L. Chung, W.L. Chen, S.L. Kuo, Treatment of pentachlorophenol-contaminated soil using nano-scale zero-valent iron with hydrogen peroxide, J. Mol. Catal. A: Chem., 265 (2007) 189-194.

[12]L. Ershadi, Ebadi, T., Ershadi V., Rabbani A.R., , Chemical oxidation of crude oil in oil contaminated soil by Fenton process using nano zero valent Iron, 2nd Int.Conf. on Environ Sci Tech, Singapore, 2011, pp. VI-89- VI-91.

[13]S. Shafieiyoun, Ebadi, T., Nikazar, M.,, Treatment of Landfill Leachate by Fenton Process with Nano sized Zero Valent Iron particles, Int. J. Environ. Res., 6 (2012) 119-128.

[14]L. Xu, J. Wang, A heterogeneous Fenton-like system with nanoparticulate zero-valent iron for removal of 4-chloro-3-methyl phenol, J. Hazard. Mater., 186 (2011) 256-264.

[15]K. Choi, W. Lee, Enhanced degradation of trichloroethylene in nano-scale zero-valent iron Fenton system with Cu(II ,(J. Hazard. Mater., 211-212 (2012) 146-153.

[16]W.X. Zhang, C.B. Wang, H.L. Lien, Treatment of chlorinated organic contaminants with nanoscale bimetallic particles, Catal. Today, 40 (1998) 387-395.

[17]C.B. Wang, W.X. Zhang, Synthesizing nanoscale iron particles for rapid and complete dechlorination of TCE and PCBs, Environ. Sci. Technol., 31 (1997) 2154-2156.

[18]L. Gomathi Devi, S. Girish Kumar, K. Mohan Reddy, C. Munikrishnappa, Photo degradation of Methyl Orange an azo dye by Advanced Fenton Process using zero valent metallic iron: Influence of various reaction parameters and its degradation mechanism, J. Hazard. Mater., 164 (2009) 459-467.

[19]M. Pagano, A. Volpe, A. Lopez, G. Mascolo, R. Ciannarella, Degradation of chlorobenzene by Fenton-like processes using zero-valent iron in the presence of Fe3+ and Cu2+, Environ. Technol., 32 (2011) 155-165.

[20]C. Liang, M.C. Lai, Trichloroethylene degradation by zero valent iron activated persulfate oxidation, Environ Eng Sci, 25 (2008) 1071-1077.

[21]S.-Y. Oh, S.-G. Kang, P.C. Chiu, Degradation of 2,4-dinitrotoluene by persulfate activated with zero-valent iron, Sci. Total Environ., 408 (2010) 3464-3468.

[22]Y. Furukawa, J.W. Kim, J. Watkins, R.T. Wilkin, Formation-of ferrihydrite and associated iron corrosion products in permeable reactive barriers of zero-valent iron, Environ. Sci. Technol., 36 (2002) 5469-5475.

[23]C. Walling, Fenton's reagent revisited, Acc. Chem. Res., 8 (1975) 125-131.

[24]F. Haber, J. Weiss, The Catalytic Decomposition of Hydrogen Peroxide by Iron Salts, Proc. Phys. Soc. London, Sect. A, 147 (1934) 332-351.

[25]G.P. Anipsitakis, D.D. Dionysiou, Radical generation by the interaction of transition metals with common oxidants, Environ. Sci. Technol., 38 (2004) 3705-3712.

[26]C. Liang, C.P. Liang, C.C. Chen, pH dependence of persulfate activation by EDTA/Fe(III) for degradation of trichloroethylene, J. Contam. Hydrol., 106 (2009) 173-182.

[27]C. Liang ,Z.S. Wang, C.J. Bruell, Influence of pH on persulfate oxidation of TCE at ambient temperatures, Chemosphere, 66 (2007) 106-113.

[28]J. Saien, Z. Ojaghloo, A.R. Soleymani, M.H. Rasoulifard, Homogeneous and heterogeneous AOPs for rapid degradation of Triton X-100 in aqueous media via UV light, nano titania hydrogen peroxide and potassium persulfate, Chem. Eng. J., 167 (2011) 172-182.

[29]R.O.C. Norman, P.M. Storey, P.R. West, Electron spin resonance studies. Part XXV. Reactions of the sulphate radical anion with organic compounds, J. Chem. Soc. B, (1970) 1087-1095.

[30]A. Burbano, D.D. Dionysiou, M. Suidan, T. Richardson, Chemical destruction of MTBE using Fenton's Reagent: effect of ferrous iron/hydrogen peroxide ratio Water Sci. Technol., 47 (2003) 165-171.

[31]C. Liang, C.J. Bruell, M.C. Marley, K.L. Sperry, Persulfate oxidation for in situ remediation of TCE. I. Activated by ferrous ion with and without a persulfate-thiosulfate redox couple, Chemosphere, 55 (2004) 1213-1223.

[32]S.Y. Oh, H.W. Kim, J.M. Park, H.S. Park, C. Yoon, Oxidation of polyvinyl alcohol by persulfate activated with heat, Fe2+, and zero-valent iron, J. Hazard. Mater., 168 (2009) 346-351.

[33]O. Wong, Carcinogenicity of trichloroethylene: an epidemiologic assessment, Clin Occup Environ Med, 4 (2004) 557-589.

[34]C.H. Liao, S.F. Kang, Y.W. Hsu, Zero-valent iron reduction of nitrate in the presence of ultraviolet light, organic matter and hydrogen peroxide, Water Res., 37 (2003) 4109-4118.

[35]Z. Qiang, W. Ben, C.P. Huang, Fenton process for degradation of selected chlorinated aliphatic hydrocarbons exemplified by trichloroethylene, 1,1-dichloroethylene and chloroform, Front Environ Sci Eng China., 2 (2008) 397-409.

[36]J.J. Pignatello, D .Liu, P. Huston, Evidence for an additional oxidant in the photoassisted Fenton reaction, Environ. Sci. Technol., 33 (1999) 1832-1839.

[37]K. Li, M.I. Stefan, J.C. Crittenden, Trichloroethene degradation by UV/H 2O 2 advanced oxidation process: Product study and kinetic modeling, Environ. Sci. Technol., 41 (2007) 1696-1703.

[38]Y. Xu, W.X. Zhang, Subcolloidal Fe/Ag particles for reductive dehalogenation of chlorinated benzenes, Ind. Eng. Chem. Res., 39 (2000) 2238-2244.

[39]H.L. Lien, W.X. Zhang, Transformation of chlorinated methanes by nanoscale iron particles, J. Environ. Eng., 125 (1999) 1042-1047.

[40]G.N. Glavee, K.J. Klabunde, C.M. Sorensen, G.C. Hadjipanayis, Chemistry of Borohydride Reduction of Iron(II) and Iron(III) Ions in Aqueous and Nonaqueous Media. Formation of Nanoscale Fe, FeB, and Fe2B Powders, Inorg. Chem., 34 (1995) 28-35.

[41]ASTM-D6889-03, Standard Practice for Fast Screening for Volatile Organic Compounds in Water Using Solid Phase Microextraction (SPME), West Conshohocken, 2003.

[42]B.W. Zhu, T.T. Lim, Catalytic reduction of chlorobenzenes with Pd/Fe nanoparticles: Reactive sites, catalyst stability, particle aging, and regeneration, Environ. Sci. Technol., 41 (2007) 7523-7529.

[43]L. Li, M. Fan, R.C. Brown, J. Van Leeuwen, J. Wang, W. Wang, Y. Song, P. Zhang, Synthesis, properties, and environmental applications of nanoscale iron-based materials: A review, Crit. Rev. Environ. Sci. Technol., 36 (2006) 405-431.

[44]Y.P. Sun, X.Q. Li, J. Cao, W.X. Zhang, H.P. Wang, Characterization of zero-valent iron nanoparticles, Adv. Colloid Interface Sci., 120 (2006) 47-56.

[45]M. Masarwa, H. Cohen, D. Meyerstein, D.L. Hickman, A. Bakac, J.H. Espenson, Reactions of low-valent transition-metal complexes with hydrogen peroxide. Are they fenton-like or not? 1. The case of Cu+ aq and Cr2+ aq, J. Chem. Soc., 110 (1988) 4293-4297.

[46]S. Yang, P. Wang, X. Yang, L. Shan, W. Zhang, X. Shao, R. Niu, Degradation efficiencies of azo dye Acid Orange 7 by the interaction of heat, UV and anions with common oxidants: Persulfate, peroxymonosulfate and hydrogen peroxide, J. Hazard. Mater., 179 (2010) 552-558.

[47]G.P. Anipsitakis, D.D. Dionysiou, Transition metal/UV-based advanced oxidation technologies for water decontamination, Appl Catal B, 54 (2004) 155-163.

[48]D.N. Clausen, I.S. Scarmínio, K. Takashima, Optimization and effects of some electron acceptors on the photocatalytic degradation of direct red 23 azo dye, J Chil Chem Soc, 54 (2009) 289-294.

[49]H. Taube, H. Myers, R.L. Rich, Observations on the mechanism of electron transfer in solution, J. Am. Chem. Soc., 75 (1953) 4118-4119.

[50]L.R. Warren, W.L. Rufus, Mechanisms of Electron Transfer 1st ed., Ronald Press, New York, 1966.

[51]J. Bolton, N. Mataga, G. McLendon, Introduction to Electron Transfer in Inorganic, Organic, and Biological Systems: Electron Transfer in Inorganic, Organic, and Biological Systems, American Chemical Society, 1991.

[52]S. Goldstein, D .Meyerstein, G. Czapski, The Fenton reagents, Free Radical Biol. Med., 15 (1993) 435-445.

[53]S.H. Bossmann, E. Oliveros, S. Göb, S. Siegwart, E.P. Dahlen, L. Payawan Jr, M. Straub, M. Wörner, A.M. Braun, New evidence against hydroxyl radicals as reactive intermediates in the thermal and photochemically enhanced fenton reactions, J. Phys. Chem. A, 102 (1998) 5542-5550.

[54]G.V. Buxton, T.N. Malone, G.A. Salmon, Reaction of SO4•- with Fe2+, Mn2+ and Cu2+ in aqueous solution, J. Chem. Soc. Faraday Trans.2897 2893 (1997) 93 ,.

[55]G.E. Hoag, J.B. Collins, J.L. Holcomb, J.R. Hoag, M.N. Nadagouda, R.S. Varma, Degradation of bromothymol blue by 'greener' nano-scale zero-valent iron synthesized using tea polyphenols, J. Mater. Chem., 19 (2009) 8671-8677.

[56]T. Satapanajaru, P. Anurakpongsatorn, P. Pengthamkeerati, H. Boparai, Remediation of atrazine-contaminated soil and water by nano zerovalent iron, Water, Air, Soil Pollut., 192 (2008) 349-359.

[57]D.M. Cwiertny, S.J. Bransfield, K.J.T. Livi, D.H. Fairbrother, A.L. Roberts, Exploring the Influence of Granular Iron Additives on 1,1,1-Trichloroethane Reduction, Environ. Sci. Tech., 40 (2006) 6837-6843.

[58]F. He, D. Zhao, Hydrodechlorination of trichloroethene using stabilized Fe-Pd nanoparticles: Reaction mechanism and effects of stabilizers, catalysts and reaction conditions, Appl Catal B, 84 (2008) 533-540.

[59]C.J. Lin, S.L. Lo, Y.H. Liou, Dechlorination of trichloroethylene in aqueous solution by noble metal-modified iron, J. Hazard. Mater., 116 (2004) 219-228.

[60]Y.H. Kim, E.R. Carraway, Reductive dechlorination of TCE by zero valent bimetals, Environ. Technol., 24 (2003) 69-75.

[61]J.G. Muller, C.J. Burrows, Metallodrug complexes that mediate DNA and lipid damage via sulfite autoxidation: copper(II) famotidine and iron(III) bis(salicyglycine), Inorg. Chim. Acta, 275–276 (1998) 314-319.

[62]G.A. McLachlan, J.G. Muller, S.E. Rokita, C.J. Burrows, Metal-mediated oxidation of guanines in DNA and RNA: a comparison of cobalt(II), nickel(II) and copper(II) complexes, Inorg. Chim. Acta, 251 (1996) 193-199.

[63]J.G. Muller, R.P. Hickerson, R.J. Perez, C.J. Burrows, DNA Damage from Sulfite Autoxidation Catalyzed by a Nickel(II) Peptide, J. Am. Chem. Soc., 119 (1997) 1501-1506.

Chapter 4:

1. C. Liang, Y. C. Chien and Y. L. Lin, *Soil Sediment Contam*, 2012, **21**, 701-719.
2. X. Xu and N. R. Thomson, *Soil Sediment Contam*, 2010, **19**, 602-616.
3. R. L. Valentine and H. C. Ann Wang, *J. Environ. Eng.*, 1998, **124**, 31-38.
4. E. Lipczynska-Kochany, G. Sprah and S. Harms, *Chemosphere*, 1995, **30**, 9-20.
5. F. J. Beltrán, M. González, F. J. Rivas and P. Alvarez, *Water, Air, Soil Pollut.*, 1998, **105**, 685-700.
6. K. G. Mumford, C. S. Lamarche and N. R. Thomson, *J. Environ. Eng.*, 2004, **130**, 1139-1146.
7. R. Mikutta, M. Kleber, K. Kaiser and R. Jahn, *Soil Sci. Soc. Am. J.*, 2005, **69**, 120-135.
8. G. W. Robinson, *Journal of Agricultural Research* 1927, **34**, 339–356.
9. G. W. Robinson and J. O. Jones, *J. Agric. Sci.*, 1925, **15**, 26-29
10. H. Cuypers, T. Grotenhuis, J. Joziasse and W. Rulkens, *Environ. Sci. Technol.*, 2000, **34**, 2057-2063.

11. F. Martin and F. J. Gonzalez-Vila, *Soil Biol. Biochem.*, 1984, **16**, 207-210.

12. K. Eusterhues, C. Rumpel, M. Kleber and I. Kögel-Knabner, *Org. Geochem.*, 2003, **34**, 1591-1600.

13. K. R .Weeks, C. J. Bruell and N. R. Mohanty, *Journal of Soil Contamination*, 2000, **9**, 331 - 345.

14. C. J. Spencer, P. C. Stanton and R. J. Watts, *J. Air Waste Manage. Assoc.*, 1996, **46**, 1067-1074.

15. A. Romero, A. Santos, F. Vicente, S. Rodriguez and A. L. Lafuente, *J. Hazard. Mater.*, 2009, **170**, 627-632.

16. C. Liang, Z. S. Wang and N. Mohanty, *Sci. Total Environ.*, 2006, **370**, 271-277.

17. L. R. Bennedsen, J. Muff and E. G. Søgaard, *Chemosphere*, 2012, **86**, 1092-1097.

18. X. Xu, University of Waterloo, 2006.

19. W. Lee and B. Batchelor, *Chemosphere*, 2004, **55**, 705-713.

20. C. Mouvet, D. Barberis and A. C. M. Bourg, *Journal of Hydrology*, 1993, **149**, 163-182.

21. ASTM-D6889-03, West Conshohocken., 2003.

22. C. J. Liang, C. J. Bruell, M. C. Marley and K. L .Sperry, *Soil Sediment Contam*, 2003, **12**, 207 - 228.

23. M. E. Lindsey and M. A. Tarr, *Water Res.*, 2000, **34**, 2385-2389.

24. M. E. Lindsey and M. A. Tarr, *Environ. Sci. Technol.*, 2000, **34**, 444-449.

25. W. P. Kwan and B. M. Voelker, *Environ. Sci. Technol* ., 2003, **37**, 1150-1158.

26. R. J. Watts and A. L. Teel, *J. Environ. Eng.*, 2005, **131**, 612-622.

Chapter 5:

APHA, 1989. Standard methods for the examination of water and wastewater. Washington, D. C.

Armstrong, S. and Green, L., 2004. Chlorinated hydrocarbon solvents. Clin Occup Environ Med, 4(3): 481-496

ASTM-D6889-03, 2003. Standard Practice for Fast Screening for Volatile Organic Compounds in Water Using Solid Phase Microextraction) SPME), West Conshohocken.

Bennett, P., He, F., Zhao, D., Aiken, B. and Feldman, L., 2010. In situ testing of metallic iron nanoparticle mobility and reactivity in a shallow granular aquifer. J. Contam. Hydrol., 116(1-4): 34-46.

Cantrell, K.J. and Kaplan, D.I., 1997. Zero-Valent Iron Colloid Emplacement in Sand Columns. J. Environ. Eng., 123(5) 499-505.

Choi, K. and Lee, W., 2012. Enhanced degradation of trichloroethylene in nano-scale zero-valent iron Fenton system with Cu(II). J. Hazard. Mater., 211-212: 146-153.

Cuypers, H., Grotenhuis, T., Joziasse, J. and Rulkens, W., 2000. Rapid persulfate oxidation predicts PAH bioavailability in soils and sediments. Environ. Sci. Technol., 34(10): 2057-2063.

Elliott, D.W. and Zhang, W.X., 2001. Field assessment of nanoscale bimetallic particles for groundwater treatment. Environ. Sci. Technol., 35(24) 4922-4926.

Furukawa, Y., Kim, J.W., Watkins, J. and Wilkin, R.T., 2002. Formation-of ferrihydrite and associated iron corrosion products in permeable reactive barriers of zero-valent iron. Environ. Sci. Technol., 36(24): 5469-5475.

He, F., Zhao, D. and Paul, C., 2010. Field assessment of carboxymethyl cellulose stabilized iron nanoparticles for in situ destruction of chlorinated solvents in source zones. Water Res., 44(7): 2360-2370.

Huling, S.G. and Pivetz, B.E., 2006. Engineering Issue Paper: In-Situ Chemical Oxidation August, U.S. EPA, Washington.

Jiemvarangkul, P., Zhang, W.X. and Lien, H.L., 2011. Enhanced transport of polyelectrolyte stabilized nanoscale zero-valent iron (nZVI) in porous media. Chem. Eng. J., 170(2-3): 482-491.

Kanel, S., Nepal, D., Manning, B. and Choi, H., 2007a. Transport of surface-modified iron nanoparticle in porous media and application to arsenic(III) remediation. J. Nanopart. Res., 9(5): 725-735.

Kanel, S.R., Goswami, R.R., Clement, T.P., Barnett, M.O. and Zhao, D., 2007b. Two Dimensional Transport Characteristics of Surface Stabilized Zero-valent Iron Nanoparticles in Porous Media. Environ. Sci. Technol., 42(3): 896-900.

Kester, J.E. and Clewell, H.J., 2004. The perils and promise of modern risk assessment: the example of trichloroethylene. Clin Occup Environ Med, 4(3): 497-512.

Li, K., Stefan, M.I. and Crittenden, J.C., 2007. Trichloroethene degradation by UV/H 2O 2 advanced oxidation process: Product study and kinetic modeling. Environ. Sci. Technol., 41(5): 1696-1703.

Liang, C., Huang, C.-F., Mohanty, N. and Kurakalva, R.M., 2008a. A rapid spectrophotometric determination of persulfate anion in ISCO. Chemosphere, 73(9) 1540-1543.

Liang, C. and Lai, M.C., 2008. Trichloroethylene degradation by zero valent iron activated persulfate oxidation. Enviro. Eng. Sci., 25(7): 1071-1077.

Liang, C., Lee, I.L., Hsu, I.Y., Liang, C.P. and Lin, Y.L., 2008b. Persulfate oxidation of trichloroethylene with and without iron activation in porous media. Chemosphere, 70(3): 426-435.

Liang, C., Liang, C.P. and Chen, C.C., 2009. pH dependence of persulfate activation by EDTA/Fe(III) for degradation of trichloroethylene. J. Contam. Hydrol., 106(3-4): 173-182.

Liang, C., Wang, Z.S. and Bruell, C.J., 2007. Influence of pH on persulfate oxidation of TCE at ambient temperatures. Chemosphere, 66(1): 106-113.

Liao, C.J., Chung, T.L., Chen, W.L. and Kuo, S.L., 2007. Treatment of pentachlorophenol-contaminated soil using nano-scale zero-valent iron with hydrogen peroxide. J. Mol. Catal. A: Chem., 265(1-2): 189-194.

Lin, Y.-H., Tseng, H.-H., Wey, M.-Y. and Lin, M.-D., 2010. Characteristics of two types of stabilized nano zero-valent iron and transport in porous media. Sci. Total Environ., 408(10): 2260-2267.

Norman, R.O.C., Storey, P.M. and West, P.R., 1970. Electron spin resonance studies. Part XXV. Reactions of the sulphate radical anion with organic compounds. J. Chem. Soc. B: 1087-1095.

NRC, 1999. Groundwater and Soil Cleanup: Improving Management of Persistent Contaminants. National Acadmy press, Washington, D.C.

O'Carroll, D., Sleep, B., Krol, M., Boparai, H. and Kocur, C., 2012. Nanoscale zero valent iron and bimetallic particles for contaminated site remediation. Advances in Water Resources. (in press).

Oh, S.-Y., Kang, S.-G. and Chiu, P.C., 2010. Degradation of 2,4-dinitrotoluene by persulfate activated with zero-valent iron. Sci. Total Environ., 408(16): 3464-3468.

Phenrat, T. et al., 2010. Transport and deposition of polymer-modified Fe0 nanoparticles in 2-D heterogeneous porous media: Effects of particle concentration, Fe0 content, and coatings. Environ. Sci. Technol., 44(23): 9086-9093.

Phenrat, T. et al., 2009. Particle Size Distribution ,Concentration, and Magnetic Attraction Affect Transport of Polymer-Modified Fe0 Nanoparticles in Sand Columns. Environ. Sci. Technol., 43(13): 5079-5085.

Pignatello, J.J., Liu, D. and Huston, P., 1999. Evidence for an additional oxidant in the photoassisted Fenton reaction. Environ. Sci. Technol., 33(11): 1832-1839.

Qiang, Z., Ben, W. and Huang, C.P., 2008. Fenton process for degradation of selected chlorinated aliphatic hydrocarbons exemplified by trichloroethylene, 1,1-dichloroethylene and chloroform . Front Environ Sci Eng China., 2(4): 397-409.

Ravikumar, J.X. and Gurol, M.D., 1994. Chemical oxidation of chlorinated organics by hydrogen peroxide in the presence of sand. Environ. Sci. Technol., 28(3): 394-400.

Raychoudhury, T., Naja, G. and Ghoshal, S,. 2010 Assessment of transport of two polyelectrolyte-stabilized zero-valent iron nanoparticles in porous media. J. Contam. Hydrol., 118(3-4): 143-151.

Saleh, N. et al., 2008. Ionic Strength and Composition Affect the Mobility of Surface-Modified Fe0 Nanoparticles in Water-Saturated Sand Columns. Environ. Sci. Technol., 42(9): 3349-3355.

Saleh, N. et al., 2007. Surface Modifications Enhance Nanoiron Transport and NAPL Targeting in Saturated Porous Media. Environ Eng Sci, 24(1): 45-57.

Schmidt, L.D., 2004. The Engineering of Chemical Reactions. Oxford University Press, New York.

Schrick, B., Hydutsky, B.W., Blough, J.L. and Mallouk, T.E., 2004. Delivery Vehicles for Zerovalent Metal Nanoparticles in Soil and Groundwater. Chem. Mater., 16(11) 2187-2193.

Schroth, M.H., Oostrom, M., Wietsma, T.W. and Istok, J.D., 2001. In-situ oxidation of trichloroethene by permanganate: effects on porous medium hydraulic properties. J. Contam. Hydrol., 50(1-2): 79-98.

Shafieiyoun, S., Ebadi, T., Nikazar ,M.,, 2012. Treatment of Landfill Leachate by Fenton Process with Nano sized Zero Valent Iron particles. Int. J. Environ. Res., 6(1): 119-128.

Shu, H.Y., Chang, M.C. and Chang, C.C., 2009. Integration of nanosized zero-valent iron particles addition with UV/H2O2 process for purification of azo dye Acid Black 24 solution. J. Hazard. Mater., 167(1-3): 1178-1184.

Siegrist, R.L., Crimi, M. and Simpkin, T.J., 2011. In situ Chemcial Oxidation for Groundwater Remediation Springer, New York.

Sra, K.S., Thomson, N.R. and Barker, J.F., 2010. Persistence of Persulfate in Uncontaminated Aquifer Materials. Environ. Sci. Technol., 44(8): 3098-3104.

Thiruvenkatachari, R., Vigneswaran, S. and Naidu, R., 2008. Permeable reactive barrier for groundwater remediation. J. Ind. Eng. Chem., 14(2): 145-156.

USEPA, 2009. IRIS Toxicological Review of Trichloroethylene, Washington, DC.

Wei, Y.-T. et al., 2010. Influence of nanoscale zero-valent iron on geochemical properties of groundwater and vinyl chloride degradation: A field case study. Water Res., 44(1): 131-140.

Wernke, M. and Schell, J., 2004. Solvents and malignancy. Clin Occup Environ Med, 4(3): 513–527.

Wong, O., 2004. Carcinogenicity of trichloroethylene: an epidemiologic assessment. Clin Occup Environ Med, 4(3): 557-589.

Xu, L. and Wang, J., 2011. A heterogeneous Fenton-like system with nanoparticulate zero-valent iron for removal of 4-chloro-3-methyl phenol. J. Hazard. Mater., 186(1): 256-264.

Xu, X., 2006. Interaction of Chemical Oxidants with Aquifer Materials, University of Waterloo, Waterloo.

Zhan, J. et al., 2008. Transport Characteristics of Nanoscale Functional Zerovalent Iron/Silica Composites for in Situ Remediation of Trichloroethylene. Environ. Sci. Technol., 42(23): 8871-8876.

Appendices

Appendix A

The Background Literature

A.1. In Situ Chemical Oxidation (ISCO)

In situ chemical oxidation, simply, is defined as using chemical oxidizing reagents to treat contaminated aquifers (Siegrist, 2000). One of the earliest applications of ISCO was in 1985 by Kubarewicz et al. when they employed Fenton's reagent to oxidize some explosive materials in the subsurface (e.g., TNT) (Tyre et al., 1991). Likewise, Watts et al. (1990) used Fenton's reagent to treat some organic compounds (i.e., pentachlorophenol). Gonullu and Farquhar (1989) used potassium permanganate ($KMnO_4$) to treat TCE contaminated soils.

Chemical oxidation technology's roots go back to 1894 when Fenton observed a color change (to a violet color) after mixing Tartaric (or racemic acids) with H_2O_2 and ferrous sulphate. As a consequence, he concluded that iron salts act as "a catalyst" for the reaction [after that date, the reaction was called Fenton's reaction, and the reagent was called Fenton's reagent] (Fenton, 1894). Since then chemical oxidation technology has developed along three parallel lines: (1) *generation and application of free radicals,* (2) *use of alternative oxidants, and* (3) *discovery and development of alternative activators* [as discussed in this chapter].

A.2. Free Radicals

A.2.1. Free Radical Generation

Bary and Gorin (1932) pointed out that an intermediate tetravalent iron "ferryl iron" FeO^{2+} could be produced during Fenton's reaction as given by

$$Fe^{2+} + H_2O_2 \longrightarrow FeO^{2+} + H_2O \qquad (A.1)$$

$$FeO^{2+} + H_2O_2 \longrightarrow Fe^{2+} + H_2O + O_2 \qquad (A.2)$$

Haber and Weiss (1934) found that free radicals and anions such as $OH^{\bullet}$ (hydroxyl free radical), $HO_2^{\bullet}$ (perhydroxyl radical), and HO_2^- (hydroperoxyde anion) could be generated from Fenton's reaction

$$Fe^{2+} + H_2O_2 \longrightarrow Fe^{3+} + HO^{\bullet} + HO^- \quad (A.3)$$

$$OH^{\bullet} + H_2O_2 \longrightarrow H_2O + HO_2^{\bullet} \quad (A.4)$$

$$HO_2^{\bullet} + H_2O_2 \longrightarrow O_2 + H_2O + HO^{\bullet} \quad (A.5)$$

$$HO^{\bullet} + Fe^{2+} \longrightarrow Fe^{3+} + HO^- \quad (A.6)$$

Particularly, the hydroxyl free radical ($HO^{\bullet}$) is a strong oxidant with an oxidation potential of 2.8v (Tsai et al., 2008; Walling, 1975).

A.2.2. Free Radical Reactivity with Organics

Merz and Waters (1947; 1949a; 1949b) studied the mechanisms of the hydroxyl free radical reactions with organic compounds (HR) (e.g., alcohols, phenols, and aromatic compounds), which can be described by

$$HO^{\bullet} + HR \longrightarrow H_2O + R^{\bullet} \quad (A.7)$$

$$R^{\bullet} + H_2O_2 \longrightarrow ROH + HO^{\bullet} \quad (A.8)$$

$$R^{\bullet} + HO^{\bullet} \longrightarrow ROH \quad (A.9)$$

$$2R^{\bullet} \longrightarrow \text{Inert products} \quad (A.10)$$

Barb et al. (1951) concluded that the ferric ion (Fe^{3+}) might react to regenerate ferrous ion Fe^{2+}, which is the main reaction catalyst; thus, ferric and ferrous ion are "different aspects of the same system", but the kinetics of the reaction from Fe^{2+} to Fe^{3+} is much faster than from Fe^{3+} to Fe^{2+}. Walling and Kato (1971) and Walling and Jonson (1975) indicated that there are three reaction pathways for the hydroxyl free radical to react with organic compounds: 1) oxidation by

Fe^{3+}, 2) dimeration to yield inert products, and 3) reduction by Fe^{2+} (where R_1, R_2, and R_3 are the first, the second, and the third pathway, respectively) as expressed by

$$\begin{aligned} R_1H + HO^{\bullet} &\longrightarrow R_1^{\bullet} + H_2O \\ R_2H + HO^{\bullet} &\longrightarrow R_2^{\bullet} + H_2O \\ R_3H + HO^{\bullet} &\longrightarrow R_3^{\bullet} + H_2O \end{aligned} \qquad \text{(A.11)}$$

$R_1^{\bullet}$ is oxidized to generate Fe^{2+}:

$$R^{\bullet} + Fe^{3+} \longrightarrow R^{+} + Fe^{2+} \qquad \text{(A.12)}$$

$R_2^{\bullet}$ is dimerized (not oxidized) to give:

$$R^{\bullet} + R^{\bullet} \longrightarrow 2\,R \qquad \text{(A.13)}$$

$R_3^{\bullet}$ reacts with ferrous ion (Fe^{2+}) instead of ferric ion (Fe^{3+}) and therefore it generates (R_3H), again, after the hydrolysis. The following demonstrates this pathway:

$$R^{\bullet} + Fe^{2+} \longrightarrow R^{-} + Fe^{3+} \qquad \text{(A.14)}$$

$$R^{-} + H_2O \longrightarrow RH + HO^{-} \qquad \text{(A.15)}$$

Walling and Johnson (1975) improved the understanding of the oxidation of aromatic compounds (e.g., benzene and toluene) by Fenton's reagent. The hydroxyl free radical can attack the aromatic compounds by three pathways:

$$HO^{\bullet} + \text{Substrate} \begin{cases} \longrightarrow R_1^{\bullet} \xrightarrow{Fe^{3+}} \text{Product} + Fe^{2+} \\ \longrightarrow R_2^{\bullet} \longrightarrow \text{Dimerization} \\ \longrightarrow R_3^{\bullet} \xrightarrow{Fe^{2+}} \text{Product} + Fe^{3+} \end{cases} \qquad \text{(A.16)}$$

Later studies showed that in the presence of organic compounds with Fenton's reagent, the reaction could form the alkoxyl free radical ($RO^{\bullet}$) and other organic free radicals such as $RO_2^{\bullet}$ and $RCO_2^{\bullet}$. These organic free radicals can also destroy organic compounds (Goldstein et al., 1993).

Recently, activated hydrogen peroxide propagations (CHP) technique has been employed to generate free radicals (non-hydroxyl free radical) from Fenton reagent such as perhydroxyl radical ($HO_2^{\bullet}$); which is a weak oxidant, hydroperoxide anion (HO_2^-); which is a strong nucleophile, and superoxide radical anion ($O_2^{\bullet -}$); which is a weak reductant. The generation of these free radicals and anions from Fenton's reagent is displayed in equation A4, A18, and A19 (Watts and Teel, 2005; Watts and Teel, 2006). CHP is a modified Fenton's reagent that uses high hydrogen peroxide concentrations (1-4 M) (Smith et al., 2009). These free radical species can oxidize organic compounds. For example, superoxide radical anion ($O_2^{\bullet -}$) can oxidize a variety of organic compounds in aqueous solutions (particularly PCE, TCE, poly chlorinated biphenyls (PCBs), and polychlorinated dibenzo-p-dioxins (PCDDs)) (Furman et al., 2010; Smith et al., 2009).

$$HO_2^{\bullet} \longleftrightarrow O_2^{\bullet -} + H^+ \qquad \text{(A.17)}$$

$$HO_2^{\bullet} + Fe^{2+} \longrightarrow Fe^{3+} + HO_2^- \qquad \text{(A.18)}$$

In 1975, in wastewater treatment, CHP technique used to oxidize organic compounds by Sato et al. (1975) without realizing the potential of the other free radical species (non-hydroxyl free radical). High H_2O_2 concentration is used by many others (Tyre et al., 1991; Watts et al., 1993; Watts et al., 1990) to oxidize many types of organic compounds (e.g., PCP, dodecylbenzenesulfonate, phenols, and polyvinyl alcohol) (Watts and Teel, 2005). Watts and Teel, (2005) highlighted the role of the other free radical species, which is generated from CHP, to oxidize organic compounds.

A.3. Alternative Oxidants

In 1894, Fenton performed other experiments with five different oxidizing reagents rather than hydrogen peroxide: chlorine water (1.3v), hypochlorites (ClO^-) (1.49v), barium peroxide

(BaO_2), sodium peroxide (Na_2O_2), and potassium permanganate ($KMnO_4$) (1.7v). The results showed that they were less able to treat organic compounds compared with hydrogen peroxide (Fenton, 1894).

Recently, many other oxidants have been used such as chlorine dioxide (ClO_2) (1.57v), calcium peroxide (CaO_2) (0.9v), peroxymonosulfate (HSO_5^-) (Osgerby, 2006), percarbonate (Kelley and Koenigsberg, 2006), peroxydisulfate ($S_2O_8^{2-}$) (House, 1962; Tsai et al., 2008), periodate (IO_4^-) and bromate (BrO_3^-) (Anipsitakis and Dionysiou, 2004).

The oxidation processes for these oxidants are divided into two categories: (1) the primary oxidation process, which relies mainly on the power of the oxidant to degrade organic compounds, and (2) the advanced oxidation process, which relies primarily on the generation of the free radicals to degrade organic compounds. For example, permanganate is not a radical based oxidant or not a catalytic-oxidant and does not generate free radicals (primary oxidation processes), while hydrogen peroxide is considered a radical based oxidant (advanced oxidation processes) (Osgerby, 2006).

Ozone (O_3), which is a gas phase oxidant, has showed a good ability to treat organic compounds (Fenton, 1894) especially, when it is coupled with hydrogen peroxide (peroxone) (Osgerby, 2006). Unfortunately, the heterogeneous oxidation reactions are beyond the scope of this research which includes hydrogen peroxide, persulfate, and peroxymonosulfate.

A.3.1. Persulfate as an Oxidant

In 1878, persulfate was discovered by Berthelot, and 17 years later, Elbs and Schenhere (1895) reported that persulfate is not a stable compound in aqueous solutions (Kolthoff and Miller, 1951). Merz and Waters (1947) used sodium persulfate as an oxidant with ferrous salts to treat alcohols, with results similar to those observed with Fenton's reagent. Merz and Waters

(1947) also described the reaction mechanism of (persulfate/ferrous salts/organics) as the following [Kolthoff et al. (1951) indicated the same reaction mechanism]:

$$Fe^{2+} + S_2O_8^{2-} \longrightarrow Fe^{3+} + SO_4^{2-} + SO_4^{-\bullet} \quad \text{(A.19)}$$

$$Fe^{2+} + SO_4^{-\bullet} \longrightarrow Fe^{3+} + SO_4^{2-} \quad \text{(A.20)}$$

$$SO_4^{-\bullet} + R\text{-}CH_2OH \longrightarrow HSO_4^{-} + R\text{-}^{\bullet}CH\text{-}OH \quad \text{(A.21)}$$

$$S_2O_8^{2-} + R\text{-}^{\bullet}CH\text{-}OH \longrightarrow HSO_4^{-} + SO_4^{-\bullet} + R\text{-}CHO \quad \text{(A.19)}$$

Five years later (1952), Latimer found that the persulfate anion has a high redox potential (2.01v), which is higher than hydrogen peroxide (1.87v). Also, the sulfate free radical ($SO_4^{-\bullet}$) is a strong oxidant (2.6v), which is close to hydroxyl free radical ($HO^{\bullet}$) (2.78v) (Liang et al., 2004).

House (1962) indicated that the hydroxyl free radical and sulfate free radical can be generated from persulfate according to

$$S_2O_8^{-2} \longrightarrow 2SO_4^{-\bullet} \quad \text{(A.20)}$$

$$SO_4^{-\bullet} + H_2O \longrightarrow HSO_4^{-} + OH^{\bullet} \quad \text{(A.21)}$$

$$S_2O_8^{-2} + OH^{\bullet} \longrightarrow HSO_4^{-} + SO_4^{-\bullet} + \tfrac{1}{2}\, O_2 \quad \text{(A.22)}$$

$$SO_4^{-\bullet} + OH^{\bullet} \longrightarrow HSO_4^{-} + \tfrac{1}{2}\, O_2 \quad \text{(A.23)}$$

Norman et al. (1970) and Neta et al. (1977) studied the reaction mechanisms between the sulfate free radical and the organic compounds, and they suggested two pathways: 1) an electron abstraction (electron transfer from the saturated carbon to the sulfate free radical), and 2) an addition to saturated or unsaturated carbon followed by hydrolysis.

Liang et al. (2007) pointed out that by using radical scavenging tests, the hydroxyl free radical dominates under basic conditions (pH= 9) while the sulfate free radical predominates under acidic conditions (pH= 4). The analogy between the two free radicals is that both of them can degrade organic compounds. The hydroxyl free radical is non-selective while the sulfate free

radical is more selective (Osgerby, 2006; Tsai et al., 2008; Watts and Teel, 2006). In addition, persulfate has gained a considerable attention in ISCO in the past decade because of its stability potential (Dahmani et al., 2006; Hoag et al., 2000; Hoag et al., 2002; Liang et al., 2003; Sra et al., 2010).

A.3.2. Peroxymonosulfate (PMS) as an Oxidant

PMS, an alternative oxidant, was observed in 1898 by Caro (so called Caro's acid) (Kolthoff and Miller, 1951). In 1920, Palinic indicated that PMS is an intermediate in persulfate decomposition (Kolthoff and Miller, 1951). Later work showed the following possible reactions for activated PMS (Anipsitakis and Dionysiou, 2003; Anipsitakis and Dionysiou, 2004):

$$M^{n+} + HSO_5^- \longrightarrow M^{(n+1)+} + SO_4^{-\bullet} + HO^- \quad \text{(A.24)}$$

or

$$M^{n+} + HSO_5^- \longrightarrow M^{(n+1)+} + SO_4^{-2} + HO^{\bullet} \quad \text{(A.25)}$$

or

$$M^{(n+1)+} + HSO_5^- \longrightarrow M^{n+} + SO_5^{-\bullet} + H^+ \quad \text{(A.29)}$$

where M^{n+} is a transition metal. Ball and Edwards (1956) indicated that the redox potential for the peroxymonosulfate free radical ($SO_5^{-\bullet}$) (1.1v) is lower than that for $SO_4^{-\bullet}$ (2.5-3.0v) (Anipsitakis and Dionysiou, 2003). Anipsitakis and Dionysiou (2004) compared the ability of three oxidants ($K_2HSO_5/KHS_2O_8/H_2O_2$) activated by different metal activators to decompose organic compounds, and the results showed that PMS is a promising oxidant.

A.4. Alternative Activators

Free radicals can be generated from the different oxidizing reagents by eight different techniques, which are called advanced oxidation processes (AOPs): (1) photochemical activation

(Haber and Weiss, 1934), (2) radiolysis activation (Goldstein et al., 1993), (3) thermal activation (House, 1962), (4) ozone activation (Osgerby, 2006; Tsai et al., 2008), (5), transition metal activation (Anipsitakis and Dionysiou, 2003; Fenton, 1894; Goldstein et al., 1993; House, 1962; Kolthoff et al., 1951; Merz and Waters, 1947; Smith et al., 2009), (6) activated carbon activation (Liang et al., 2009), (7) peroxide activation (Boulos et al., 2008; Crimi and Taylor, 2007; Goi and Trapido, 2010), and (8) high pH activation (Siegal et al., 2009; Yukselen-Aksoy et al., 2010).

Many of these AOPs have the potential to treat organic compounds; however, in this work, we are focusing on the activation processes by transition metals without supported by, or coupling with, other activation processes (e.g., hv, O_3, thermal, and radiolysis).

A.5. Activation of Oxidants by Transition Metals

The activation process by transition metals can involve: (1) use of metal complexes and chelates (e.g., iron oxides, Fe^{2+}-EDTA), (2) use of different types of metals (e.g., Cu, Ni, Ag.) (3) use of different sizes of metals (e.g., granular, nano-scale, micro-scale), and (4) use of different forms of metals (e.g., iron salts (soluble form), iron metals (powder form)).

Different chelates (or metal complexes) provides different solubility for the metals in the solution. Fenton (1894) employed ferrous sulfate as an activator for H_2O_2. Fenton and Jones (1900) used different ferrous salts (ferrous sulphate and ferrous acetate), and concluded that both forms were able to achieve the desired reaction (without any comment on which one is faster or stronger). In 1934, Haber and Weiss used Fe^{+2}-EDTA to activate H_2O_2 (Luzzatto et al., 1995). Luzzatto et al. (1995) compared the activation ability for four iron complexes with H_2O_2 (Fe^{2+}-EDTA, Fe^{2+}-HEDTA, Fe^{2+}-TCMA, and Fe^{2+}-NTA).

Different types of metals have different activation ability toward oxidants. Milas (1937) used vanadium pentaoxide (V_2O_5) and chromium trioxide (CrO_3) to activate H_2O_2 to treat organic compounds (e.g., BTEX, naphthalene). Dixon and Norman (1962) coupled tri-valent titanium (Ti^{3+}) with H_2O_2 to generate free radicals (e.g., $OH^{\bullet}$) as shown by

$$Ti^{3+} + H_2O_2 \longrightarrow Ti^{4+} + HO^- + HO^{\bullet} \quad \text{(A.26)}$$

Cr^{2+}, V^{4+} as well as Ti^{+3} were employed to activate H_2O_2. The results showed that the organic compound reaction rate by chromium activated H_2O_2 was higher than those for titanium or vanadium activated H_2O_2 (Samuni et al., 1972).

The oxidation states of the activators can play an important role in improving the activation processes. Iron was used as an activator for H_2O_2 in its higher oxidation states like FeO_4^{2-}, FeO_4^{3-}, and FeO_4^{4-} (Bielski, 1991). Goldstein et al. (1993) indicated that a number of metal ions were used with H_2O_2 in their lower oxidation states like mono-valent copper (Cu^{1+}) and di-valent cobalt (Co^{2+}). In contrast, other metals were used in their higher oxidation states such as Ce^{4+}, U^{4+}, Ag^{2+}, Mn^{3+}, Co^{3+} (Goldstein et al. 1993). In terms of free radical generation, most of these metal ions in their higher oxidation states decompose H_2O_2 to $HO_2^{\bullet}$, which is less able to oxidize organic compounds compared to $HO^{\bullet}$.

Ferrous ion is the most popular metal in chemical oxidation with H_2O_2 (Barb et al., 1951; Bray and Gorin, 1932; Fenton, 1894; Fenton and Jones, 1900; Haber and Weiss, 1934; Merz and Waters, 1947; Merz and Waters, 1949a; Merz and Waters, 1949b), persulfate (Anipsitakis and Dionysiou, 2004; Balazs et al., 2000; Kolthoff et al., 1951; Kolthoff and Miller, 1951; Merz and Waters, 1947), peroxymonosulfate (Ball and Edwards, 1956) and other oxidants (Fenton, 1894)

The first activation of persulfate was by silver ion in 1900 (without organic compounds in the reaction) by Marshall (Walling and Camaioni, 1978). A number of metal ions have been

coupled with persulfate to treat organic substances: Ag^{1+}, Cu^{2+}, Mn^{2+}, Ce^{3+} (House, 1962), Co^{2+} (Balazs et al., 2000) Ni^{2+}, Fe^{3+}, and Ru^{3+} (Anipsitakis and Dionysiou, 2004). In addition, peroxymonosulfate was activated to yield free radicals using different metal ions: Fe^{2+} (Ball and Edwards, 1956), Co^{2+}, Ru^{3+} (Anipsitakis and Dionysiou, 2003), Ag^{1+}, and Fe^{3+} (Anipsitakis and Dionysiou, 2004).

Balazs et al. (2000) compared five metal ions as activators for persulfate to treat organic compounds and found that the treatment effectiveness of these metal ions was as the following Ag >> Co > Cu > Fe > Pt. Anipsitakis and Dionysiou (2004) investigated the decomposition of the organic compound, 2,4-dichlorophenol, by employing nine metal ions (i.e., Fe^{2+}, Fe^{3+}, Co^{2+}, Ru^{3+}, Ag^{1+}, Ce^{2+}, V^{3+}, Mn^{2+}, and Ni^{2+}) with three oxidants (i.e., H_2O_2/persulfate/PMS). They pointed out that Co^{2+} showed the best performance with PMS, Fe^{2+} with H_2O_2 , and Ag^{1+} with persulfate.

A.6. Chemical Reduction Using Metals

Chemical reduction technology is defined as employing a metal (e.g., iron, nickel or zinc) to degrade organic substances. To illustrate, metals, electron donors (electron-rich), provide electrons to organic compounds in order to degrade them (Satapanajaru et al., 2008). To be more specific, the reaction between a chlorinated compound ($C_xH_yCl_z$) and iron in aqueous solutions can be shown as the following (Zhang et al., 1998b):

$$C_xH_yCl_z + zH^+ + zFe^0 \longrightarrow C_xH_{y+z} + zFe^{2+} + zCl^- \qquad (A.27)$$

Iron reduction technology roots go back to 1925 when Rhodes and Carty (1925) reported that organic compounds (particularly carbon tetrachloride) can degrade metals (e.g., Al, Cu, Ni), and they found that copper and bronze were more sensitive (for loss) with organic compounds.

Sweeny and Fischer (1972) used metallic zinc to decompose halogenated pesticides (e.g., DDT, chlordane, and lindane). In 1988, Senzaki indicated that PCE and TCE can be treated by iron powder (Reynolds et al., 1990). Reynolds et al. (1990) evaluated the potential loss of organic compounds, TCE, by metals, and found that some of these metals could treat organic compounds. In 1992, Gillham and O'Hannesin pointed out that aluminum and copper could also be used to decompose organic compounds (Gillham and O'Hannesin, 1994).

Gillham and O'Hannesin (1994) concluded that zero-valent iron (ZVI) efficiently degrades 13 of 14 organic compounds (e.g., tetrachloroethylene (PCE), trichloroethylene (TCE), dichloroethylene (DCE), and vinyl chloride (VC)). Unlike Fe^{2+} and Fe^{3+} oxides, ZVI is a manufactured material (Li et al., 2006b). This early work formed the foundation of permeable reactive barrier (PRB) technology.

A.6.1. Iron Powder or Iron Salts

Using metal iron (iron powder), rather than iron salts (e.g., ferrous sulfate and Fe(II)EDTA), as an activator for oxidizing reagents is a new approach. Tang and Chen (1996) found that H_2O_2/iron powder is more effective to degrade organic compounds (particularly with three types of dyes) than H_2O_2/iron salts. Lücking et al. (1998) evaluated the decomposition of 4-chlorophenol by three various methods (H_2O_2/iron powder, H_2O_2/graphite, and H_2O_2/activated carbon). The results showed that the decomposition of 4-chlorophenol using H_2O_2/iron powder was much faster than the two other methods.

A.6.2. Zero-Valent Iron (ZVI) as an Activator

Doong and Chang (1998) applied a novel method by combining UV/H_2O_2 with zero-valent iron (Fe^0) to treat pesticides, and they found that Fe^0/UV/H_2O_2 could increase the removal of pesticides faster than UV/H_2O_2 and similar to Fe^{2+}/UV/H_2O_2.

A Fe^0/H_2O_2 system was used to treat MTBE in aqueous solutions, and the results showed that Fe^0/H_2O_2 was able to degrade over 99% of MTBE within a short period (10 min) (Bergendahl and Thies, 2004). Bremner et al. (2006) indicated that phenols were treated effectively by Fe^0/H_2O_2. Liang and Lai (2008) employed ZVI with persulfate, rather than H_2O_2, in order to generate the sulfate free radical to treat TCE. They reported that the reaction was fast and the decomposition of TCE was effective. Oh et al. (2009) investigated the oxidation of Polyvinyl alcohol using both Fe^0/ $S_2O_8^{2-}$ and Fe^{+2}/ $S_2O_8^{-2}$. They concluded that Fe^0/ $S_2O_8^{2-}$ is more effective than Fe^{2+}/ $S_2O_8^{2-}$.

In aqueous solutions, ZVI corrosion releases Fe^{2+} into the solution by three mechanisms. Equations (A33) and (A34) display the corrosion of ZVI in aerobic and anaerobic conditions, respectively (Furukawa et al., 2002). Equation (A35) shows the direct corrosion of ZVI by persulfate (Liang and Lai, 2008). Fe^{2+} reacts with the sulfate anion $S_2O_8^{2-}$ to produce ferric ion (Fe^{3+}) and the sulfate free radical anion ($SO_4^{-\bullet}$) (Liang et al., 2004). Fe^{2+} can be regenerated through the reaction of Fe^{3+} at the ZVI surface as can be shown in equation (A37) (Bremner et al., 2006).

$$Fe^0 + \tfrac{1}{2} O_2 + H_2O \longrightarrow Fe^{2+} + 2\ OH^- \quad \text{(A.28)}$$

$$Fe^0 + 2\ H_2O \longrightarrow Fe^{2+} + 2\ OH^- + H_2 \quad \text{(A.29)}$$

$$Fe^0 + S_2O_8^{2-} \longrightarrow Fe^{2+} + 2\ SO_4^{2-} \quad \text{(A.30)}$$

$$Fe^{2+} + S_2O_8^{2-} \longrightarrow Fe^{3+} + SO_4^{2-} + SO_4^{-\bullet} \quad \text{(A.31)}$$

$$2\ Fe^{3+} + Fe^{0} \longrightarrow 3\ Fe^{2+} \qquad (A.32)$$

A.7. NanoParticles

Nanoparticles are defined by many authors to be particles with a diameter that ranges from 1 to 100 nanometer (nm) (the most popular definition) (Masciangioli and Zhang, 2003; Oh et al., 2009; Zhang, 2003); however, others define nano-particles as any particle with a diameter that is between 1 to 1000 nm (Huber, 2005). Sun et al. (2006) indicated that the average size of nano-particles (420 nano-ZVI particles were measured) was 105 nm (by acoustic spectrum) and 70.2 nm (by TEM). They observed that 90% of the nano-particles were between 1 and 100 nm, but some particles were larger than 300 nm. Li et al. (2006b) found that over 80% of nano-particles were less than 100 nm, but some were larger than 400 nm. In this work, we will adapt the broader definition to include all particles with a diameter from 1 to 1000 nm.

A.7.1. Structure

As a consequence of size change from micro-scale to nano-scale, the physical, chemical, and biological properties might be changed (for the same compound) (Masciangioli and Zhang, 2003). In other words, nano-materials are novel functional materials (Sun et al., 2006). For example, the surface area, surface reactivity, mechanical strength, structure, and other properties might be changed when going from micro- to nano-scale (Li et al., 2006a). To be more specific, the surface area of nZVI-particles is 30 m^2/g compared with 0.02-0.9 m^2/g for micro-particles (micro-ZVI) (Nyer and Vance, 2001). In general, the surface area per mass increases with a diameter decrease. For example, the surface area of nZVI particles is changed from 7.6 m^2/g for 100 nm diameter particles to 76.3 m^2/g for 10 nm diameter particles (Nyer and Vance, 2001). Not all the surface area in a nano-particle is available to react due to the aggregation between

nano-particles. The surface reactivity (or the reactive surface sites) is heavily dependent on the behavior of these particles in aqueous solutions (Zhang, 2003).

The composition of a nZVI particle consists of two phases of iron (Theron et al., 2008). The core consists of nZVI while the shell consists of iron oxides (FeO) such as magnamite (Fe_2O_3) and magnetite (Fe_3O_4) (Sun et al., 2006). Sun et al. (2006) pointed out that the core of nZVI consists of 44% ZVI, and the shell consists of 56% of iron oxides (FeO). In contrast, Nurmi et al. (2005) found that the core consists of 70% of ZVI while the shell consists of 30% of FeO (by using XRD).

Li et al. (2006a) indicated eleven different methods to synthesize nZVI. Every one of these methods produce nano-particles with different properties (e.g., size, surface area, surface reactivity, aggregates in solutions) (Li et al., 2006a). nZVI can be combined with other metals like Pd, Pt, Ag, Co, Cu, and Ni (Zhang, 2003).

A.7.2. nZVI for Environmental Applications

nZVI particles are relatively high reductive materials (E° -440 mV) (Sun et al., 2006).

$$Fe^{2+} + 2\ e^- \longrightarrow Fe^0 \qquad \text{(A.33)}$$

nZVI has been used in the laboratory to treat a wide variety of contaminants such as chlorinated organics (Katsenovich and Miralles-Wilhelm, 2009; Varanasi et al., 2007; Wang and Zhang, 1997), pesticides (Elliott et al., 2009; Satapanajaru et al., 2008), dyes (Lin et al., 2008), anions, heavy metals, and radionuclides (Zhang, 2003). The reduction of chlorinated organics by nZVI is given by

$$Fe^0 + R\text{-}Cl_2 \longrightarrow R + Fe^{2+} + 2Cl^- \qquad \text{(A.34)}$$

One of the earliest applications of nano-particles in the environmental field was by Wang and Zhang (1997) who used micro-Fe^0, nano-Fe^0, micro-Fe^0/Pd, and nano-Fe^0/Pd to treat TCE and

PCE. Their results showed that the organic compound degradation rate by nZVI was higher than that by micro-Fe^0.

Nano-bimetallic-particles (or two-component intermetallics or two metal alloys (Gonsalves et al., 2002)) have been used to degrade chlorinated organic compounds effectively. The best performance was by nFe^0/Pd compared to nFe^0/Zn, nFe^0/Pt, and nFe^0/Ni. Moreover, nFe^0/Pd was more effective than nZVI and nano-Pd together (mixing two types of nano-particles, which are nZVI and nano-Pd, not bimetallic-particles, which are nFe^0/Pd) (Zhang et al., 1998b).

A.8. In-Situ Application of Nano-ZVI Particles

Cantrell and Kaplan (1997) tried to flush colloidal ZVI-particles (1-3 um in size) through long columns (i.e., L= 1.0 m and 3.05 m, D.I. = 4.4 cm) containing ether a geological (i.e., quartz sand) or non-geological porous medium. They observed a filtration of ZVI-particles near the front of the columns, and that filtration increased with either an increasing ZVI concentration or decreasing injection rate. Generally, the colloidal ZVI flushed through the sand packed columns but the porous medium was affected (the porosity was reduced about 3%). Schrick et al. (2004) used soil columns (i.e., glass buret columns with I.D. 1.2 cm) with four types of soils to flush nZVI-particles. They pointed out that nZVI-particles are efficiently filtered by all the soils, except by the clay-rich soil. They concluded that clay might act as a stabilizer for nZVI-particles (an anionic support material). Kanel et al. (2007a) found that nZVI-particles (10-160 nm) were immobile and aggregated on the porous medium surfaces near the inlet of the columns (soil columns with two lengths 10cm x 2.5cm and 50cm x 6cm). Saleh et al. (2007) found similar filtration results with different column experiments (i.e., stainless steel, 12.5 cm x 1.09 cm, packed with silica sand). In addition, they found a proportional relationship between nZVI concentration and nZVI filtration in sand (when the particle concentration decreases, the

filtration of the particles decreases). Kanel et al. (2007b) studied the flow of nZVI-particles by injecting them in soil box model (i.e., two-dimensional, L=50cm, W=28.5cm, H=5cm, packed with silica beads). They concluded that nZVI-particles could not be transported into groundwater systems (they observed the flow for only 10 minutes). Lin et al. (2010), also, pointed out that no nZVI was detected in the column effluent (i.e., glass column 10.8 cm x 2.66 cm, packed with glass beads, 350 um in diameter) (they used high nZVI concentration, 2000 mg/L). In conclusion, nZVI particles are, relatively, immobile in a porous medium, and the mobility of nZVI is heavily dependent on (1) nZVI diameter, (2) nZVI concentration, (3) nZVI load (or volume), and (4) aquifer material types.

To overcome this problem, delivery vehicles [many other names have been used such as chemical stabilizing agents or surface modifiers or supported materials] have been developed to improve the movement and the transport of nZVI through porous media. These stabilizers are hydrophilic carbon (Schrick et al., 2004), poly acrylic acid (PAA) (Kanel et al., 2007b; Lin et al., 2010; Schrick et al., 2004), poly styrene sulfonate (PSS) (Phenrat et al., 2009; Saleh et al., 2007), carboxymethyl cellulose (CMC) (Lin et al., 2010; Phenrat et al., 2009), polyasparate (PAP) (Phenrat et al., 2009), starch (He and Zhao, 2005), surfactant (Kanel et al., 2007a), oil emulsions (Quinn et al., 2005), silica composites (Zhan et al., 2008; Zheng et al., 2008) and noble metals (Elliott and Zhang, 2001). Stabilized-nZVI particles [if nZVI particles are coupled with delivery vehicles or stabilizing agents, they call Stabilized-nano-ZVI] can be injected through porous media; however, these stabilizing agents, generally, decrease the reactivity of nZVI particles. Phenrat et al. (2009) indicated that all modifiers (i.e., PSS, CMC, and PAP) decrease the reactivity of nZVI particles toward TCE (up to 24 times).

In contrast, this was not an issue with iron-based bimetallic-nanoparticles; they enhanced the reactivity of nZVI (Zhang et al., 1998a). Furthermore, Elliott and Zhang (2001) used nano-bimetallic-particles (Fe^0/Pd) in a field-test, and PCE and TCE were treated (96% of TCE was removed) in some wells by this method. Using a second metal (e.g., palladium, cobalt, or silver) on nZVI surfaces as a stabilizing agent (or delivery vehicle) for nZVI was investigated in the research. The other stabilizing methods were not explored.

A.9. Nano-Activators in Chemical Oxidation

Advanced oxidation technologies (AOTs) were improved by using nano-activators, especially in wastewater treatment where they usually apply more than one activation process to degrade contaminants. To be more specific, nano-particles are considered to be one of these activation processes but not the solo activation process. As noted above, thermal, photochemical, ozonation, and other processes could be employed to generate free radicals from the oxidants (e.g., H_2O_2, PMS, PDS), or enhance the degradation directly (without oxidizing reagents). Therefore, the ambiguity is high regarding the role that nano-activators play to activate oxidants.

As examples, Shu et al. (2009) applied UV/nZVI/H_2O_2 to treat dyes (Azo dye acid black 24), but hydrogen peroxide was activated by UV before adding nZVI to the reaction. In other words, these researchers used nZVI as a second source of treatment not as an activator for hydrogen peroxide. Furthermore, Yang et al. (2009; 2007) applied nano-activators (Co/TiO_2 and FeCo/ TiO_2) with PMS at 300-700 C°. Kumar et al. (2009) used nano-activators (Ag-ZnO) with photo and thermal-assistance (250 C°) to activate H_2O_2, PDS, and PMS. Ben-Moshe et al. (2009) activated hydrogen peroxide by UV, irradiation and nano-copper oxide particles (CuO) to degrade organic compounds (alachor and phenanthrene). They concluded that nano-copper

oxide particles effectively activated hydrogen peroxide without requiring irradiation, and the photo-assistance did not aid in the activation of hydrogen peroxide.

Some investigations have applied nano-activators as a solo activation process. For instance, Shi et al. (2008) found that nano-Fe_2O_3 can activate H_2O_2 to treat benzyl alcohols, aliphatic alcohols, and olefins. One of the first efforts to activate H_2O_2 by nZVI (solo-process) was by Liao et al. (2007) who used this system to treat pentachlorophenol.

A.10. Soil Slurry Batch Experiments

Aqueous experiments do not really capture the situation in aquifers since the ability of any treatment technology might be changed in the presence of aquifer solids. In 1985, Kubarewicz et al. oxidized TNT and RDX (explosive materials) by means of Fenton's reagent (Fe^{2+} activated H_2O_2) in a soil slurry (Tyre et al., 1991). Later, the same approach was used widely with Fenton's reagent to treat soils contaminated by a variety of organic compounds such as PCP (Watts et al., 1993; Watts et al., 1990), dieldrin, hexadecane, trifluralin (Tyre et al., 1991), trichloroethylene (Baciocchi et al., 2004; Gates and Siegrist, 1995), diesel (Watts and Dilly, 1996) and petroleum hydrocarbons (Kong et al., 1998). Soil slurry tests have been used to examine the treatability of other oxidants such as persulfate (Dahmani et al., 2006; Killian et al., 2007; Liang et al., 2004; Liang et al., 2003), permanganate (Gates et al., 1995; Hønning et al., 2007; Nelson, 1999), and recently, peroxymonosulfate (Do et al., 2009).

A.11. Physical Model Experiments

A soil slurry test does not exactly reflect what happens in an aquifer system. Some reagents cannot flow through geological porous media, and some might block the pore throats and pore bodies reducing the porosity and permeability. In other words, not all remediation technologies

can successfully be applied in situ even if they show promising treatment potential in aqueous and slurry tests. To deal with this concern, this treatment approach was evaluated using physical models that mimic and simulate the fate and transport of a solute (e.g., nZVI particles) in an aquifer with one-dimensional flow (i.e., a soil packed column).

The root of using a soil box model highlights the validity of using this technique in many fields, including ISCO. Bear (1972) indicated that Slichter first reported the hydrodynamic dispersion phenomenon of a solute in groundwater. Slichter (1905) constructed a soil box model (a horizontal tank) containing aquifer materials to study the dispersion of a solute in groundwater. Others have employed a column (a cylindrical tube) containing a porous medium (to mimic hydrogeological conditions) to study the hydrodynamic dispersion (or displacement) of various solutes such as chloride (Day, 1956; Krupp and Elrick, 1968; List, 1965; Nielsen and Biggar, 1962), cations (i.e., Mg, Na, Ca) (Bower et al., 1957), viscous liquids (i.e., sodium sulphate, coloured with methylene blue) (Wooding, 1959), and tritium (Nielsen and Biggar, 1961; Nielsen and Biggar, 1962).

For ISCO, Gonullu and Farquhar (1989) were among the first to employ a soil packed column (with silica sand) to treat TCE and PCE by using $KMnO_4$. Ravikumar and Gurol (1994) employed a sand column (91 cm long) to evaluate PCP and TCE decomposition in soils by Fe^{2+} activated H_2O_2. Kakarla and Watts (1997) evaluated the movement of stabilized H_2O_2 (with four different stabilizing agents) through soil columns (25 cm long). Ho et al. (1995) constructed a soil box model (i.e., a soil tank, x=76.2, y=0.64, z=91.4 cm) to test nitrobenzene degradation by H_2O_2. Chen et al. (2001) studied the mechanism of TCE degradation by Fe^{2+} activated H_2O_2 using short stainless steel columns (7.6 cm long and 4.3cm internal diameter with two sampling ports). The movement of some other chemical oxidants was examined using soil columns such

as permanganate (Al et al., 2006; Schnarr et al., 1998; Schroth et al., 2001; Xu and Thomson, 2009), and persulfate (Liang et al., 2008; Sra et al., 2010).

A.12. Advantages and Limitations of In Situ Technologies

The advantages and limitations for some innovative subsurface remediation technologies. (summarized from (NRC, 1999)).

Technology	Advantages	Limitations
Soil vapor extraction (SVE)	- Installing beneath buildings. - Effective with high volatile compounds.	- Ineffective with low volatile compounds. - Disable to remove metals and radionuclides.
Air sparging	- Inexpensive. - Optimum to treat fuel source zones.	- Ineffective with low volatile compounds.
Co solvent	- Not sorbed on the geological materials. - Effectively dealing with high saturated sites.	- Less ability with high hydraulic conductivity aquifers (above 10^{-4} cm/sec).
Surfactant	- Applied beneath buildings.	- Less ability with high hydraulic conductivity aquifers. - Long treatment periods. - Increasing downward mobilization on DNAPLs.
In situ chemical oxidation (ISCO)	- Short treatment period (weeks to months). - Remediating a wide variety of organic compounds	- Some oxidants have short lifetime (i.e., H_2O_2).
Steam injection	- Remove petroleum hydrocarbons effectively.	- Increase the DNAPL mobility (downward).
Electrical heating	- Suitable with fine grained soils.	- Limited with the low volatile compounds.
In situ vitrification	- Treating a wide variety of contaminants. - Helpful as a foundation for constriction.	- Limited with the dry and high organic matter soils. - Limited with depth (under six meters).
Electokientic	- Effective with low permeable sites.	-

In situ bioremediation	- Inexpensive technology. - Not transferring the contaminants to other medias. - Remediating a wide verity of organic compounds.	- Some contaminants are toxic for the microorganisms. - Not treating NAPLs in the free phase but only on the dissolved phase. - Long treatment term.
Phyto-remediation	- inexpensive. - not generating any waste (eco-friendly).	- limited with the depth. - long treatment term.
Permeable reactive barrier (PRB)	- Not requiring any ongoing energy or installation above the ground. - Treating metals and organics.	- Its longevity is questionable. - Limited with the depth..
Physical barrier	- protecting some aquifers by using non-permeable walls.	- Costly to install. - Not treating contaminants.

References:

Al, T.A., Banks, V., Loomer, D., Parker, B.L. and Ulrich Mayer, K., 2006. Metal mobility during in situ chemical oxidation of TCE by KMnO4. Journal of Contaminant Hydrology, 88(1-2): 137-152.

Anipsitakis, G.P. and Dionysiou, D.D., 2003. Degradation of organic contaminants in water with sulfate radicals generated by the conjunction of peroxymonosulfate with cobalt. Environmental Science and Technology, 37(20): 4790-4797.

Anipsitakis, G.P. and Dionysiou, D.D., 2004. Radical generation by the interaction of transition metals with common oxidants. Environmental Science and Technology, 38(13): 3705-3712.

Baciocchi, R., Boni, M.R. and D'Aprile, L., 2004. Application of H2O2 lifetime as an indicator of TCE Fenton-like oxidation in soils. Journal of Hazardous Materials, 107(3): 97-102.

Balazs, G., Cooper, J., Lewis, P. and Adamson, M., 2000. Transition Metal Catalysts for the Ambient Temperature Destruction of Organic Wastes Using Peroxydisulfate, pp. 229-239.

Ball, D.L. and Edwards, J.O., 1956. The kinetics and mechanism of the decomposition of Caro's acid. I. Journal of the American Chemical Society, 78(6): 1125-1129.

Barb, W.G., Baxendale, J.H., George, P. and Hargrave, K.R., 1951. Reactions of ferrous and ferric ions with hydrogen peroxide. Part I. - The ferrous ion reaction. Transactions of the Faraday Society, 47: 462-500.

Bear, J., 1972. Dynamics of Fluids in Porous Media. Dover Publications, INC., New York.

Ben-Moshe, T., Dror, I. and Berkowitz, B., 2009. Oxidation of organic pollutants in aqueous solutions by nanosized copper oxide catalysts. Applied Catalysis B: Environmental, 85(3-4): 207-211.

Bergendahl, J.A. and Thies, T.P., 2004. Fenton's oxidation of MTBE with zero-valent iron. Water Research, 38(2): 327-334.

Bielski, B.H., 1991. Studies of hypervalent iron. Free radical research communications, 12-13 Pt 2: 469-477.

Billings, J.F. and Gale, K., 1999. Contaminant remediation, biodegradation and removel methods and apparatus. Environmental Improvement Technologies, Inc

Boulos, N., Carvel, D. and Muessig, J., 2008. Ex Situ and in Situ Remediation with Activated Persulfate, United States Patent.

Bower, C.A., Gardner, W.R. and Goertzen, J.O., 1957. Dynamics of Cation Exchange in Soil Columns. Soil Science Society of America journal, 21: 20-24.

Bray, W.C. and Gorin, M.H., 1932. Ferryl ion, a compound of tetravalent iron [5]. Journal of the American Chemical Society, 54(5): 2124-2125.

Bremner, D.H., Burgess, A.E., Houllemare, D. and Namkung, K.C., 2006. Phenol degradation using hydroxyl radicals generated from zero-valent iron and hydrogen peroxide. Applied Catalysis B: Environmental, 63(1-2): 15-19.

Cantrell, K.J. and Kaplan, D.I., 1997. Zero-Valent Iron Colloid Emplacement in Sand Columns. Journal of Environmental Engineering, 123(5): 499-505.

Chen, G., Hoag, G. E., Chedda, P., Nadim, F., Woody, B., and Dobbs, G. M., 2001. The mechanism and applicability of in situ oxidation of trichloroethylene with Fenton's reagent. Journal of Hazardous Materials, 87(1-3): 171-186.

Conrad, S.H., Glass, R.J. and Peplinski, W.J., 2002. Bench-scale visualization of DNAPL remediation processes in analog heterogeneous aquifers: urfactant floods and in situ oxidation using permanganate. Journal of Contaminant Hydrology, 58(1-2): 13-49.

Crimi, M.L. and Taylor, J., 2007. Experimental Evaluation of Catalyzed Hydrogen Peroxide and Sodium Persulfate for Destruction of BTEX Contaminants. Soil Sediment Contam, 16(1): 29 - 45.

Dahmani, M., Huang, K. and Hoag, G., 2006. Sodium Persulfate Oxidation for the Remediation of Chlorinated Solvents (USEPA Superfund Innovative Technology Evaluation Program). Water, Air, & Soil Pollution: Focus, 6(1): 127-141.

Day, P.R., 1956. dispersion on a moving salt water boundary advancing through a saturated sand. Trans. Am. Geophys. Union, 37: 595–601.

Dixon, W.T. and Norman, R.O.C., 1962. Free radicals formed during the oxidation and reduction of peroxides. Nature, 196(4857): 891-892.

Do, S.-H., Jo, J.-H., Jo, Y.-H., Lee, H.-K. and Kong, S.-H., 2009. Application of a peroxymonosulfate/cobalt (PMS/Co(II)) system to treat diesel-contaminated soil. Chemosphere, 77(8): 1127-1131.

Doong, R.A. and Chang, W.H., 1998. Photoassisted iron compound catalytic degradation of organophosphorous pesticides with hydrogen peroxide. Chemosphere, 37(13): 2563-2572.

Elliott, D.W., Lien, H.L. and Zhang, W.X., 2009. Degradation of lindane by zero-valent iron nanoparticles. Journal of Environmental Engineering, 135(5): 317-324.

Elliott, D.W. and Zhang, W.X., 2001. Field assessment of nanoscale bimetallic particles for groundwater treatment. Environmental Science and Technology, 35(24): 4922-4926.

Fenton, H.J.H., 1894. LXXIII. - Oxidation of tartaric acid in presence of iron. Journal of the Chemical Society, Transactions, 65: 899-910.

Fenton, H.J.H. and Jones, H.O., 1900. VII. - The oxidation of organic acids in presence of ferrous iron. Part I. Journal of the Chemical Society, Transactions, 77: 69-76.

Furman, O.S., Teel, A.L. and Watts, R.J., 2010. Volume reduction of nonaqueous media contaminated with a highly halogenated model compound using superoxide. Journal of Agricultural and Food Chemistry, 58(3): 1838-1843.

Furukawa, Y., Kim, J.-w., Watkins, J. and Wilkin, R.T., 2002. Formation of Ferrihydrite and Associated Iron Corrosion Products in Permeable Reactive Barriers of Zero-Valent Iron. Environmental Science & Technology, 36(24): 5469-5475.

Gates, D.D. and Siegrist, R.L., 1995. In-Situ Chemical Oxidation of Trichloroethylene Using Hydrogen Peroxide. Journal of Environmental Engineering, 121(9): 639-644.

Gates, D.D., Siegrist, R.L. and Cline, S.R., 1995. Chemical oxidation of contaminants in clay or sandy soil, pp. 582-588.

Gillham, R.W. and O'Hannesin, S.F., 1994. Enhanced degradation of halogenated aliphatics by zero valent iron. Ground Water, 32(6): 958-967.

Goi, A. and Trapido, M., 2010. Chlorophenols Contaminated Soil Remediation by Peroxidation. Journal of Advanced Oxidation Technologies, 13: 50-58.

Goldstein, S., Meyerstein, D. and Czapski, G., 1993. The Fenton reagents. Free Radical Biology and Medicine, 15(4): 435-445.

Gonsalves, K.E., Rangarajan, S.P. and Wang, J., 2002. Chemical synthesis of nanostructured metals, metal alloys, and semiconductors. In: N. Hari Singh (Editor), Nanostructured Materials and Nanotechnology. Academic Press, San Diego, pp. 1-56.

Gonullu. T. and Farquhar. G., 1989. Oxidation to remove TCE from soil. Department of Civil engineering, University of Waterloo.

Haber, F. and Weiss, J., 1934. The Catalytic Decomposition of Hydrogen Peroxide by Iron Salts. Proceedings of the Royal Society of London. Series A, Mathematical and Physical Sciences, 147(861): 332-351.

He, F. and Zhao, D., 2005. Preparation and Characterization of a New Class of Starch-Stabilized Bimetallic Nanoparticles for Degradation of Chlorinated Hydrocarbons in Water. Environmental Science & Technology, 39(9): 3314-3320.

Ho, C.L., Shebl, M.A. and Watts, R.J., 1995. Development of an Injection System for In Situ Catalyzed Peroxide Remediation of Contaminated Soil. Hazardous Waste & Hazardous Materials, 12(1): 15-25.

Hoag, G.E., Chheda, P.V., Woody, B.A. and Dobbs, G.M., 2000. Chemical oxidation of volatile organic compounds, U.S. Patent. United Tech. Corp., University of Connecticut.

Hoag, G.E., Chheda, P.V., Woody, B.A. and Dobbs, G.M., 2002. Chemical oxidation of volatile organic compounds, US Patent. United Tech. Corp., University of Connecticut.

Hønning, J., Broholm, M.M. and Bjerg, P.L., 2007. Quantification of potassium permanganate consumption and PCE oxidation in subsurface materials. Journal of Contaminant Hydrology, 90(3-4): 221-239.

House, D.A., 1962. Kinetics and mechanism of oxidations by peroxydisulfate. Chemical Reviews, 62: 185-203.

Huber, D.L., 2005. Synthesis, properties, and applications of iron nanoparticles. Small, 1(5): 482-501.

Huling, S.G. and Pivetz, B.E., 2006. Engineering Issue Paper: In-Situ Chemical Oxidation August, U.S. EPA, Washington.

Kakarla, P.K.C. and Watts, R.J., 1997. Depth of Fenton-Like Oxidation in Remediation of Surface Soil. Journal of Environmental Engineering, 123(1): 11-17.

Kanel, S., Nepal, D., Manning, B. and Choi, H., 2007a. Transport of surface-modified iron nanoparticle in porous media and application to arsenic(III) remediation. Journal of Nanoparticle Research, 9(5): 725-735.

Kanel, S.R., Goswami, R.R., Clement, T.P., Barnett, M.O. and Zhao, D., 2007b. Two Dimensional Transport Characteristics of Surface Stabilized Zero-valent Iron Nanoparticles in Porous Media. Environmental Science & Technology, 42(3): 896-900.

Katsenovich, Y.P. and Miralles-Wilhelm, F.R., 2009. Evaluation of nanoscale zerovalent iron particles for trichloroethene degradation in clayey soils. Science of the Total Environment, 407(18): 4986-4993.

Kelley, B. and Koenigsberg, S., 2006. Chemical oxidation treats soil and groundwater. Pollution Engineering, 38(3): 34-37.

Killian, P.F., Bruell, C.J., Liang, C. and Marley, M.C., 2007. Iron (II) Activated Persulfate Oxidation of MGP Contaminated Soil. Soil Sediment Contam, 16(6): 523 - 537.

Kolthoff, I.M., Medalia, A.I. and Raaen, H.P., 1951. The reaction between ferrous iron and peroxides. IV. Reaction with potassium persulfate. Journal of the American Chemical Society, 73(4): 1733-1739.

Kolthoff, I.M. and Miller, I.K., 1951. The chemistry of persulfate. I. The kinetics and mechanism of the decomposition of the persulfate ion in aqueous medium. Journal of the American Chemical Society, 73(7): 3055-3059.

Kong, S.-H., Watts, R.J. and Choi, J.-H., 1998. Treatment of petroleum-contaminated soils using iron mineral catalyzed hydrogen peroxide. Chemosphere, 37(8): 1473-1482.

Krupp, H.K. and Elrick, D.E., 1968. Miscible Displacement in an Unsaturated Glass Bead Medium. Water Resour. Res., 4(4): 809-815.

Kumar, P.S.S., Manivel, A. and Anandan, S., 2009. pp. 1423-1430.

Li, L. et al., 2006a. Synthesis, properties, and environmental applications of nanoscale iron-based materials: A review. Critical Reviews in Environmental Science and Technology, 36(5): 405-431.

Li, X.Q., Elliott, D.W. and Zhang, W.X., 2006b. Zero-valent iron nanoparticles for abatement of environmental pollutants: Materials and engineering aspects. Critical Reviews in Solid State and Materials Sciences, 31(4): 111-122.

Liang, C., Bruell, C.J., Marley, M.C. and Sperry, K.L., 2004. Persulfate oxidation for in situ remediation of TCE. I. Activated by ferrous ion with and without a persulfate-thiosulfate redox couple. Chemosphere, 55(9): 1213-1223.

Liang, C. and Lai, M.C., 2008. Trichloroethylene degradation by zero valent iron activated persulfate oxidation. Environmental Engineering Science, 25(7): 1071-1077.

Liang, C., Lee, I.L., Hsu, I.Y., Liang, C.P. and Lin, Y.L., 2008. Persulfate oxidation of trichloroethylene with and without iron activation in porous media. Chemosphere, 70(3): 426-435.

Liang, C., Lin, Y.T. and Shih, W.H., 2009. Treatment of trichloroethylene by adsorption and persulfate oxidation in batch studies. Industrial and Engineering Chemistry Research, 48(18): 8373-8380.

Liang, C., Wang, Z.S. and Bruell, C.J., 2007. Influence of pH on persulfate oxidation of TCE at ambient temperatures. Chemosphere, 66(1): 106-113.

Liang, C.J., Bruell, C.J., Marley, M.C. and Sperry, K.L., 2003. Thermally Activated Persulfate Oxidation of Trichloroethylene (TCE) and 1,1,1-Trichloroethane (TCA) in Aqueous Systems and Soil Slurries. Soil Sediment Contam, 12(2): 207 - 228.

Liao, C.J., Chung, T.L., Chen, W.L. and Kuo, S.L., 2007. Treatment of pentachlorophenol-contaminated soil using nano-scale zero-valent iron with hydrogen peroxide. Journal of Molecular Catalysis A: Chemical, 265(1-2): 189-194.

Lin, Y.-H., Tseng, H.-H., Wey, M.-Y. and Lin, M.-D., 2010. Characteristics of two types of stabilized nano zero-valent iron and transport in porous media. Science of The Total Environment, 408(10): 2260-2267.

Lin, Y.T., Weng, C.H. and Chen, F.Y., 2008. Effective removal of AB24 dye by nano/micro-size zero-valent iron. Separation and Purification Technology, 64(1): 26-30.

List, E.J., 1965. The stability and mixing of a density-stratified horizontal flow in a saturated porous medium, California Institute of Technology, Pasadena, CA.

Lücking, F., Köser, H., Jank, M. and Ritter, A., 1998. Iron powder, graphite and activated carbon as catalysts for the oxidation of 4-chlorophenol with hydrogen peroxide in aqueous solution. Water Research, 32(9): 2607-2614.

Luzzatto, E., Cohen, H., Stockheim, C., Wieghardt, K. and Meyerstein, D., 1995. Reactions of low valent transition metal complexes with hydrogen peroxide. Are they "Fenton-like" or

not? 4. The case of Fe(II)L, L = edta; hedta and tcma. Free radical research, 23(5): 453-463.

MacKinnon, L.K. and Thomson, N.R., 2002. Laboratory-scale in situ chemical oxidation of a perchloroethylene pool using permanganate. Journal of Contaminant Hydrology, 56(1-2): 49-74.

Masciangioli, T. and Zhang, W.X., 2003. Environmental technologies at the nanoscale. Environmental Science and Technology, 37(5).

Merz, J.H. and Waters, W.A., 1947. A. - Electron-transfer reactions. The mechanism of oxidation of alcohols with Fenton's reagent. Discussions of the Faraday Society, 2: 179-188.

Merz, J.H. and Waters, W.A., 1949a. The oxidation of aromatic compounds by means of the free hydroxyl radical. Journal of the Chemical Society (Resumed): 2427-2433.

Merz, J.H. and Waters, W.A., 1949b. Some oxidations involving the free hydroxyl radical. Journal of the Chemical Society (Resumed).

Milas, N.A., 1937. The hydroxylation of unsaturated substances. III. The use of vanadium pentoxide and chromium trioxide as catalysts of hydroxylation. Journal of the American Chemical Society, 59(11): 2342-2344.

Nelson, C.H., 1999. Treatment of TCE-impacted groundwater using in situ chemical oxidation. Battelle Memorial Institute International In Situ and On-Site Bioreclamation Symposium Proceedings, 5.

Neta, P., Madhavan, V., Zemel, H. and Fessenden, R.W., 1977. Rate constants and mechanism of reaction of so4·- with aromatic compounds. Journal of the American Chemical Society, 99(1): 163-164.

Nielsen, D.R. and Biggar, J.W., 1961. Miscible Displacement in Soils: I. Experimental Information. Soil Science Society of America journal, 25: 1-5.

Nielsen, D.R. and Biggar, J.W., 1962. Miscible Displacement in Soils: II. Behavior of Tracers. Soil Science Society of America journal, 26: 125-128.

Norman, R.O.C., Storey, P.M. and West, P.R., 1970. Electron spin resonance studies. Part XXV. Reactions of the sulphate radical anion with organic compounds. Journal of the Chemical Society B: Physical Organic: 1087-1095.

NRC, 1994. Alternatives for ground water cleanup, Washington, D.C.

NRC, 1999. Groundwater and Soil Cleanup: Improving Management of Persistent Contaminants. National Acadmy press, Washington, D.C.

Nurmi, J.T. et al., 2005. Characterization and properties of metallic iron nanoparticles: Spectroscopy, electrochemistry, and kinetics. Environmental Science and Technology, 39(5): 1221-1230.

Nyer, E.K. and Vance, D.B., 2001. Treatment Technology: Nano-scale iron for dehalogenation. Ground Water Monitoring and Remediation, 21(2): 41-46.

Oh, S.-Y., Kang, S.-G. and Chiu, P.C., 2010. Degradation of 2,4-dinitrotoluene by persulfate activated with zero-valent iron. Science of The Total Environment, 408(16): 3464-3468.

Oh, S.Y., Kim, H.W., Park, J.M., Park, H.S. and Yoon, C., 2009. Oxidation of polyvinyl alcohol by persulfate activated with heat, Fe2+, and zero-valent iron. Journal of Hazardous Materials, 168(1): 346-351.

Osgerby, I.T., 2006. ISCO technology overview: Do you really understand the chemistry? In: E.J. Calabrese, P.T. Kostecki and J. Dragun (Editors). Contaminated Soils, Sediments and Water: Success and Challenges, MA, pp. 287-308.

Padmanabhan, A.R., 2008. Novel Simultaneous Reduction/Oxidation Process for Destroying Organic Solvents, Worcester Polytechnic Institute.

Phenrat, T., Liu, Y., Tilton, R.D. and Lowry, G.V., 2009. Adsorbed Polyelectrolyte Coatings Decrease Fe0 Nanoparticle Reactivity with TCE in Water: Conceptual Model and Mechanisms. Environmental Science & Technology, 43(5): 1507-1514.

Pignatello, J.J. and Baehr, K., 1994. Ferric complexes as catalysts for Fenton degradation of 2,4-D and metolachlor in soil. Journal of Environmental Quality, 23(2): 365-370.

Quinn, J. et al., 2005. Field Demonstration of DNAPL Dehalogenation Using Emulsified Zero-Valent Iron. Environmental Science & Technology, 39(5): 1309-1318.

Ravikumar, J.X. and Gurol, M.D., 1994. Chemical oxidation of chlorinated organics by hydrogen peroxide in the presence of sand. Environmental Science & Technology, 28(3): 394-400.

Reynolds, G.W., Hoff, J.T. and Gillham, R.W., 1990. Sampling bias caused by materials used to monitor halocarbons in groundwater. Environmental Science and Technology, 24(1): 135-142.

Rhodes, F.H. and Carty, J.T., 1925. The Corrosion of Certain Metals by Carbon Tetrachloride. Industrial and Engineering Chemistry, 17(9): 909-911.

Saleh, N. et al., 2007. Surface Modifications Enhance Nanoiron Transport and NAPL Targeting in Saturated Porous Media. Environmental Engineering Science, 24(1): 45-57.

Samuni, A., Meisel, D. and Czapski, G., 1972. The kinetics of the oxidation of chromium(II), titanium(III), and vanadium(IV) by hydrogen peroxide and hydroxyl radicals. Journal of the Chemical Society, Dalton Transactions(12): 1273-1277.

Satapanajaru, T., Anurakpongsatorn, P., Pengthamkeerati, P. and Boparai, H., 2008. Remediation of atrazine-contaminated soil and water by nano zerovalent iron. Water, Air, and Soil Pollution, 192(1-4): 349-359.

Schnarr, M. et al., 1998. Laboratory and controlled field experiments using potassium permanganate to remediate trichloroethylene and perchloroethylene DNAPLs in porous media. Journal of Contaminant Hydrology, 29(3): 205-224.

Schrick, B., Hydutsky, B.W., Blough, J.L. and Mallouk, T.E., 2004. Delivery Vehicles for Zerovalent Metal Nanoparticles in Soil and Groundwater. Chemistry of Materials, 16(11): 2187-2193.

Schroth, M.H., Oostrom, M., Wietsma, T.W. and Istok, J.D., 2001. In-situ oxidation of trichloroethene by permanganate: effects on porous medium hydraulic properties. Journal of Contaminant Hydrology, 50(1-2): 79-98.

Shi, F. et al., 2008. Nano-iron oxide-catalyzed selective oxidations of alcohols and olefins with hydrogen peroxide. Journal of Molecular Catalysis A: Chemical, 292(1-2): 28-35.

Shu, H.Y., Chang, M.C. and Chang, C.C., 2009. Integration of nanosized zero-valent iron particles addition with UV/H2O2 process for purification of azo dye Acid Black 24 solution. Journal of Hazardous Materials, 167(1-3): 1178-1184.

Siegal, J., Rees, A.A., Eggers, K.W. and Hobbs, R.L., 2009. In situ chemical oxidation of residual LNAPL and dissolved-phase fuel hydrocarbons and chlorinated alkenes in groundwater using activated persulfate. Remediation Journal, 19(2): 19-35.

Siegrist, R.L., 2000. In Situ Chemical Oxidation for Remediation of Contaminated Soil and Ground Water. EPA(37).

Siegrist, R.L., Crimi, M. and Simpkin, T.J., 2011. In situ Chemcial Oxidation for Groundwater Remediation Springer, New York.

Slichter, C.S., 1905. Field measurements of the rate of movement of underground waters, US Geological Survey.

Smith, B.A., Teel, A.L. and Watts, R.J., 2009. Destruction of trichloroethylene and perchloroethylene DNAPLs by catalyzed H2 O2 propagations. Journal of Environmental Engineering, 135(7): 535-543.

Sra, K.S., Thomson, N.R. and Barker, J.F., 2010. Persistence of Persulfate in Uncontaminated Aquifer Materials. Environmental Science & Technology, 44(8): 3098-3104.

Sun, Y.P., Li, X.Q., Cao, J., Zhang, W.X. and Wang, H.P., 2006. Characterization of zero-valent iron nanoparticles. Advances in Colloid and Interface Science, 120(1-3): 47-56.

Sweeny, K.H. and Fischer, J.R., 1972. Reductive degradation halogenated pesticides, U S. Patent, United States.

Tang, W.Z. and Chen, R.Z., 1996. Decolorization kinetics and mechanisms of commercial dyes by H2O2/iron powder system. Chemosphere, 32(5): 947-958.

Theron, J., Walker, J.A. and Cloete, T.E., 2008. Nanotechnology and water treatment: Applications and emerging opportunities. Critical Reviews in Microbiology, 34(1): 43-69.

Thiruvenkatachari, R., Vigneswaran, S. and Naidu, R., 2008. Permeable reactive barrier for groundwater remediation. Journal of Industrial and Engineering Chemistry, 14(2): 145-156.

Tsai, T.T., Kao, C.M., Yeh, T.Y. and Lee, M.S., 2008. Chemical oxidation of chlorinated solvents in contaminated groundwater: Review. Practice Periodical of Hazardous, Toxic, and Radioactive Waste Management, 12(2): 116-126.

Tyre, B.W., Watts, R.J. and Miller, G.C., 1991. Treatment of four biorefractory contaminants in soils using catalyzed hydrogen peroxide. Journal of Environmental Quality, 20(4): 832-838.

Varanasi, P., Fullana, A. and Sidhu, S., 2007. Remediation of PCB contaminated soils using iron nano-particles. Chemosphere, 66(6): 1031-1038.

Walling, C., 1975. Fenton's reagent revisited. Accounts of Chemical Research, 8(4): 125-131.

Walling, C. and Camaioni, D.M., 1978. Role of silver(II) in silver-catalyzed oxidations by peroxydisulfate. Journal of Organic Chemistry, 43(17): 3266-3271.

Walling, C. and Johnson, R.A., 1975. Fenton's reagent. V. Hydroxylation and side-chain cleavage of aromatics. Journal of the American Chemical Society, 97(2): 363-367.

Walling, C. and Kato, S., 1971. The oxidation of alcohols by Fenton's reagent. The effect of copper ion. Journal of the American Chemical Society, 93(17): 4275-4281.

Wang, C.B. and Zhang, W.X., 1997. Synthesizing nanoscale iron particles for rapid and complete dechlorination of TCE and PCBs. Environmental Science and Technology, 31(7): 2154-2156.

Watts, R.G., Greenberg, R.S., 1998. Soil and/or groundwater remediation process. Anesys Corp., U.S. Patent.

Watts, R.J. and Dilly, S.E., 1996. Evaluation of iron catalysts for the Fenton-like remediation of diesel-contaminated soils. Journal of Hazardous Materials, 51(1-3): 209-224.

Watts, R.J. and Teel, A.L., 2005. Chemistry of modified Fenton's reagent (catalyzed H2O2 propagations-CHP) for in situ soil and groundwater remediation. Journal of Environmental Engineering, 131(4): 612-622.

Watts, R.J. and Teel, A.L., 2006. Treatment of contaminated soils and groundwater using ISCO. Practice Periodical of Hazardous, Toxic, and Radioactive Waste Management, 10(1): 2-9.

Watts, R.J., Udell, M.D. and Monsen, R.M., 1993. Use of iron minerals in optimizing the peroxide treatment of contaminated soils. Water Environment Research, 65(7): 839-844.

Watts, R.J., Udell, M.D. and Rauch, P.A., 1990. Treatment of pentachlorophenol-contaminated soils using Fenton's reagent. Hazardous Waste and Hazardous Materials, 7(4): 335-345.

Wooding, R.A., 1959. The Stability of a Viscous Liquid in a Vertical Tube Containing Porous Material. Proceedings of the Royal Society of London. Series A, Mathematical and Physical Sciences, 252(1268): 120-134.

Xu, X. and Thomson, N.R., 2009. A long-term bench-scale investigation of permanganate consumption by aquifer materials. Journal of Contaminant Hydrology, 110(3-4): 73-86.

Yang, Q., Choi, H., Al-Abed, S.R. and Dionysiou, D.D., 2009. Iron-cobalt mixed oxide nanocatalysts: Heterogeneous peroxymonosulfate activation, cobalt leaching, and ferromagnetic properties for environmental applications. Applied Catalysis B: Environmental, 88(3-4): 462-469.

Yang, Q., Choi, H. and Dionysiou, D.D., 2007. Nanocrystalline cobalt oxide immobilized on titanium dioxide nanoparticles for the heterogeneous activation of peroxymonosulfate. Applied Catalysis B: Environmental, 74(1-2): 170-178.

Yukselen-Aksoy, Y., Khodadoust, A. and Reddy, K., 2010. Destruction of PCB 44 in Spiked Subsurface Soils Using Activated Persulfate Oxidation. Water, Air, and Soil Pollution, 209(1): 419-427.

Zhan, J. et al., 2008. Transport Characteristics of Nanoscale Functional Zerovalent Iron/Silica Composites for in Situ Remediation of Trichloroethylene. Environmental Science & Technology, 42(23): 8871-8876.

Zhang, W.X., 2003. Nanoscale iron particles for environmental remediation: An overview. Journal of Nanoparticle Research, 5(3-4): 323-332.

Zhang, W.X., Wang, C.B. and Lien, H.L., 1998a. Treatment of chlorinated organic contaminants with nanoscale bimetallic particles. Catalysis Today, 40(4): 387-395.

Zhang, W.X., Wang, C.B. and Lien, H.L., 1998b. Treatment of chlorinated organic contaminants with nanoscale bimetallic particles. Catal. Today, 40(4): 387-395.

Zheng, T. et al., 2008. Reactivity Characteristics of Nanoscale Zerovalent Iron−Silica Composites for Trichloroethylene Remediation. Environmental Science & Technology, 42(12): 4494-4499.

Appendix B

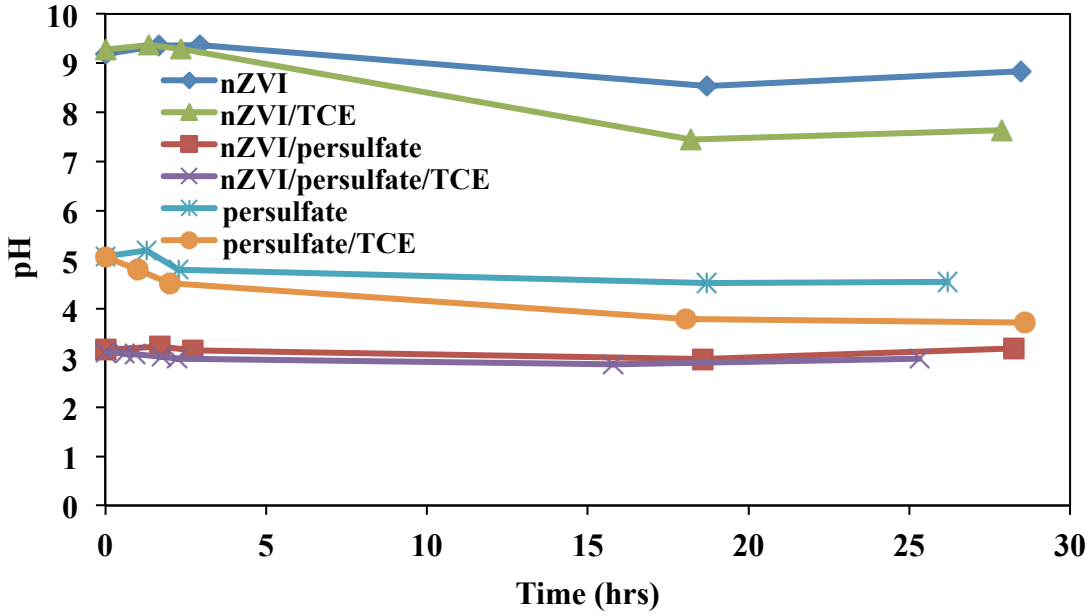

Figure B.1. pH of persulfate/nZVI system based on a molar ratio of 1:1 between persulfate: nZVI with 1811.49 mg/l as an initial persulfate concentration. (In the presence of TCE, the molar ratio is 1:20:20 between TCE/Persulfate/nZVI). (The error bars represent a standard deviation with duplicates).

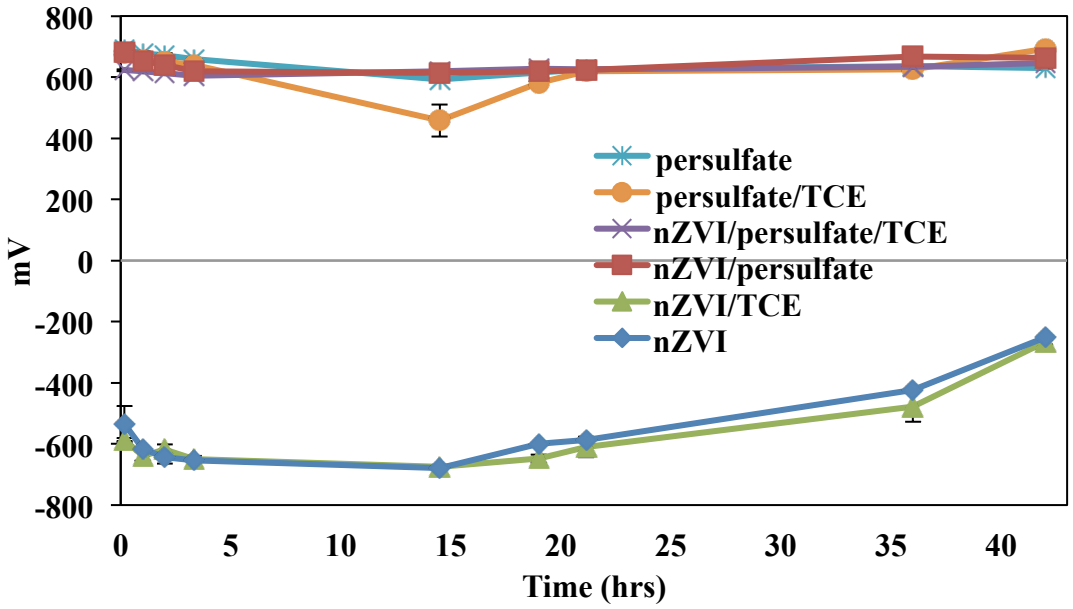

Figure B.2. Redox potential values of persulfate/nZVI system based on a molar ratio of 1:1 between persulfate: nZVI with 1811.49 mg/l as an initial persulfate concentration. (In the presence of TCE, the molar ratio is 1:20:20 between TCE/Persulfate/nZVI). (The error bars represent a standard deviation with duplicates).

Appendix C

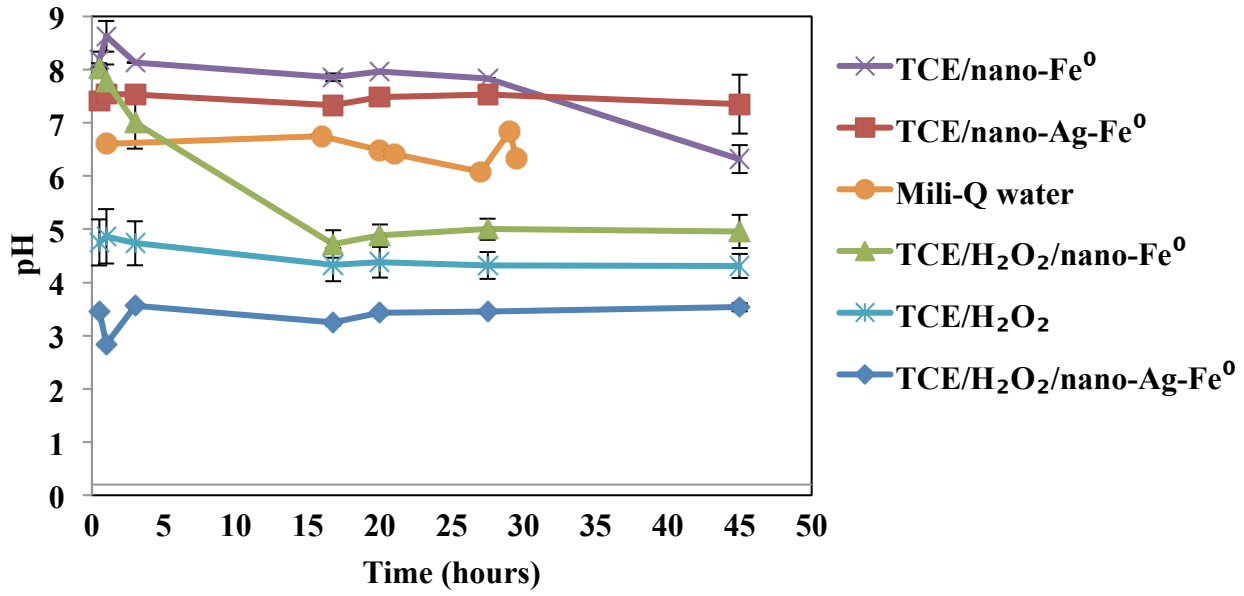

Figure C.1. pH of H_2O_2/nano-Ag-Fe^0 (or nano-Fe^0) system based on a molar ratio of 1:1 between H_2O_2: nano-Ag-Fe^0 with 1811.49 mg/l as an initial H_2O_2 concentration. (In the presence of TCE, the molar ratio is 1:20:20 between TCE/H_2O_2/ nano-Ag-Fe^0). (The error bars represent a standard deviation with triplicates).

Appendix D

Table D.1. Degree of success in the mobility of stabilized nZVI in column test, soil box model, and field test

Stabilizing agents	nZVI concentration	Flow rate	Reference	Experimental design		Soil properties		Degree of success
				Type	Details	Type	Details	
Hydrophilic carbon or PAA or PSS with Pd or Ni	5 g/L	1-19 ml/min	(Schrick et al., 2004)	Column test	Glass buret column, 1.2cm (i.d.), Vertical setting	4 types: Ottawa sand, sand, silt, and clay	Porosity= 0.4-0.48	60% was recovered in some cases
Poly acrylic acid (PAA) or Carboxymethyl cellulose (CMC)	2 g/L	6.28- 38.2 m/d	(Lin et al., 2010)	Column test	Glass column, 2.66cm (i.d.), 10.8cm (length), vertical setting,	Glass beads	Size= 350 um, porosity = 0.365	>99% of mass recovery with PAA and CMC
-Triblock copolymers: PMAA, PMMA, and PSS[1] -SDBS[2]	120 mg/L to 3 g/L	4.66- 93 m/day	(Saleh et al., 2007)	Column test	Stainless steel column, 12.5cm (length), 1.09cm (i.d.)	Silica sand	Size= 300 um, porosity = 0.33	95-98% of mass was recovered with triblock copolymers, and ~ 40% with SDBS
PSS	0.03- 6 g/L	27.6 m/day	(Phenrat et al., 2009)	Column test	Stainless steel column, 25.5cm (length), 1.09cm (i.d.), up flow mode	Silica sand	porosity = 0.33	0.6-0.97 of C/C. was detected
0.5% non-ionic	1 g/L	1.8 ml/min	(Kanel et al.,	Column test	Pyrex glass column (2	Sand Jumunji	Size= 600 um, porosity	100% of arsenic

[1] Poly (methacrylic acid) (PMAA), hydrophobic poly (methyl methacrylate) (PMMA) ,and Poly styrene sulfonate (PSS).
[2] Sodium dodecyl benzyl sulfonate

Surfactant[3]			2007a)		designs): 10cm (L) x 2.5 (i.d.) and 50cm (L) x 6cm (i.d.)	(South Korea	= 0.51	was treated
Nano-porous silica (functionalized with ethyl group)	3g/L	0.1ml/min, 18ml/min	(Zhan et al., 2008)	Column test	10cm Length, 1.8mm i.d., Vertical setting	Ottawa sand	Porosity= 0.32	~ 70% of mass was recovered
-Triblock copolymers -SDBS	10-30 mg/L	0.1 ml/min	(Saleh et al., 2008)	Column test	Stainless steel column, 61cm (length), 1.1cm (i.d.)	Silica sand	Size= 300 um, porosity = 0.33	nZVI with triblock polymers was mobile (less mobility with SDBS)
0.1% Pd	-	0.58 ml/min	(Katsenovich and Miralles-Wilhelm, 2009)	Column test	Pyrex glass column, 45cm (length), 5cm (i.d.), up flow mode	Clay	Porosity = 0.54	~50% of TCE was treated
PAA or CMC	0.1, 0.5, and 3 g/L	2.88 m/day	(Raychoudhury et al., 2010)	Column test	4.5 cm (length), 2.5cm (i.d.)	Sand	Porosity = 0.3, d_{50}= 375 um	Effluent concentration of iron was >99% with PAA and CMC[4]
PAA or soy proteins or PV3A[5]	10 g/L (200 ml)	3-10 ml/min	(Jiemvarangkul et al., 2011)	Column test	Glass column, 30 cm (length), 2.5cm (i.d.)	Standard Ottawa sand	Porosity = 0.3, size= 0.6-0.85 mm	43% of iron mass was recovered with PAA, and >99% with PV3A

[3] Polyoxyethylene sorbtitan monolaurate
[4] The results showed a higher nZVI mobility when CMC was used as a stabilizer agent compared to PAA.
[5] Polyvinyl alcohol-co-vinyl acetate-co-itaconic acid (PV3A)

2.5, 5, and 10% of Cu	2, 5, 8 g/L	108, 216, and 324 m/day	(Mossa Hosseini et al., 2011)	Column test	Plexiglass column, 120 cm (length), 6.5cm (i.d.), down flow mode	Sand	Porosity = 0.37, size= 0.2-1.2 mm	33-75% nitrate was removed
Poly acrylic acid (PAA)	4 g/L	75ml/min	(Kanel et al., 2007b)	Soil box model test (2D)	50cm x 28.5cm x 2cm	A-110 silica beads	Size= 1.1mm porosity = 0.385	Stabilized nZVI transport like a tracer test (Visually observation)
PSS	0.3, 3, and 6 g/L	-	(Phenrat et al., 2010)	Soil box model (2-D)	30cm x 18cm x 2.5cm	Unimin, New cannan CT	Fine, medium, coarse sands[6]	~ 40-80% of mass recovery for some cases
Oil emulsions: 37% oil (sunlight and corn oil) and 1.5% surfactant[8]	170 g/L (2,536 L)	-	(Quinn et al., 2005)	Field test	~ 5.3-8 m depth	LC34 sand[7]	Porosity= 0.33	57-100% of TCE was treated at all depths
Metal additives: (0.1% Pd)	0.75-1 g/L (~ 1.7 kg)	3700- 7500 ml/min	(Elliott and Zhang, 2001)	Field test	4.5 m distance and 6m depth	(Trenton, NJ, USA)	Porosity= 0.25	~ 96% of TCE was treated in 4 weeks
0.1- 0.6% CMC and 0.1% Pd	0.2-1 g/L	<5 psi (pressure)	(He et al., 2010)	Field test	5 m distance and 15m depth	South USA[9]	Porosity= 0.3	40-60% of chlorinated solvents (in long

[6] Arranged as porosity, size, and hydraulic conductivity (K): (I) Fine sand: 0.3, 99 um, 2.85m/d. (II) Medium sand:0.3, 330 um, 28.5 m/d. (III) Coarse sand:0.4, 880 um, 475.2 m/d.

[7] At Cape Canaveral air force station, Florida

[8] Non-ionic surfactant (sorbitan triolate)

[9] No more information was provided about soil's properties.

	(1,136L)							period)
0.5-1% Pd and non-ionic surfactant[10]	~ 40-370 mg/L (2,250 L)	20,000 ml/min	(Wei et al., 2010)	Field test	5 m distance and 4-18 m depth	Kaohsiung, Taiwan	-	50-99% of vinyl chloride was treated
0.4-0.8% of CMC and 0.1% of Pd	0.2-1 g/L	5300 ml/min	(Bennett et al., 2010)	Field test	15.9 m depth,	Palo Alto, San Francisco, CA, USA	Shallow granular aquifer	Mass recovery were 2.6, 21, and 31% in various locations

[10] Not specified

Bennett, P., He, F., Zhao, D., Aiken, B. and Feldman, L., 2010. In situ testing of metallic iron nanoparticle mobility and reactivity in a shallow granular aquifer. Journal of Contaminant Hydrology, 116(1-4): 34-46.

Elliott, D.W. and Zhang, W.X., 2001. Field assessment of nanoscale bimetallic particles for groundwater treatment. Environmental Science and Technology, 35(24): 4922-4926.

He, F., Zhao, D. and Paul, C., 2010. Field assessment of carboxymethyl cellulose stabilized iron nanoparticles for in situ destruction of chlorinated solvents in source zones. Water Research, 44(7): 2360-2370.

Jiemvarangkul, P., Zhang, W.X. and Lien, H.L., 2011. Enhanced transport of polyelectrolyte stabilized nanoscale zero-valent iron (nZVI) in porous media. Chemical Engineering Journal, 170(2-3): 482-491.

Kanel, S., Nepal, D., Manning, B. and Choi, H., 2007a. Transport of surface-modified iron nanoparticle in porous media and application to arsenic(III) remediation. Journal of Nanoparticle Research, 9(5): 725-735.

Kanel ,S.R., Goswami, R.R., Clement, T.P., Barnett, M.O. and Zhao, D., 2007b. Two Dimensional Transport Characteristics of Surface Stabilized Zero-valent Iron Nanoparticles in Porous Media. Environmental Science & Technology, 42(3): 896-900.

Katsenovich, Y.P. and Miralles-Wilhelm, F.R., 2009. Evaluation of nanoscale zerovalent iron particles for trichloroethene degradation in clayey soils. Science of the Total Environment, 407(18): 4986-4993.

Lin, Y.-H., Tseng, H.-H., Wey, M.-Y. and Lin, M.-D., 2010. Characteristics of two types of stabilized nano zero-valent iron and transport in porous media. Science of The Total Environment, 408(10): 2260-2267.

Mossa Hosseini, S., Ataie-Ashtiani, B. and Kholghi, M., 2011. Nitrate reduction by nano-Fe/Cu particles in packed column. Desalination, 276(1-3): 214-221.

Phenrat, T. et al., 2010. Transport and deposition of polymer-modified Fe 0 nanoparticles in 2-D heterogeneous porous media: Effects of particle concentration, Fe 0 content, and coatings. Environmental Science and Technology, 44(23): 9086-9093.

Phenrat, T. et al., 2009. Particle Size Distribution, Concentration, and Magnetic Attraction Affect Transport of Polymer-Modified Fe0 Nanoparticles in Sand Columns. Environmental Science & Technology, 43(13): 5079-5085.

Quinn ,J. et al., 2005. Field Demonstration of DNAPL Dehalogenation Using Emulsified Zero-Valent Iron. Environmental Science & Technology, 39(5): 1309-1318.

Raychoudhury, T., Naja, G. and Ghoshal, S., 2010. Assessment of transport of two polyelectrolyte-stabilized zero-valent iron nanoparticles in porous media. Journal of Contaminant Hydrology, 118(3-4): 143-151.

Saleh, N. et al., 2008. Ionic Strength and Composition Affect the Mobility of Surface-Modified Fe0 Nanoparticles in Water-Saturated Sand Columns. Environmental Science & Technology, 42(9): 3349-3355.

Saleh, N. et al., 2007. Surface Modifications Enhance Nanoiron Transport and NAPL Targeting in Saturated Porous Media. Environmental Engineering Science, 24(1): 45-57.

Schrick, B., Hydutsky, B.W., Blough ‚J.L. and Mallouk, T.E., 2004. Delivery Vehicles for Zerovalent Metal Nanoparticles in Soil and Groundwater. Chemistry of Materials, 16(11): 2187-2193.

Wei, Y.-T. et al., 2010. Influence of nanoscale zero-valent iron on geochemical properties of groundwater and vinyl chloride degradation: A field case study. Water Research, 44(1): 131-140.

Zhan, J. et al., 2008. Transport Characteristics of Nanoscale Functional Zerovalent Iron/Silica Composites for in Situ Remediation of Trichloroethylene. Environmental Science & Technology, 42(23): 8871-8876.